LBL-8062

REMOTE REFERENCE MAGNETOTELLURICS WITH SQUIDS

Thomas D. Gamble
(Ph.D. thesis)

August 1978

Prepared for the U. S. Department of Energy
under Contract W-7405-ENG-48

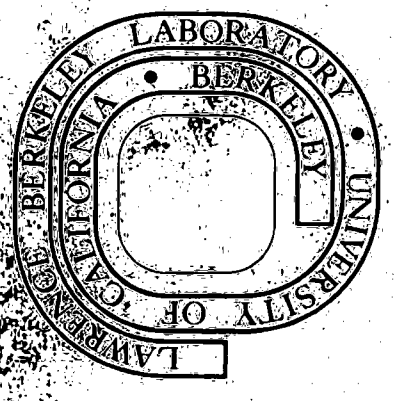

REMOTE REFERENCE MAGNETOTELLURICS WITH SQUIDs

Thomas D. Gamble

Materials and Molecular Research Division, Lawrence Berkeley Laboratory
and Department of Physics, University of California
Berkeley, California 94720

ABSTRACT

This dissertation is concerned with the measurement of the relationship between the natural fluctuations of the earth's magnetic field and the voltages they produce in the surface of the earth. This relationship is approximately defined by the electromagnetic impedance of the surface of the earth for normally incident plane waves. Measurements of the impedance have been used as a method of geophysical survey called magnetotellurics. Because the electrical resistivities of different types of ground differ by several orders of magnitude this method has met with moderate success in spite of the fact that the estimates of the impedance have not been very precisely reproducible.

The tunnel junction dc SQUID magnetometer designed by Clarke, Goubau and Ketchen has superior noise and drift characteristics. I describe the design, construction and operation of a 3 axis dc SQUID magnetometer suitable for field measurements. Repeated magnetotelluric surveys with this instrument showed that the reduced intrinsic noise of the magnetometer did not significantly improve the reproducibility of the estimates of the impedance. Nonetheless, I demonstrate that the discrepancies between the surveys are consistent with the noise bias errors of the least squares linear regression technique that was used to estimate the impedance

rather than with the errors inherent in the approximations made in the consideration of the physical problem. I also argue that the difficulties in the calculation of average power spectra, which have been blamed for the scattered results, are not significant.

I tried dozens of alternative methods of estimating the impedance. Four classes of methods are described that failed to produce satisfactory estimates. However, they did unambiguously demonstrate the presence of correlations between the noises in different field components.

In order to avoid bias caused by local sources of electric or magnetic noise, it is necessary to make simultaneous measurements of two components of the field fluctuations at a site remote from the magnetotelluric sounding site. The equations for the estimation of the impedance, for the calculation of the confidence limits and for the calculation of the signal and noise power spectra of all the measurements are derived for the remote reference method. The basic equations are remarkably simple, symmetric, unique and easily generalized.

A test of the remote reference method is described in detail. Data were taken simultaneously at two sounding sites and the magnetic field at each site used as the reference for the other. The remote reference method unambiguously gave superior estimates of the impedance. The reproducibility of the results was everywhere consistent with the expected random error which was as small as 0.4% for the apparent resistivity of the ground at frequencies where copious data were recorded.

ACKNOWLEDGEMENTS

This work has depended on a community not only of scholars but also of technicians, craftsmen and administators. I can not possibly acknowledge them all though I am deeply grateful for their efforts, guidance and friendship. However, the contributions of two people must be mentioned specifically. First, this work could never have reached its successful conclusion were it not for the generous support and almost unlimited tolerance of my research advisor, Professor John Clarke. Second, throughout my research I have worked so closely with a member of the Clarke group, Dr. Wolfgang Goubau, that to the outside observer our thought processes must seem identical. In fact, both of us are blessed with such cantankerous natures that, if possible, we will take opposing views of any problem. It is largely for this reason that my graduate career has been both productive and strenuous.

This work was supported by the Divisions of Basic Energy Sciences and of Geothermal Energy, U.S. Department of Energy, and by the USGS under grant #14-08-0001-G-328.

To those who search for the truth

and those who put up with us while we do

Table of Contents

SECTION I: INTRODUCTION 1

The Physical Problem 1

Previous Estimation of $\underline{\underline{Z}}$ 11

Outline 15

SECTION II: SQUID Magnetometers for the Field 19

Characteristics of the dc SQUID Magnetometer 19

Electronics Design 20

Field Operation of SQUIDs 23

SECTION III: Signal Processing 25

SECTION IV: Failures 30

Data 30

Method I: solution of 8 equations 39

Method II: weighted averages of cross powers 48

Method III: one reference channel 52

Method IV; double averaging 59

SECTION V; Remote Reference 64

The estimate 64

Error analysis - variances of $\underline{\underline{Z}}^R$ 66

Variances of functions of $\underline{\underline{Z}}^R$ 72

Confidence limits 79

Determination of signal and noise powers 81

Generalizations-the referenced tipper 85

SECTION VI: Test of the Remote Reference Method 89

Data 89

Results 94

Reproducibility of apparent resistivities 121

CONCLUSION 126

REFERENCES 128

SECTION I: INTRODUCTION

The Physical Problem

In 1722 an English instrument maker named Graham discovered diurnal variations in the direction of a very accurate compass, thus becoming the first person aware of natural short term fluctuations in the earth's magnetic field.[7] After having discovered the laws of electromagnetic induction Faraday in 1831 attempted to measure the electric potentials in the earth's surface that he knew must be generated by these fluctuations.[27] He failed because of the low sensitivity of his instruments. These telluric potentials were first observed by accident on early telegraph lines whose ends had been grounded while not in use. The early telegraphic receiver was just a magnetized needle in a coil. Spontaneous fluctuations of the needle were frequently observed. In 1849 a British telegraph engineer named Barlow described a nice informal series of experiments in which he established that the currents were indeed produced by ground potential differences which were roughly homogeneous over the array of his telegraph lines and generally associated with high levels of natural magnetic phenomena.[1] Thus Faraday and Barlow became the first in a long line of experimenters extending to the present day who have attempted with either unambiguous failure or ambiguous success to measure the relationship between these natural electric and magnetic fields.[10,19] This is the goal of magnetotellurics: to measure the electromagnetic impedance of the surface of the earth for the naturally occurring fluctuations and ultimately to use that information to determine the electrical resistivity of the ground.

This long and somewhat confused history may have in part been caused by the fact that the problem might seem to be totally intractable. The impedance of any system depends on the configuration of the incident electromagnetic energy and this configuration is never known in any detail for the magnetotelluric problem. In fact, the dependence of the magnetotelluric impedance on the incident wave form is small and the incident wave can be approximated as a normally incident plane wave.

This approximation actually consists of two physically distinct sets of assumptions. 1) The incident electromagnetic energy is composed of plane waves. 2) The impedance is independent of the angle of incidence and polarization of the incident wave, and the vertical magnetic field is a linear function of the horizontal magnetic fields.

I will now define my notation and describe the physical picture of the problem that convinced me that extensive efforts to improve the method for estimating the impedance were justified. Each electromagnetic quantity will be described by a complex number with the time dependence $e^{-i\omega t}$ where $\omega = 2\pi f$ is the angular frequency. The time dependence will be dropped from all equations. I will use a right handed coordinate system with the $\hat{z}$ axis pointing down into the earth. The earth has a conductivity σ, resistivity $\rho = 1/\sigma$, magnetic permiability μ equal to the free space value $\mu_o = 4\pi \times 10^{-7}$ and permittivity or dielectric constant $\varepsilon = \varepsilon_o = \frac{1}{\mu_o c^2}$; $c = 3 \times 10^8$ m/sec. All equations will be in MKS units. The atmosphere has $\varepsilon = \varepsilon_o$, $\mu = \mu_o$ and $\sigma = 0$. With these conventions Maxwell's equations are

$$\nabla \times \vec{H} = \sigma\vec{E} - i\omega\varepsilon\vec{E} \tag{1.1}$$

$$\nabla \times \vec{E} = i\omega\vec{B} \tag{1.2}$$

$$\nabla \cdot \vec{E} = 0 \tag{1.3}$$

$$\nabla \cdot \vec{B} = 0 \tag{1.4}$$

where $\vec{B} = \mu\vec{H}$.

Combining these equations yields

$$\nabla^2 F = -i\omega\mu(\sigma - i\omega\varepsilon)F \tag{1.5}$$

for any field component F of $\vec{E}$ or $\vec{H}$. Since $\sigma=0$ in the air, waves propagate with velocity c. Typical values of ρ in the earth are 0.1 to 10,000 Ωm while $\varepsilon \simeq 10^{-11}$ farads/m. Thus we can ignore $\omega\varepsilon$ compared to σ in the earth up to about 10^5 Hz. In the earth the wave will decay to an amplitude of 1/e in a distance

$$\sqrt{2/(\mu\omega\sigma)} = 500\sqrt{\rho/f} \tag{1.6}$$

called the skin depth.

The pattern of electromagnetic energy in the earth induced by an incident wave can be constructed through Huygens' principle.[27] The progress of the wave can be constructed by considering each point of the wave front at the time t as a new source of electromagnetic energy. Adding together the waves from all sources produces a new wave front at time $t+\delta t$ at positions where the waves from all sources are in phase and interfere constructively. Huygens' principle is extremely general. It can be applied to any wave phenomenon, longitudinal or transverse, on any scale, including the realm of quantum mechanics.

Consider a small flat section of ground, one square inch, for example. Consider an incident wave that is sufficiently homogeneous that it can be approximated as a plane wave over that inch and consider only the energy that passes through that surface. If the incoming plane wave has an angle of incidence of θ_i with the outward normal to the surface and wave vector $\vec{k}$ then the wave crossing that surface will form a plane wave at the angle of transmission θ_t to the inward normal with wave vector $\vec{k}_t$. From equation (1.5), $\vec{k}_t = \sqrt{i\omega\sigma\mu}\ \hat{k}_t$. Thus the phase velocity in the earth

$$v_p = \left|\frac{\omega}{k}\right| = \sqrt{\frac{\omega}{\mu\sigma}} \quad . \tag{1.7}$$

Matching phases at the boundary gives

$$\sin\theta_t = \sqrt{\omega/(\mu\sigma c^2)}\ \sin\theta_i \quad . \tag{1.8}$$

Thus as long as

$$\omega\varepsilon << \sigma \tag{1.9}$$

the angle of transmission will be essentially zero regardless of the angle of incidence. Thus for typical values of 0.1 Hz and 10 Ωm a normal angle of incidence should be one of the better assumptions of experimental physics.

If the flat surface under consideration is large compared to the skin depth at frequency ω then the only energy reaching points below the center of the flat surface will be due to the plane transmitted wave. Additional waves produced by surface features or inhomogeneities

beyond the flat surface will be attenuated to an insignificant level before reaching this area. For this transmitted wave there will be nonzero components of $\vec{E}$ and $\vec{H}$ only parallel to the surface and these will be related by

$$E_x = (1-i)\sqrt{\omega\mu\rho/2}\ H_y$$
$$E_y = (i-1)\sqrt{\omega\mu\rho/2}\ H_x \qquad (1.10)$$

from equation (1.1) or (1.2). Thus E_x leads H_y by 45° in phase and $|\vec{E}|/|\vec{H}|$ becomes small for low frequencies or resistivity.

The most important point of the preceeding paragraph is that the scale length of the problem is the skin depth. It is over such distances rather than the wavelength in air that the incident wave must be homogeneous in order for it to be approximated as a plane wave. The effects of inhomogeneities in the earth will be significant over distances of the order of the skin depth. The many investigators[32,14,5] who have considered the incident energy as a plane wave must have implicitly understood this but there is still such confusion that one of the most experienced investigators in the field, T. Rikitaki, in 1966 called the most basic and general results, equations (1.8) and (1.10), "ridiculous".[26]

A second point which needs clarification is that when inequality (1.9) is satisfied, only two components of the magnetic field fluctuations need be measured to specify all the electromagnetic fields. The pattern of energy under an irregular surface will no longer be a plane wave. Nevertheless the pattern could in principle

be constructed using Huygens' principle from wavelets originating simultaneously everywhere at the surface, regardless of θ_i. In other words, one of the three degrees of freedom of an electromagnetic wave has been lost at the surface. While inhomogeneous incident waves certainly could produce independent fluctuations of the third component of the magnetic field, such independent fluctuations will depend on the nature of the inhomogeneity. No additional information about the earth would be obtained by relating the electric field to all three magnetic fields unless the nature of the incident inhomogeneity were known. Thus all the approximations in group 2 should be reasonable as long as the inequality (1.9) holds.

The validity of assumption 1 about the homogeneity of the incident wave depends not only on the nature of the incident wave and the skin depth but also on the conductivity structure. In a horizontally layered earth it may not be obvious which layer it is whose skin depth defines the range of the effects of inhomogeneities at a particular frequency. The classic case of the effect of structure is the "coast effect".[17] Comparatively large currents are generated in a very large conductive sheet such as the ocean so that it may take a large number of skin depths in the continental material before the secondary fields from the ocean are reduced to an insignificant level. It is obvious then that in this case the impedance of the earth near the coast will be strongly affected by the incident field over the ocean so that this structure will severely test the assumption of homogeneous incident fields.

The effects of inhomogeneous fields have been studied for a large number of models of the earth[17,19,23,24] usually with a dipole or line

source at approximately 150 km elevation. The general conclusion is that for these models one would expect to see variations of the impedance of the order of 10% at 100 second period, increasing with period. All these model calculations are rather academic, however. "We simply do not have adequate knowledge of the sources of geomagnetic disturbance to permit us to predict the scale length"[20] of the source fields. Numerous investigators[35] have attempted to augment our knowledge by simultaneous measurements of the magnetic fluctuations in different locations. Gross inhomogeneities of the total field have been demonstrated in the auroral and equitorial zones. Such measurements can not directly establish that the incident field is homogeneous however, because the total magnetic field is modified by the local conductivity structure. One thing is certain: the natural field fluctuations are generated in many modes whose amplitudes and locations vary with time. Because of these variables there can be no single answer to the question of the validity of the plane wave assumption. I feel it can best be answered experimentally, through systematic investigation of the reproducibility of the impedance over stable geological areas. The limits to the accuracy of magnetotellurics will be much better than the worst case variations caused by inhomogeneities. With extentions of the techniques presented in this dissertation it may be possible to detect the presence of significant inhomogeneities and correct for them. At the least, one could reject data that produced significantly anomalous estimates of the impedance.

I conclude from this physical picture that at least from 10^{-2} to 10^{5} Hz the horizontal electric field in the surface of the earth due to distant sources, $\vec{E}_s(\omega)$ (s denotes signal), should have a time independent linear relationship to the horizontal components of the magnetic field, $\vec{H}_s(\omega)$. The linear relationship between two two component vectors is of course a rank two tensor and the impedance, which will be denoted by $\underset{\approx}{Z}$, is defined by

$$\vec{E}_s(\omega) = \underset{\approx}{Z}(\omega)\ \vec{H}_s(\omega) \quad . \tag{1.11}$$

Consider the form of the impedance tensor for a few models of the earth. Equations (1.10) for a homogeneous flat earth in matrix form are

$$\vec{E}_s = \begin{pmatrix} 0 & (1-i)\sqrt{\omega\mu\rho/2} \\ (i-1)\sqrt{\omega\mu\rho/2} & 0 \end{pmatrix} \vec{H}_s \tag{1.12}$$

A model of the earth whose conductivity is a function of depth only will be called one dimensional. In such a case the form of equation (1.12) would be unchanged if one replaced ρ by the apparent resistivities $\rho_w(\omega)$, w=xy, yx, defined by

$$\rho_w(\omega) = |Z_w(\omega)|^2/(\omega\mu) \tag{1.13}$$

It is convenient to use units of mV/km for the electric field and $\gamma = 10^{-5}$ Gauss for the magnetic. In these units the apparent resistivity in Ω-m is

$$\rho_w(\omega) = 0.2 \left|Z_w\right|^2/f \tag{1.14}$$

A two dimensional earth is one in which the conductivity is invariant under translation in one horizontal direction. This is a reasonable model for many geological situations where an originally layered structure has been displaced along fault lines which are all in the same direction, called the strike direction. Thus the strike direction is the direction of translational invariance. If $\underline{\underline{Z}}$ is expressed as a matrix in a coordinate system aligned with the strike direction then the diagonal elements are still zero. Even more generally, if there is any vertical plane of reflection symmetry passing through the magnetotelluric sounding site then the currents and voltages induced in the ground must also have that symmetry. Thus the diagonal elements of $\underline{\underline{Z}}$ in a coordinate system aligned with the plane of symmetry will still be zero. For a two dimensional earth the plane of reflection symmetry is perpendicular to the strike direction. In a coordinate system not aligned with the plane of symmetry the diagonal elements will not be zero. The strike direction for a two dimensional earth could be found by minimizing the magnitude of the difference of the diagonal elements as a function of the rotation angle θ about the $\hat{z}$ axis. The same rotation angle maximizes the sum of the squared magnitudes of the off diagonal elements.

The rotation properties of $\underline{\underline{Z}}$ are determined by its tensor nature. For any tensor $\underline{\underline{T}}$, rotating the coordinate system by an angle θ about the $\hat{z}$ axis changes the matrix representation of $\underline{\underline{T}}$ to

$$\underset{\approx}{T}'(\theta) = \underset{\approx}{R}(\theta)\ \underset{\approx}{T}\underset{\approx}{R}^{-1}(\theta) \tag{1.15}$$

where

$$\underset{\approx}{R}(\theta) = (\underset{\approx}{R}^{-1}(\theta))^{\dagger} = \begin{pmatrix} \cos\theta & \sin\theta \\ -\sin\theta & \cos\theta \end{pmatrix} \tag{1.16}$$

and $\dagger$ denotes the conjugate transpose.

A three dimensional earth has an arbitrary conductivity structure. Then the rotation angle which maximizes the sum of the squared magnitudes of the off diagonal elements indicates what is called the apparent strike direction. The apparent strike direction is ambiguous by 90° since rotation by 90° just interchanges the x and y axes. By rotated apparent resistivity I will mean the apparent resistivity from equation (1.13) in a coordinate system aligned with the apparent strike direction. A measure of the "three dimensionality" of the earth is the skewness

$$W = \left| \frac{Z_{xx} + Z_{yy}}{Z_{xy} - Z_{yx}} \right| \tag{1.17}$$

which is invariant under rotation.

The rotated apparent resistivities, apparent strike direction, skewness, and also the phase angles of the off diagonal elements are real parameters of the complex impedance tensor elements that have a relatively straightforward qualitative relation to the resistivity of the ground. They are also easier to present graphically. I therefore will use these parameters to describe the impedance tensor estimates.

Previous estimation of $\underline{\underline{Z}}$

The problem of actually measuring the impedance tensor would be trivial if all the measurements of the electric and magnetic fields were noise free. Unfortunately all measurements contain noise so the measured fields $\vec{E}$ and $\vec{H}$ contain noise contributions $\vec{E}_n$ and $\vec{H}_n$. I will include in the definition of noise ionospherically generated signals that do not satisfy the plane wave assumption so that $\underline{\underline{Z}}$ is well defined and time independent. Thus

$$\vec{\eta} = \vec{E} - \underline{\underline{Z}}\,\vec{H} \tag{1.18}$$

is the total error in $\vec{E}$ and $\vec{H}$. In addition to the noise there is the problem that the defining equation for $\underline{\underline{Z}}$, equation (1.11), is just the two component equations

$$E_{sx} = Z_{xx}H_{sx} + Z_{xy}H_{sy} \tag{1.19}$$

and

$$E_{sy} = Z_{yx}H_{sx} + Z_{yy}H_{sy} \tag{1.20}$$

in the four unknown impedance tensor elements.

Some investigators, following Cagniard,[5] simply ignored the tensor nature of the relationship, thus in effect assuming that $Z_{xx} = Z_{yy} = 0$ and $|Z_{xy}| = |Z_{yx}|$. This was not successful since Z_{xy} and Z_{yx} often differ in magnitude by more than an order of magnitude and it confused the discussion of source effects. Others[13,6,19] estimated $\underline{\underline{Z}}$ by attempting to find two relatively noise free measurements, a and b, of each component of $\vec{E}$ and $\vec{H}$, thus producing two sets of

equations (1.19) and (1.20) that could be solved simultaneously if the determinant

$$\begin{vmatrix} H_x^a & H_x^b \\ H_y^a & H_y^b \end{vmatrix}$$

is not zero, that is, if the magnetic fields have a different polarization for the two measurements. Although it is theoretically possible to get an accurate impedance tensor estimate from this approach, the location of noise free signals of significantly different polarizations that can be analyzed without significant error for every frequency of interest requires both great effort and luck.

In 1964 Madden and Nelson[17] recognized that an estimate of $\underline{\underline{Z}}$ could be made incorporating all of the measured data by substituting the measured fields into equation (1.11), multiplying by $\vec{H}^*$ to form the diadic matrix products of the vectors and averaging over the products from a narrow band of frequencies or from different times to produce

$$[EH] = \underline{\underline{Z}}[HH] \tag{1.21}$$

where, by definition

$$[AB] = \begin{pmatrix} \overline{A_x B_x^*} & \overline{A_x B_y^*} \\ \overline{A_y B_x^*} & \overline{A_y B_y^*} \end{pmatrix} \tag{1.22}$$

is the average power spectral matrix, which is a tensor, and the bar indicates the average.

This particular estimate for $\underline{\underline{Z}}$, which will be denoted by $\underline{\underline{Z}}^H$, has been used frequently enough[31,33] to be called the usual method of analysis. From equation (1.21)

$$\underline{\underline{Z}}^H = [EH][HH]^{-1} \quad . \tag{1.23}$$

Sims, Bostick, and Smith[30] recognized that $\underline{\underline{Z}}^H$ is the estimate of $\underline{\underline{Z}}$ that minimizes the mean square error of the prediction of the electric field from the magnetic. That is,

$$\frac{\partial}{\partial Z^H_{ij}} \left(\overline{|\vec{E} - \underline{\underline{Z}}^H \vec{H}|^2} \right) = 0, \quad i,j=x,y \quad . \tag{1.24}$$

Sims et al also pointed out that there are six such least squares estimates of $\underline{\underline{Z}}$ corresponding to the use of any pair of E_x, E_y, H_x, or H_y to predict the other two. For instance, one could calculate the least squares admittance tensor $\underline{\underline{Y}}$ defined by

$$\frac{\partial}{\partial Y_{ij}} \left(\overline{|\vec{H} - \underline{\underline{Y}}\vec{E}|} \right) = 0 \tag{1.25}$$

and then obtain another estimate of $\underline{\underline{Z}}$, $\underline{\underline{Z}}^E$, from $\underline{\underline{Z}}^E = \underline{\underline{Y}}^{-1}$. The difficulty with each of these least squares estimates, recognized by all these investigators, is that they contain the measured autopowers of the predicting fields, for example $\overline{|H_x|^2}$ and $\overline{|H_y|^2}$ in equation (1.23). This is unsatifactory because the autopowers are always biased estimates of the signal powers, even if the noises are not correlated with the signals. For example,

$$\langle \overline{|H_x|^2} \rangle = \langle \overline{|H_{sx}|^2} \rangle + \langle \overline{H_{sx} H^*_{nx}} \rangle + \langle \overline{H_{nx} H^*_{sx}} \rangle + \langle \overline{|H_{nx}|^2} \rangle = \langle \overline{|H_{sx}|^2} \rangle + \langle \overline{|H_{nx}|^2} \rangle > \langle \overline{|H_{sx}|^2} \rangle \tag{1.26}$$

where $\langle\ \rangle$ indicates an ensemble average. On the other hand averaged measured crosspowers are not biased by the noise powers if the noises are not correlated with the signals or each other. That is

$$\langle \overline{E_x H^*_y} \rangle = \langle \overline{E_{sx} H^*_{sy}} \rangle + \langle \overline{E_{nx} H^*_{sy}} \rangle + \langle \overline{E_{sx} H^*_{ny}} \rangle + \langle \overline{E_{nx} H^*_{ny}} \rangle = \langle \overline{E_{sx} H^*_{sy}} \rangle \ . \tag{1.27}$$

Thus equation (1.23) gives estimates of the impedance tensor whose magnitudes are biased downward by the autopowers in the denominator of $[HH]^{-1}$. If $\vec{H}_s$ where known, it could be used in equation (1.23) to obtain an unbiased estimate for $\underline{\underline{Z}}$.

The least squares estimates for $\underline{\underline{Z}}$ were a major advance at least in the sense that they made possible a quantitative measure of the combined noise in all the measurements via

$$\overline{|\delta_i|^2} \equiv \overline{|E_i - Z^H_{ix} H_x - Z^H_{iy} H_y|^2} \ . \tag{1.28}$$

Usually the size of $\overline{|\delta_i|^2}$ is measured by the correlation coefficient C_i where

$$C_i^2 \equiv \frac{\overline{|E_i|^2} - Z^{H*}_{ix}\, \overline{E_i H^*_x} - Z^{H*}_{iy}\, \overline{E_i H^*_y}}{\overline{|E_i|^2}} = 1 - \frac{\overline{|\delta_i|^2}}{\overline{|E_i|^2}} \tag{1.29}$$

C_i^2 is sometimes called the coherency. If $C_i=1$ then E_i, H_x, and H_y are completely noise free and there is no measurement error. If all of the measurements are pure noise then C_i approaches zero as the number of data in the average increases.

By monitoring $\vec{\delta}$ and selecting only data for which it is small, one can ensure that one obtains relatively error free results. However, there is no guarantee that one will obtain many, if any, noise free data at every frequency. Conversely, if the noise were in $\vec{E}$ only and not in $\vec{H}$, then $\underline{\underline{Z}}^H$ would be unbiased, but the least squares estimates alone do not permit one to identify the noisy fields.

Outline

With the development of the low noise dc SQUID it seemed reasonable to hope that a fieldworthy 3 axis magnetometer employing these devices might improve the estimation of $\underline{\underline{Z}}$ by reducing the magnetic field noise. Section II describes the design considerations in the construction of such an instrument.

Magnetotelluric surveys using our dc SQUID magnetometer were performed in Grass Valley, near Winnemucca, Nevada in 1975 and 1976 as a joint effort of the Engineering Geoscience group and Physics department of the University of California, Berkeley. Comparison of the impedance tensor estimates from the two years using $\underline{\underline{Z}}^H$ proved that we had joined the ranks of the ambiguously successful. Although the dc SQUID magnetometer proved to be accurate and convenient, the reduced intrinsic instrument noise did not seem to improve the quality of the data. Some values of the correlation coefficient, C_i, below

0.1 were obtained and the magnitudes of the impedance tensor elements were sometimes so small as to be physically unreasonable. Thus the intrinsic noise of the magnetometer did not seem to be a crucial factor. On the other hand, for data of high coherency the impedance tensor estimates were reproducible between the two surveys within about 5% on the average and the discrepancies were all consistent with the hypothesis that the autopower measurement bias was the cause. Thus an investigation of tensor estimation seemed in order. Section III considers signal processing techniques, including the fast Fourier transform (FFT). The main point is that signal processing is also not the crucial factor in producing the large scatter in magnetotelluric results.

Section IV discusses alternative tensor estimation techniques that were tested on the 1976 data. In that survey we recorded an extra channel of information by adding a third telluric line. This provided a reference signal to estimate the impedance in a simple way from the average crosspowers alone. The most straightforward estimators were spectacular failures. It seems that the most likely explanation for this is that there were real noise voltages in the ground, correlated between the telluric lines. In order to avoid the possibility of correlated noise from local sources it is necessary to record two simultaneous remote reference channels.

Section V contains the linear algebra and statistics of tensor estimation by the remote reference technique. This method requires a number of reference channels equal to the rank of the tensor to be

estimated. As long as the references are not correlated with the noises in $\vec{E}$ and $\vec{H}$ the method yields an unbiased estimate of the tensor regardless of the correlations between the noises in $\vec{E}$ and $\vec{H}$. Perhaps just as important is the fact that the equations are simple. The distributions of errors in the tensor estimate and associated parameters such as the rotated apparent resistivities are calculated and shown to be essentially the same as those in the least squares estimate $\underline{\underline{Z}}^H$ when $\underline{\underline{Z}}^H$ is an unbiased estimator. With the remote reference one can calculate the power spectra of both the signals and the noises, provided the noises are uncorrelated with each other and the signals. This calculation provides checks for such correlations. All these equations are extremely general and their application to tipper measurement is given as an example. It is a beautiful set of equations.

The remote reference technique was tested on real magnetotelluric data taken near Hollister, California in 1977. Data from two magnetotelluric sounding sites were recorded simultaneously so that the magnetic channels at each could be used as the reference for the other. This test was an unambiguous success. It is described in section VI. At frequencies higher than 0.3 Hz, where copious data were taken, the impedance tensor estimates were reproducible within approximately 1% between different data sets. The calculated random errors were everywhere consistent with the agreement between the results from data recorded in different overlapping frequency bands and at different times.

SECTION II. SQUID MAGNETOMETERS FOR THE FIELD

The theory, fabrication, operation and performance of the cylindrical dc SQUID are discussed by Clarke, Goubau and Ketchen.[8] Here I will discuss only those principles of design and elements of performance that are particularly important to geophysical applications.

The three axis magnetometer is essentially three one axis magnetometers. The three SQUID sensors are place in orthogonally drilled holes in a single block of fiberglass. The block is immersed in liquid helium in a five liter superinsulated fiberglass dewar with a hold time of approximately five days. The electronics are mounted on top of the dewar.

Characteristics of the dc SQUID magnetometer

This dc SQUID makes use of two Nb-NbO_x-Pb tunnel junctions in a superconducting loop. The large area of the tunnel junctions compared to point contact junctions makes them very resistant to distruction by accidental electrical discharge and physically and thermally stable. They can be operated at any temperature below 6°K because the critical current is relatively independent of temperature. At frequencies above 2×10^{-2} Hz the equivalent flux noise is white with level of about 10^{-10} γ^2/Hz. At lower frequencies the power spectrum is approximately $10^{-11}/f$ γ^2/Hz with an average long term drift of less than 10^{-5} γ/hour. The achievement of this low drift rate requires the stabilization of the bath temperature but this is easily accomplished. The system is enclosed in the dewar so the temperature can easily be regulated by controlling the pressure of the vapor.[11]

We did not bother to regulate the bath pressure in our surveys because the barometric pressure changes very little over the period of our lowest frequency tensor estimates (100 seconds).

The dc SQUID is operated by passing a dc current greater than the critical current through the junctions so that a dc voltage and a Josephson ac voltage of frequency 2e/h = 480 MHz/μV appear across the junctions. The resistance of the junctions is a periodic function of the flux through the ring with flux period $\phi_o = h/2e = 2.07 \times 10^{-7}$ gauss-cm^2.

Commercially available rf SQUID magnetometers use a superconducting ring containing only one Josephson junction. The ring is then excited by an external rf oscillator and the energy dissipated in the SQUID is a periodic function of the flux through the ring. From this point on there is no difference between the operation of a dc SQUID and an rf SQUID excited at the Josephson frequency. Thus the electronics for the two types of SQUIDs are identical except that the rf SQUID requires an rf oscillator that is stable over a wide temperature range and the rf injection circuitry.

The SQUID is placed in a negative feedback circuit. A coil modulates the flux through the SQUID at a high audio frequency, 100 kHz for our electronics. This modulates the voltage across the SQUID at 100 kHz and the amplitude of the voltage modulation is a periodic function of the flux through the SQUID. The negative feedback circuit acts as a null detector. Any 100 kHz signal across the SQUID is amplified, demodulated by a lock in detector and integrator and

fed back through the modulation coil. This changes the dc flux through the SQUID to reduce the 100 kHz output. The feedback current necessary to null the 100 kHz signal is then proportional to the externally applied flux.

Electronics Design

The design of the electronics is a straightforward exercise in circuit analysis with the following requirements: the circuit must be stable, the noise of the electronics should not dominate the intrinsic noise of the sensor, the frequency response of the circuit should be flat and the slewing rate, the maximum rate of flux change that can be nulled, should be as high as possible.

The total flux through the SQUID is the externally applied flux ϕ_a plus the feedback flux ϕ_f. Thus the output of the circuit at the frequency ω is

$$\phi_f = G(\omega)\ (\phi_f + \phi_a) \tag{2.1}$$

where $G(\omega)$ is the frequency response of the open loop. I shall refer to the SQUID as the beginning of the loop and the modulation coil as the end. The frequency response of the closed loop is then simply

$$\phi_f/\phi_a = G(\omega)/(1 - G(\omega)) \equiv R(\omega) \tag{2.2}$$

and the response at any stage in the loop can be calculated by dividing R by the forward gain between that stage and the end. The complication of the audio frequency modulation and demodulation can usually be ignored. Circuits resonant at the audio frequency f_m with bandwidth

f/Q can be included in the open loop gain $G(\omega)$ as a simple pole, $1/(1-i\omega\tau)$, with

$$\tau = Q/(\pi f_m) \tag{2.3}$$

For low frequencies $G(0)$ is usually a large negative number so $R(0) = -1$ and is essentially independent of the exact value of $G(0)$. $|G(0)|$ should be made as large as possible to minimize variations in $R(0)$. From equation (2.2), the loop will be stable as long as there is no solution of $1-G(\omega) = 0$ for any complex ω with a positive imaginary part (remember that all amplitudes proceed in time as $e^{-i\omega\tau}$). The sensor noise will dominate the noise of the electronics as long as the sensor noise times the forward gain between the sensor and each stage is greater than the noise generated in that stage.

The frequency response and slewing rate can be made independent of frequency by introducing a zero, $(1-i\omega\tau_o)$, into the open loop gain G to cancel each pole, $1/(1-i\omega\tau_p)$, in G other than the integrator pole, with $\tau_o = \tau_p$. However, poles near the beginning of the loop will reduce the signal level from the sensor at high frequency so that the sensor noise will no longer dominate the noise of later stages. Zeros added later in the loop to whiten the frequency response will cause high amplification of the noise at high frequencies. As the low frequency open loop gain, $|G(0)|$, or the compensating time constant, τ_o, are increased the high frequency noise will eventually saturate the SQUID. Thus if $|G(0)|$ is large the pole cannot be completely neutralized.

The slewing rate is limited in two ways. First, the maximum slewing rate at angular frequency ω is $\omega\phi_f^s$ where ϕ_f^s is the amplitude of feedback flux which saturates some stage of the loop. The maximum slewing rate will be obtained if the first stage to saturate is the stage which provides the feedback current. The two stages most likely to saturate are the last stage of audio frequency amplification and the SQUID itself, where $|\phi_f + \phi_a|$ can not exceed $\phi_o/4$. Second, the slewing rate at the modulation frequency obviously should be less than $2\pi f_m \phi_m$ where ϕ_m is the amplitude of the flux modulation so that the feedback loop does not cancel the modulation. If $R(\omega)$ and thus the slewing rate are essentially independent of frequency then this limits the slewing rate at all frequencies to approximately $\pi f_m \phi_o/2$ since $\phi_m \simeq \phi_o/4$. This limitation on the slewing rate can be circumvented at low frequencies by adding a pole, $1/(1-i\omega\tau_p)$, to the loop gain G. This solution greatly reduces the slewing rate and makes $R(\omega)$ a strong function of frequency at frequency $1/\tau_p$ and higher. One could also increase the second limit on the slewing rate by increasing f_m. This could not be done to any great extent for an rf SQUID operated with a typical rf excitation frequency of about 30 MHz because the audio modulation frequency has to be very small compared to the excitation frequency. In contrast our tunnel junction dc SQUIDs are operated at a dc bias of approximately 2 μV so the Josephson frequency is on the order of 1 GHz. Thus a modulation frequency of the order of 10 MHz could be used.

Unfortunately, the first limitation on the slewing rate is about the same as the second for our present design. This comes about because the preamplifiers require a source impedance of approximately 10^5 ohms for optimum noise performance. The dc SQUID magnetometer used in the 1975 and 1976 surveys employed resonant tank circuits with a Q of about 100 to match the low impedance of the SQUIDs ($\simeq 1\Omega$). These were later replaced by resonant transformers with $Q \simeq 10$. The time constant associated with this Q, equation (2.3) can be reasonably well neutralized to give a white frequency response up to about 30 kHz and a slewing rate of approximately 3×10^5 ϕ_o/second = 10^5 γ/second. This time constant τ_m can not easily be further decreased because it is essentially the capacitance of the transformer and the line connecting the matching circuit to the electronics input (300 pf) times the impedance (10^5 ohms), producing $\tau \simeq 3 \times 10^{-5}$ seconds. Since the frequency response can not be fully neutralized there is a phase shift between ϕ_a and ϕ_f so that the SQUID saturates to limit the slewing rate. A lumped 10^5 to 1 impedance matching circuit with less than 300 pf capacitance is hard to build.

Field Operation of SQUIDs

SQUIDs are also very sensitive detectors of rf energy so a SQUID magnetometer must be shielded for field use. Copper screening was found to be excellent for this. It was also generally beneficial to enclose the wires connecting the SQUIDs and the electronics in stainless steel capillary tubing and to enclose a separate dc ground wire.

Atmospheric electrical activity at high frequencies can produce flux changes more rapid than 10^5 γ/second. Thus it is usually necessary to attenuate the high frequency fluctuations with a metal can. We most frequently used a can external to the dewar with a 3db cutoff frequency of 55 Hz. Fields produced by Johnson noise currents are a consideration in the design of such cans. The amplitude of such fields is proportional to $\ell^{-3/2}$ where ℓ is a typical linear dimension of the can.

For the measurement of small magnetic fluctuations in the presence of the earth's magnetic field it is essential that the magnetometer be held very rigidly. Our magnetometer was held by a wooden tripod and protected from the wind by a plywood pyramid. On soft ground the force of the wind on the pyramid moved the ground itself to a noticeable degree and it was necessary to bury the magnetometer.

SECTION III. SIGNAL PROCESSING

There are several ways of calculating average powers. In this section I describe the method I have used and argue that the choice between methods is one of practical considerations only. The one fundamental point is that the goal of magnetotellurics is the estimation of the linear response function, $\underline{\underline{Z}}$, not the estimation of the power spectral densities. The response $\vec{E}_s$ is causally related to the input $\vec{H}_s$ and that relationship does not depend on the statistics of the signals.

The approximation of signals of infinite duration by finite segments must always introduce error. However, such errors as spectral aliasing and trucation errors would have no effect on the tensor estimates if the electric and magnetic signals were simply proportional. Then the errors would be in the same ratio as the signals and one would still obtain the correct estimate for $\underline{\underline{Z}}$. The estimates are affected only by the difference between the errors in the measurement of $\vec{E}$ and $\vec{H}$. Thus these errors are less important for magnetotellurics than they are for spectral estimation. Nonetheless one will certainly want to minimize the errors in signal processing.

There are three basic ways of computing average powers: 1) Fourier transformation of the data followed by multiplication by the conjugate Fourier components and averaging, 2) Fourier transformation of the time averaged autocorrelation and crosscorrelation functions and 3) narrow band filtering of the data followed by multiplication by the direct and quadrature (delayed by 90°) filter outputs and

time averaging. Theoretically any of these methods could be carried out with either digital or analog hardware to yield results of equivalent accuracy. The errors inherent in each method have corresponding errors in the others. The balance of truncation error against spectral resolution for method one corresponds to the competition between the number of data that can be averaged and the maximum time lag for method two and to the relationship between transient response and filter Q for method three. The errors due to both limitations can be decreased for each method as the length of the data segments is increased. The only criteria for the selection of a particular method are the practical limits and efficiency. For instance analog multipliers will always introduce noise proportional to the signals because of their nonlinearities whereas the precision of averaged digital products can be increased without limit by increasing the number of products in the average. The great efficiency of the fast Fourier transform (FFT) makes method one the most economical digital technique. Therefore I have used method one in all the data analysis.

Sims and Bostick, in the 1969 edition of their excellent series of technical reports on magnetotellurics,[29] give quantitative calculations and practical examples of the effects of truncation errors and digitizer resolution. They show that twelve bit digitizer accuracy is required and sufficient to obtain accurate power spectral estimates for the steep magnetotelluric power spectra. All our data were digitized with 12 bit resolution. Sims and Bostick also quantify the obvious result that truncation errors are likely to be large for

the fundamental of the FFT and decrease for higher order harmonics.

The severest test of the spectral resolution is at the lowest harmonics. This is because the resolution on a linear frequency scale is the same for all harmonics so that the fractional resolution (or the Q) of the harmonic is proportional to the order of the harmonic. The severest spectrum that must be dealt with in magnetotellurics is the magnetic spectrum near 0.1 Hz which may be as steep as $1/f^8$. The easiest and most certain way to obtain high spectral resolution is simply to use data segments for that spectral region that are very long compared to 10 seconds. I have used data segments at least 500 seconds long for these frequencies so that the 0.1 Hz harmonic has a Q of about 50. Such high spectral resolution is really not necessary however, because as discussed above, the error in the estimates of $\underline{\underline{Z}}$ produced by spectral overlap is small. Wight, Bostick and Smith[34] have reported that they have obtained the best results in their experience while using only the 6th and 8th Fourier harmonics of the fundamental in a real time analysis system.

Because of the large truncation errors and low spectral resolution of the lowest harmonics I have used only the fifth and higher harmonics to calculate average powers.

The mean and linear trend of each data segment were subtracted before any other digital processing. This procedure has both a physical and mathematical justification. Physically, while the signals can be filtered to remove spectral components outside the range of the harmonics of the FFT, the analog electronics almost

invariably introduce some dc offset and temperature drift. Offsets and drifts can then be clearly identified as noise and should be subtracted. Mathematically, one might consider analyzing the data into Legendre polynomials and subtracting the Legendre components up to any order to remove noise. The first two Legendre polynomials, the mean and the linear trend, are best fit over the length of the data segment by sinusoidal components of frequency lower than the fundamental and thus can reasonably be subtracted. The higher order polynomicals, however, primarily contain frequency components that are at higher frequency. The Legendre polynomials of order 2n+1 and 2n+2 are roughly equal to the cosine and sine components of the nth Fourier harmonic. If the measurements at some frequency within the range of the harmonics were suspected of being noise, it could best be eliminated by discarding the appropriate Fourier harmonics.

All the details of truncation error and spectral resolution depend on the choice of the time window. Any time window that tapers smoothly to zero at the ends has greatly reduced sideband sensitivity compared to a square time window. Otherwise the differences are not drastic. I used time windows tapered to zero with a cosine bell shape over various fractions from 1/12 to 1/8 of the data segment length.

Finally, average powers were calculated by multiplying by the conjugate Fourier coefficients and averaging the products from the Fourier harmonics contained in nonoverlapping frequency windows of $Q = 3$ and from all the data collected at different times. N will be

reserved throughout this dissertation to denote the number of products in the average.

I should note that prewhitening of the signals can greatly alleviate the problems of spectral resolution and truncation errors as well as the demands on the dynamic range of the equipment. Wight et al employed a digital prewhitening of the signals in their real time analysis system. While none of the data analyzed here were prewhitened we now pass the magnetic signals through a simple single pole high pass filter with a one second time constant.

SECTION IV. FAILURES

In the search for a good estimator of $\underline{\underline{Z}}$ a very large number of methods were generated and discarded. This section describes four classes of methods that were further unambiguous failures or ambiguous successes. They yield some information about the character of the signals and noises in magnetotellurics and there are some interesting mathematical points but the major value of this section may lie in preventing wasted effort with these methods in the future.

The first method is a solution for $\underline{\underline{Z}}$ in terms of the average crosspowers between the components of $\vec{E}$ and $\vec{H}$. The second uses higher moments of the crosspowers. Both methods have relatively high random errors. The third method involves the use of one reference channel and would always be effective if the noises were uncorrelated. The fourth attempts to exploit the quasisinusoidal nature of the signals by employing two stages of averaging. This was the most successful estimator for real magnetotelluric data using only local measurements. It was not an unambiguous success however for its random errors are larger than for the least squares estimators, it is too complex for thorough analysis and its success depends on matching an adjustable parameter to the statistics of the signals.

Data

These methods were tested both with simulated data on a PDP-11 minicomputer and with real data from the 1976 Grass Valley survey. Data were simulated for a known impedance tensor $\underline{\underline{Z}}$ by choosing complex random numbers with real and imaginary parts uniformly distributed

over the range -1 to 1 to represent the magnetic signals H_{sx} and H_{sy}. Electric field signals were calculated from $\vec{H}$ using equation (1.11). Then noise was introduced by adding a random complex number with an adjustable weighting factor to each vector component of the signals. The weighting factors were adjusted to give the desired signal to noise ratios. The products of the noisy fields were then calculated and average powers obtained by repeating the process N times. Then the tensor estimates were calculated. In order to determine the statistics of the estimates the whole calculation was repeated K times with independent sets of random numbers. The mean value, $\bar{Z}_{ij}$, and the sample variance, σ^2_{ij}, for each impedance element were computed from the expressions

$$\bar{Z}_{ij} = K^{-1} \sum_{\ell=1}^{K} Z_{ij}^{(\ell)} \quad , \tag{4.1}$$

and

$$\sigma^2_{ij} = \left\{ K^{-1} \sum_{\ell=1}^{K} |Z_{ij}^{(\ell)} - \bar{Z}_{ij}|^2 \right\} \quad . \tag{4.2}$$

The expected standard deviation in $|\bar{Z}_{ij}|$, ΔZ_{ij}, was taken as $\pm \sigma_{ij}/K^{1/2}$. Since the probability densities were fixed the simulated signals were stationary, unlike real magnetotelluric data.

The Grass Valley data were taken using the dc SQUID magnetometer and a commercial rf SQUID magnetometer. Figure 1 is a map of the sites. The electric fields were measured with telluric dipoles 500 m long in an L array, with the equipment truck at the vertex. The telluric signals were amplified with PAR 113 preamplifiers and all the

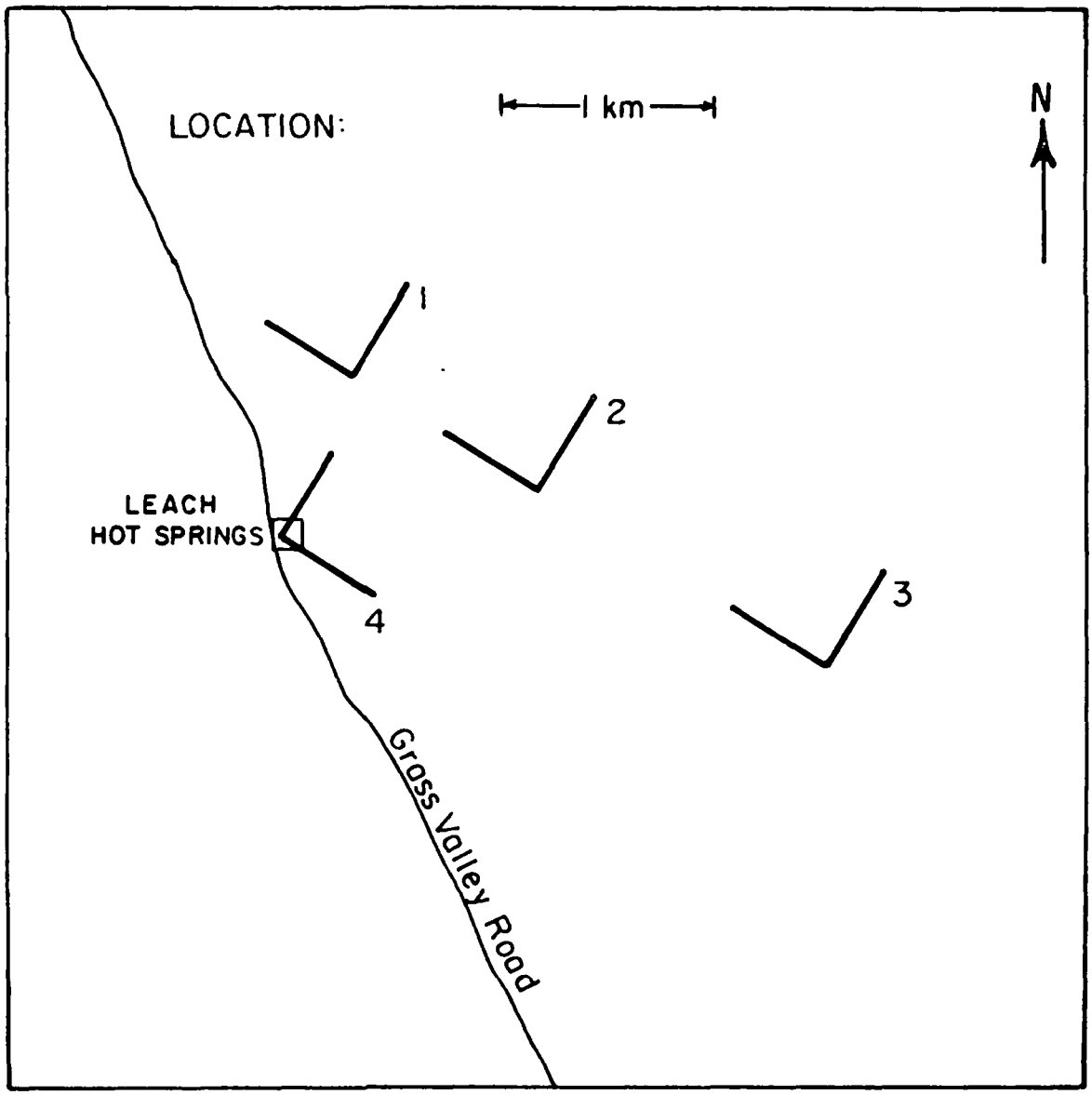

XBL 777-5808

Fig. 1. Location of the telluric arrays for the 1975 and 1976 survey sites whose results are graphed in figures 2 through 5.

data recorded on a Honeywell 5600 FM analog tape recorder. The data were later digitized with twelve bit resolution and analyzed using the signal processing techniques discussed in section III on the CDC 7600 computer system of the Lawrence Berkeley Laboratory. Further details of the equipment used in the survey, a description of the physical site, a review of other studies done in the area in connection with geothermal assessment and more complete results of the 1975 survey are described by Beyer et al.[4]

The rotated apparent resistivities from $\underline{\underline{Z}}^H$ for four of the stations are plotted vs period in figures 2 through 5 parts a and b for the 1975 and 1976 surveys, respectively. No results are plotted for some of the frequency windows because estimates with skewness (equation 1.17) greater than 0.6 were discarded as being grossly contaminated by noise.* A casual glance will reveal that this was at best an ambiguous success in measuring $\underline{\underline{Z}}$. The apparent resistivities differ between the two years by as much as three orders of magnitude. The rotated apparent resistivies at locations 2 and 4 calculated from the 1976 data using $\underline{\underline{Z}}^E$ (equation 1.25) are shown in figure 6 for comparison. On the other hand the results from high coherency data were in reasonable agreement between the two years. The magnitude of C is indicated in figures 2 through 5 by a good rating if $0.95 < C < 1$, fair if $0.89 < C < 0.95$ and poor if $C < 0.89$ for low frequencies (< 1Hz). For high frequencies (> 1 Hz) the ratings were

*Large values of skewness are physically impossible. We have not produced any skewness estimates greater than 0.6 from good data and so have chosen this as an arbitrary upper limit for reasonable estimates.

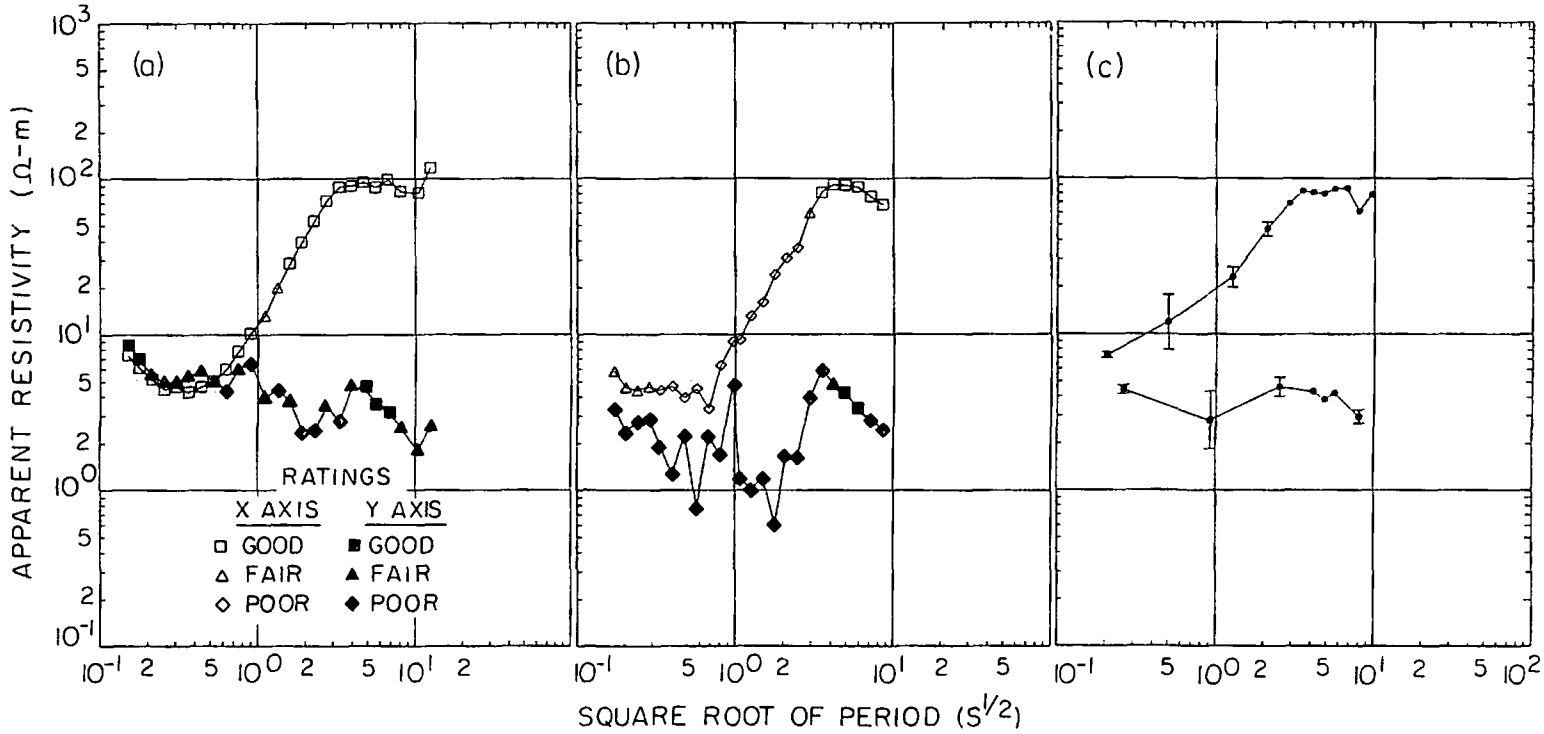

XBL775-5415

Fig. 2. Rotated apparent resistivities versus square root of period for location 1, a) 1975 data using $\underline{\underline{Z}}^H$, b) 1976 data using $\underline{\underline{Z}}^H$, c) 1976 data with double average analysis, method IV.

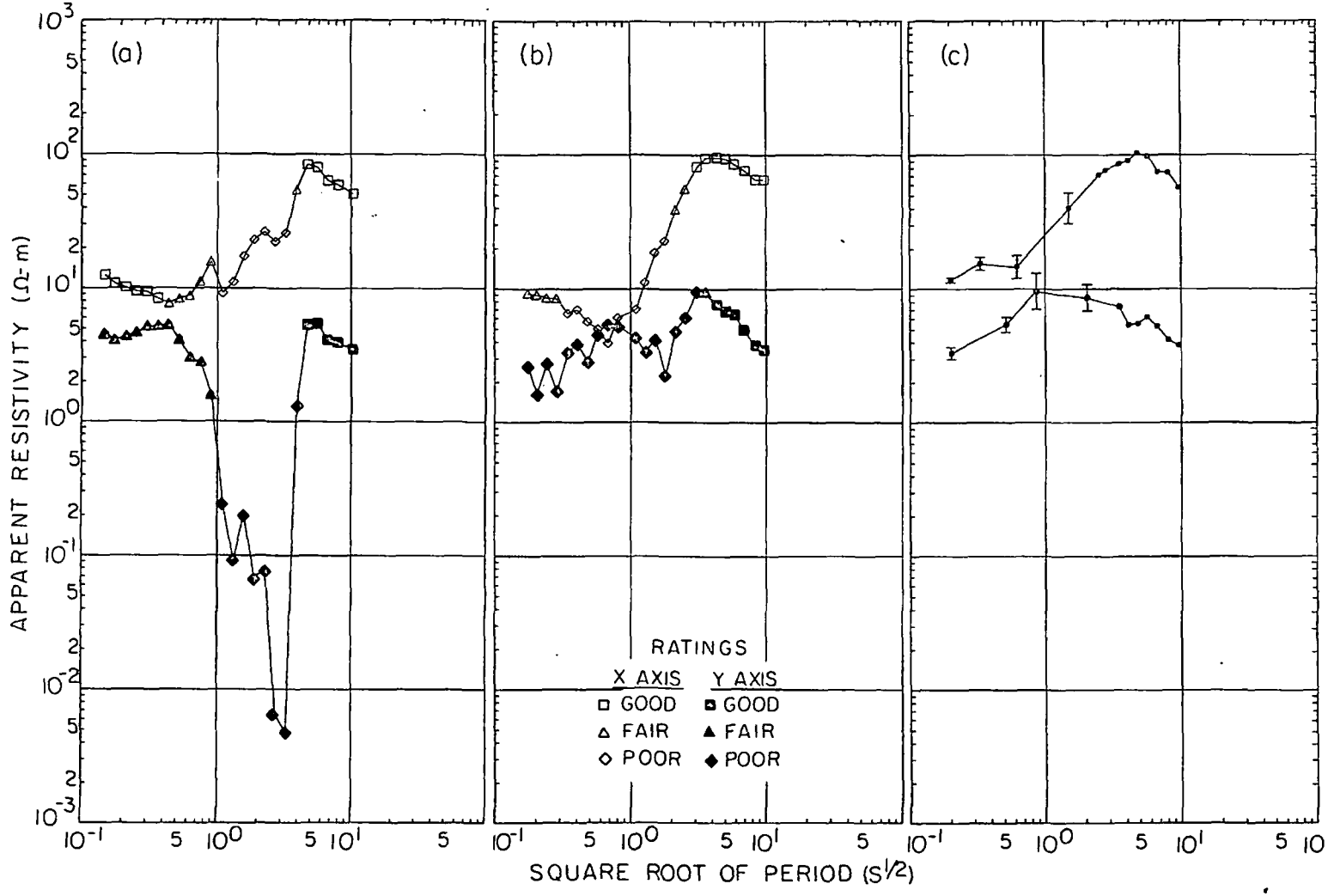

XBL 775-5416

Fig. 3. Rotated apparent resistivities versus square root of period for location 2. a) 1975 data using $\underline{\underline{Z}}^H$, b) 1976 data using $\underline{\underline{Z}}^H$, c) 1976 data with double average analysis, method IV.

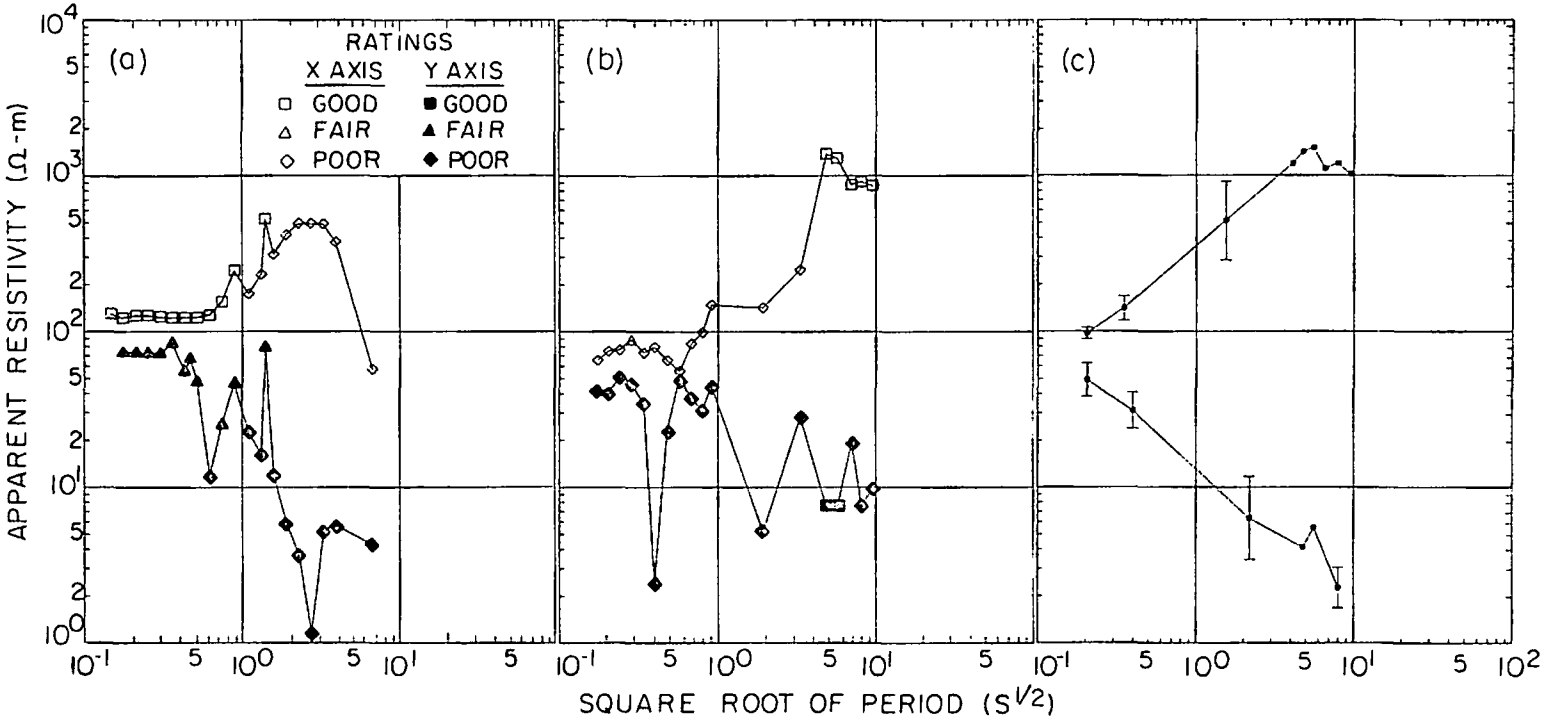

XBL 775-5418

Fig. 4. Rotated apparent resistivities versus square root of period for location 3. a) 1975 data using $\underline{\underline{Z}}^H$, b) 1976 data using $\underline{\underline{Z}}^H$, c) 1976 data with double average analysis, method IV.

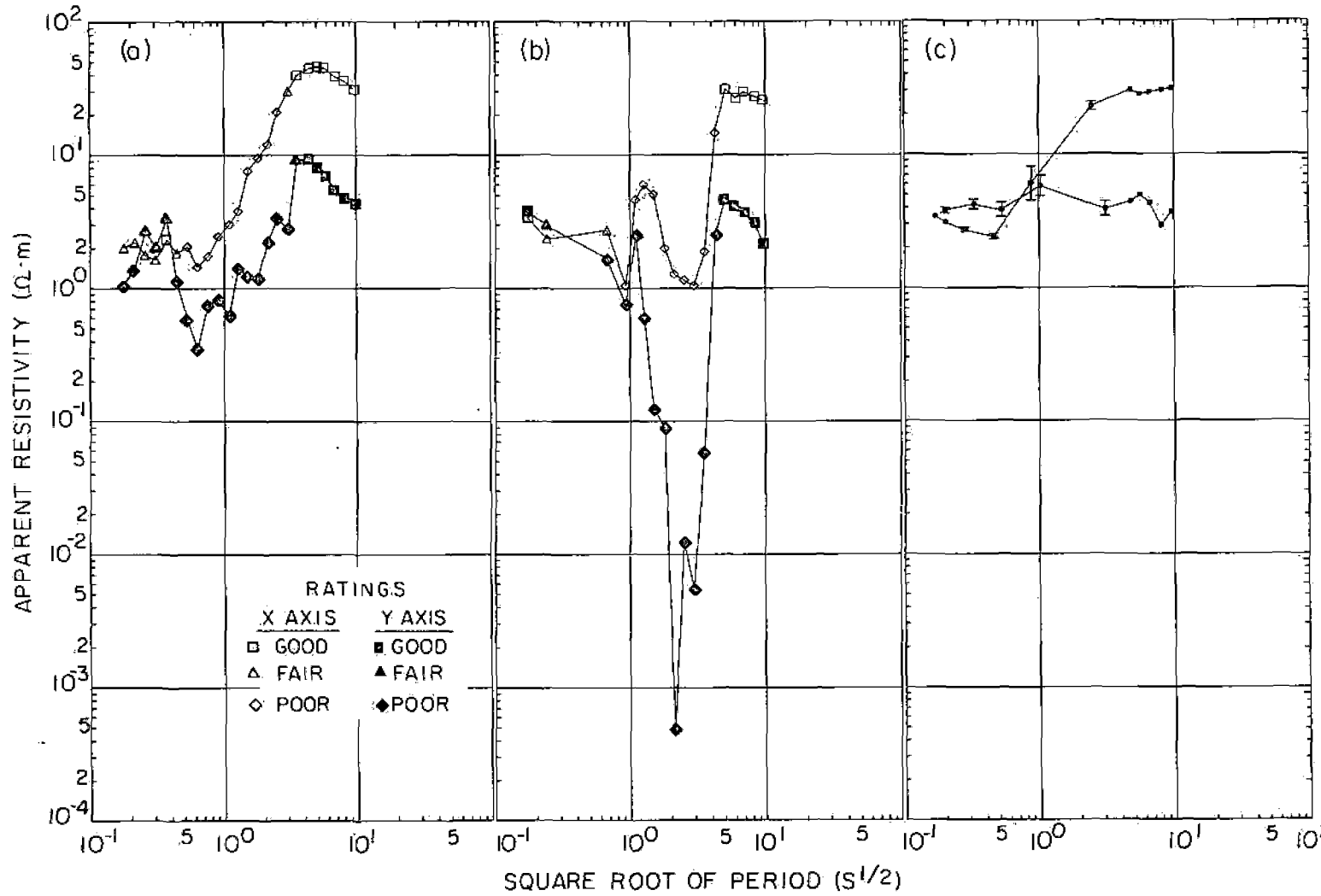

XBL775-5417

Fig. 5. Rotated apparent resistivities versus square root of period for location 4. a) 1975 data using $\underline{\underline{Z}}^H$, b) 1976 data using $\underline{\underline{Z}}^H$, c) 1976 data with double average analysis, method IV.

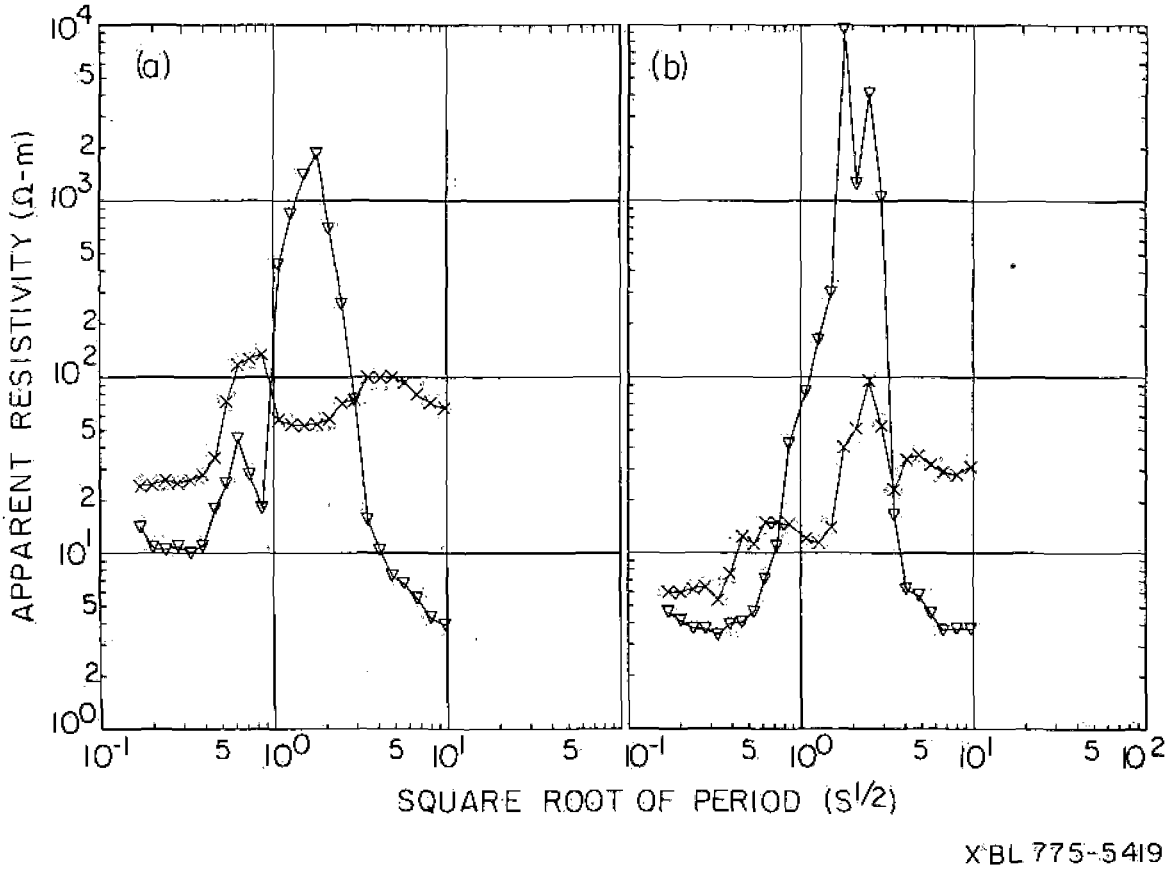

Fig. 6. Rotated apparent resistivities versus square root of period from the 1976 data using the least squares admittance tensor, equation (1.25), and $\underset{\approx}{Z}^E = \underset{\approx}{Y}^{-1}$. a) location 2, b) location 4.

good if $0.90 < C < 1$, fair if $0.72 < C < 0.90$ and poor if $C < 0.72$. These are purely subjective ranges chosen to display as much information as possible in a simple way. Note that more than half the time the apparent resistivies from "good" data agree between the two years to within 10%. Also "poor" data consistently gave apparent resistivities lower than those from "good" data when $\underline{\underline{Z}}^H$ was used and the apparent resistivies from $\underline{\underline{Z}}^E$ are invariably higher than those from $\underline{\underline{Z}}^H$. Thus the bias errors are large compared to the random errors and the results are consistent with the hypothesis that the sole important source of error was the autopower bias.

There are, of course, possible sources of bias other than the measured autopowers, such as systematic errors in the measurements. Also, the strict definition of the bias in an estimate is the difference between the ensemble average of that estimate and the ensemble average of the quantity to be estimated. Any random error in a nonlinear function of the measurements will produce some bias in the estimate. However, this bias error will always be smaller than the random error and thus will not be of any practical importance. I shall use "unbiased" to mean practially unbiased by the noises in the measurements.

Method I: Solution of 8 Equations

Multiplying the defining equations (1.19) and (1.20) through by E_x^*, E_y^*, H_x^* and H_y^* in turn, averaging and dropping the subscript s produces the eight equations:

$$\overline{|E_x|^2} = Z_{xx}\, b^* + Z_{xy}\, c^* \quad , \tag{4.3}$$

$$a = Z_{xx}\, d^* + Z_{xy}\, e^* \quad , \tag{4.4}$$

$$b = Z_{xx}\, \overline{|H_x|^2} + Z_{xy}\, f^* \quad , \tag{4.5}$$

$$c = Z_{xx}\, f + Z_{xy}\, \overline{|H_y|^2} \quad , \tag{4.6}$$

$$\overline{|E_y|^2} = Z_{yx}\, d^* + Z_{yy}\, e^* \quad , \tag{4.7}$$

$$d = Z_{yx}\, |H_x|^2 + Z_{yy}\, f^* \quad , \tag{4.8}$$

$$e = Z_{yx}\, f + Z_{yy}\, |H_y|^2 \quad , \tag{4.9}$$

and

$$a^* = Z_{yx}\, b^* + Z_{yy}\, c^* \quad . \tag{4.10}$$

Here a, b, c, d, e, and f are crosspowers defined by $a = \overline{E_x E_y^*}$, $b = \overline{E_x H_x^*}$, $c = \overline{E_x H_y^*}$, $d = \overline{E_y H_x^*}$, $e = \overline{E_y H_y^*}$, and $f = \overline{H_x H_y^*}$.

These equations contain all of the information available from the average powers. In principle one could substitute the measured average powers into these equations and then use any pair from equation (4.3) through (4.6) to calculate Z_{xx} and Z_{xy} and any pair from (4.7) through (4.10) for Z_{yx} and Z_{yy}. These 36 possible solutions contain all the least squares solutions. $\underline{\underline{Z}}^H$ is the simultaneous solution of (4.5), (4.6), (4.8) and (4.9). $\underline{\underline{Z}}^E$ is the simultaneous solution of the other four.

If the noises are uncorrelated with each other and the signals then the measured average crosspowers are unbiased estimates of the signal crosspowers. Since the measured autopowers are biased by the noise powers the signal autopowers in the eight equations must be considered as unknowns if one is to obtain an unbiased estimate for $\underline{\underline{Z}}$. Kao and Rankin[16] have attempted to get unbiased estimates for $\underline{\underline{Z}}$ by an iterative solution of these equations in terms of the crosspowers. However, there are eight equations with eight unknowns and they can in fact be solved directly.

It is easiest to solve first for $\overline{|H_x|^2}$ and $\overline{|H_y|^2}$, and to express all of the other unknown quantities in terms of these two autopowers. From equations (4.5) and (4.6).

$$Z_{xx} = \frac{b\,\overline{|H_y|^2} - cf^*}{\overline{|H_x|^2}\,\overline{|H_y|^2} - |f|^2} \quad , \tag{4.13}$$

and

$$Z_{xy} = \frac{c\,\overline{|H_x|^2} - bf}{\overline{|H_x|^2}\,\overline{|H_y|^2} - |f|^2} \quad . \tag{4.14}$$

Substituting equations (4.13) and (4.14) into equation (4.4) we find

$$|a|^2(\overline{|H_x|^2}\,\overline{|H_y|^2} - |f|^2) = (e^*ca^*)\overline{|H_x|^2} + d^*ba^*\overline{|H_y|^2} - a^*(d^*cf^* + e^*bf) \quad . \tag{4.15}$$

Similarly, by substituting into equation (4.10) solutions for Z_{yx} and Z_{yy} obtained from equations (4.8) and (4.9), one finds

$$|a|^2(\overline{H_x^2}\,\overline{H_y^2} - |f|^2) = ec^*a\,\overline{|H_x|^2} + db^*a\,\overline{|H_y|^2} - a(dc^*f + eb^*f^*) . \quad (4.16)$$

Subtracting equation (4.16) from equation (4.17) we obtain the relationship between $\overline{H_x^2}$ and $\overline{H_y^2}$:

$$\overline{|H_x|^2} = \frac{1}{\mathrm{Im}(e^*ca^*)} \left\{ - \mathrm{Im}(d^*ba^*)\,\overline{|H_y|^2} + \mathrm{Im}[a^*(d^*cf^* + e^*bf)] \right\} , \quad (4.17)$$

where Im(x) is the imaginary part of x. Substituting this result for $\overline{|H_x|^2}$ into equation (4.15) we find a quadratic equation for $\overline{|H_y|^2}$,

$$\left(\overline{|H_y|^2}\right)^2 - \overline{2u|H_y|^2} - w = 0 \quad (4.18)$$

where $u = \mathrm{Im}[d^*c^*eb + a^*(d^*cf^* + e^*bf)]/2\mathrm{Im}(d^*ba^*)$,

and $w = - \{\mathrm{Im}[ec^*(d^*cf^* + e^*bf)] + |f|^2\mathrm{Im}(e^*ca^*)\}/\mathrm{Im}(d^*ba^*)$.

The solution to equation (4.18) is

$$\overline{|H_y|^2} = u[1 \pm (1 + w/u^2)^{1/2}] . \quad (4.19)$$

The calculated autopower $\overline{|H_y|^2}$ will be real only if $1 + w/u^2 \geq 0$. Data leading to complex values of $\overline{|H_y|^2}$ should be rejected since complex autopowers are not physically possible. $\overline{|H_x|^2}$ is obtained by substituting equation (4.19) into equation (4.17). In terms of $\overline{|H_x|^2}$ and $\overline{|H_y|^2}$, the impedance elements and electric field autopowers are given by

$$Z_{xx} = (b\ \overline{|H_y|^2} - cf^*)/D \ , \tag{4.20}$$

$$Z_{xy} = (c\ \overline{|H_x|^2} - bf)/D \ , \tag{4.21}$$

$$Z_{yx} = (d\ \overline{|H_y|^2} - ef^*)/D \ , \tag{4.22}$$

$$Z_{yy} = (e\ \overline{|H_x|^2} - fd)/D \ , \tag{4.23}$$

$$\overline{|E_x|^2} = [|c|^2\ \overline{|H_x|^2} + |b|^2\ \overline{|H_y|^2} - 2\mathrm{Re}(c^* bf)]/D \ , \tag{4.24}$$

and

$$\overline{|E_y|^2} = [|e|^2\ \overline{|H_x|^2} + |d|^2\ \overline{|H_y|^2} - 2\mathrm{Re}(e^* fd)]/D \ , \tag{4.25}$$

where $D = \overline{|H_x|^2}\ \overline{|H_y|^2} - |f|^2$, and $\mathrm{Re}(x)$ is the real part of x.

In equation (4.19) there are two possible solutions for $\overline{|H_y|^2}$ corresponding to the positive and negative values of the square root. The remaining problem is to determine which of the two solutions is correct. It is evident from equation (4.17) that $\overline{|H_x|^2}$ is real when $\overline{|H_y|^2}$ is real and, therefore, that the electric field autopowers obtained from equations (4.24) and (4.25) are also real when $\overline{|H_y|^2}$ is real. Consequently, no information regarding the selection of the correct root in equation (4.19) is obtained from the imaginary parts of equations (4.3) and (4.7), since they are identically zero. All of the information in equations (4.3) to (4.10) has been utilized.

In the absence of noise it is obvious that one can determine the correct value for $\overline{|H_y|^2}$ by comparing the calculated and measured autopowers. In the presence of noise, the situation is, in general, rather

complicated. If there is noise on one channel only (for example, H_x), the autopowers for the remaining (noise-free) channels (for example, E_x, E_y, H_y) calculated using the correct solution of equation (4.19) agree *exactly* with the measured autopowers. If there is noise on more than one channel, all of the calculated autopowers are influenced by noise, and none agrees exactly with the measured value. In this general case the computer simulation has shown that the following procedure produces unbiased estimates of the impedance elements and the autopowers.

(i) Compute all autopowers using both signs in equation (4.19). If one sign leads to autopowers that are all positive, and the other leads to one or more negative autopowers, assume that the former sign is correct. If each sign leads to one or more negative autopowers, the data should be rejected.

(ii) If both signs lead to positive autopowers, compute the absolute values of the logarithms of $\overline{|E_x|^2_c}/\overline{|E_x|^2_m}$, $\overline{|E_y|^2_c}/\overline{|E_y|^2_m}$, $\overline{|H_x|^2_c}/\overline{|H_x|^2_m}$, and $\overline{|H_y|^2_c}/\overline{|H_y|^2_m}$ for each sign, where the subscripts c and m denote calculated and measured quantities. The sign in equation (4.19) that produces the <u>smallest</u> absolute value of any of the logarithms is assumed to be correct. This procedure ensures that we obtain the correct root in the case where there is significant noise in only one channel.

(iii) If the value of the calculated autopower is significantly higher than the measured autopower, there is a significant

error due to random noise. Data that meet criterion (ii) can be further screened by rejecting those for which the ratios of calculated to measured autopowers are significantly greater than a cut-off value S ($\geqslant 1$). The value of S can be selected at will, but must be the same for all channels to avoid biasing the impedance tensor. As the cut-off value is made closer to unity, the computed impedance tensor becomes more accurate, but fewer sets of data pass the criterion.

The ability to express the impedance and autopowers entirely in terms of crosspowers is due to the correlation between E_x and E_y. In equation (4.4), E_y acts as a reference signal (in the sense of lock-in detection) for E_x, while in equation (4.10) E_x acts as a reference signal for E_y. If Z_{xx} or $Z_{yy} = 0$ the solution to equations (4.3) through (4.10) becomes indeterminate. Thus, an unbiased estimate of the impedance tensor cannot be obtained when Z_{xx} or Z_{yy} is zero, for example, when the geology is 1-dimensional ($Z_{xx} = Z_{yy} = 0$, $Z_{xy} = -Z_{yx}$), or when the geology is 2-dimensional ($Z_{xx} + Z_{yy} = 0$) with one electrode in the strike direction ($Z_{xx} = Z_{yy} = 0$). To avoid the instability for a 2-dimensional geology, one should first roughly locate the strike direction, and make sure that neither electric field measurement is parallel to the strike. Ideally, one would choose the orientation so that $|Z_{xy}| \approx |Z_{yx}|$.

An example of the results of the computer simulation for the impedance tensor $Z_{xx} = -Z_{yy} = 2(1-i)$ and $Z_{xy} = -Z_{yx} = 3(1-i)$ is given in table I. The noise-to-signal power ratios were 1.5 for the electric

Table I. Calculation of impedance tensor elements from computer-simulated data and the crosspower solution of equations (4.3) through (4.10). The noise-to-signal power ratios were 1.5 and 1.0 for the electric and magnetic channels respectively and S = 1.5.

Element	True value	Calculated value, $\bar{Z}_{ij}$	σ_{ij}	$\Delta\bar{Z}_{ij}$
Z_{xx}	2(1 - i)	2.15 - 2.04 i	± 1.19	± 0.12
Z_{xy}	3(1 - i)	3.08 - 3.14 i	± 1.83	± 0.18
Z_{yx}	-3(1 - i)	-3.03 + 3.11 i	± 1.67	± 0.17
Z_{yy}	-2(1 - i)	-1.99 + 2.01 i	± 1.21	± 0.12

channels, and 1.0 for the magnetic channels. The impedance tensor was estimated from equations (4.20) to (4.23) using the criteria (i) to (iii) with S=1.5 to determine $\overline{|H_y|^2}$. N was 256. The calculation was repeated 256 times, each time using new data for the electric and magnetic fields. Of the 256 repetitions of the calculation, the selection criteria were satisfied 110 times, so that K = 110. The discrepancy between the true and calculated values of the impedance tensor is generally within one standard deviation. Hence there is no significant bias.

For the real data from Grass Valley this method was an unambiguous failure. Very often the crosspowers were not consistent with any real value for the autopowers. More than half the time the solution for neither sign passed the selection criteria. The apparent resistivities from those data that did pass were so scattered that no additional information about the structure of the ground could be obtained. Examples of the results from this method will be given in section VI for the data used to test the remote reference method. Those data usually passed the selection criteria but the results were still usually too scattered to be useful.

Although this failure could be explained by assuming that Z_{xx} and Z_{yy} happened to be too small with the electrode orientation used in Grass Valley, the other methods in this section will demonstrate that there were definitely significant correlations in the noises for these data. This method is particularly sensitive to correlation between the noises in the two vector components of $\vec{E}$ because the calculated autopowers (equation 4.19) depend strongly on the value of $a = \overline{E_x E_y^*}$

and E_{sx} and E_{sy} often are not strongly correlated.

Method II: Weighted Averages of Crosspowers

In the previous method an unbiased estimate of $\underline{\underline{Z}}$ was obtained by multiplying equations (1.19) and (1.20) in turn by a single field component, and solving the resulting eight equations for the impedance elements in terms of the average crosspowers. Each estimate made use of all the information contained in the crosspowers, and hence was the only possible unbiased estimate. One could also multiply equations (1.19) and (1.20) by more complicated functions of the various fields to obtain estimates of the impedance elements in terms of weighted averages of crosspowers. This technique yields an infinite number of estimates which do not contain measured autopowers.

Consider again equation (1.19). Let λ and λ' be two distinct, but as yet unspecified functions. For the ith values of E_x, H_x, and H_y, λ and λ' take the values λ_i and λ_i'. If one multiplies equation (1.19) in turn by λ and λ', and averages over all N data points, one obtains

$$\overline{\lambda E_x} = Z_{xx}\,\overline{\lambda H_x} + Z_{xy}\,\overline{\lambda H_y}\ , \tag{4.26}$$

and

$$\overline{\lambda' E_x} = Z_{xx}\,\overline{\lambda' H_x} + Z_{xy}\,\overline{\lambda' H_y}\ , \tag{4.27}$$

where $\overline{\lambda E_x} = (1/N) \sum_{i=1}^{N} \lambda_i E_x^{(i)}$, etc. These equations are linearly independent provided that the determinant $\overline{\lambda H_x}\,\overline{\lambda' H_y} - \overline{\lambda' H_x}\,\overline{\lambda H_y} \neq 0$, in which case they can be solved for Z_{xx} and Z_{xy}:

$$Z_{xx} = \frac{\overline{\lambda E_x}\ \overline{\lambda' H_y} - \overline{\lambda H_y}\ \overline{\lambda' E_x}}{\overline{\lambda H_x}\ \overline{\lambda' H_y} - \overline{\lambda' H_x}\ \overline{\lambda H_y}} \tag{4.28}$$

and

$$Z_{xy} = \frac{\overline{\lambda H_x}\ \overline{\lambda' E_x} - \overline{\lambda' H_x}\ \overline{\lambda E_x}}{\overline{\lambda H_x}\ \overline{\lambda' H_y} - \overline{\lambda' H_x}\ \overline{\lambda H_y}} \tag{4.29}$$

In a similar way, provided that $\overline{\xi H_x}\ \overline{\xi' H_y} - \overline{\xi' H_x}\ \overline{\xi H_y} \neq 0$, one obtains expressions for Z_{yx} and Z_{yy} from equation (1.20),

$$Z_{yx} = \frac{\overline{\xi E_y}\ \overline{\xi' H_y} - \overline{\xi H_y}\ \overline{\xi' E_y}}{\overline{\xi H_x}\ \overline{\xi' H_y} - \overline{\xi' H_x}\ \overline{\xi H_y}}\ , \tag{4.30}$$

and

$$Z_{yy} = \frac{\overline{\xi H_x}\ \overline{\xi' E_y} - \overline{\xi' H_x}\ \overline{\xi E_y}}{\overline{\xi H_x}\ \overline{\xi' H_y} - \overline{\xi' H_x}\ \overline{\xi H_y}}\ , \tag{4.31}$$

where ξ and ξ' are again unspecified functions, and $\overline{\xi E_y} = (1/N) \sum_{i=1}^{N} \xi_i E_y^{(i)}$, etc.

In the absence of noise there are no constraints on λ, λ', ξ, and ξ'. These functions could depend on the electric and magnetic fields, but equally well could be sequences of random numbers. In the presence of noise certain restrictions must be imposed to obtain stable, unbiased estimates of the impedance elements from equations (4.28) through (4.31). The estimates are stable provided that the denominators do not tend to zero as $N \to \infty$. This requirement implies that λ, λ', ξ, and ξ' must be functions of the electric and/or magnetic fields since otherwise all the averages (for example, $\overline{\lambda E_x}$) tend to zero as $N \to \infty$.

The estimates will be unbiased if all the weighted averages approach the noise-free weighted averages in the limit $N \to \infty$. If the impedance elements are to be both stable and unbiased it is straightforward to show that λ and λ' must be of the form

$$\lambda = \rho E_y^* \quad , \tag{4.32}$$

and

$$\lambda' = \eta E_y^* \quad , \tag{4.33}$$

where ρ and η are either unity or any combination of $E_x E_y^*$, $H_x E_y^*$, $H_y E_y^*$ and $E_y E_y^*$. Thus, the weighted averages $\overline{\lambda E_x}$, $\overline{\lambda' E_x}$, etc. become $\overline{\rho E_x E_y^*}$, $\overline{\eta E_x E_y^*}$, etc., where ρ and η represent weighting functions for the crosspowers $E_x E_y^*$, $H_x E_y^*$, and $H_y E_y^*$. The weighting function $E_y E_y^*$ contains the noise power in E_y, but it can be shown that this does not introduce bias into equations (4.26) and (4.27) provided that the noise in E_y is uncorrelated with that in E_x, H_x, and H_y.

By similar arguments, one can show that ξ and ξ' must be of the form

$$\xi = \mu E_x^* \quad , \tag{4.34}$$

and

$$\xi' = \nu E_x^* \quad , \tag{4.35}$$

where μ and ν are unity or any combination of $E_y E_x^*$, $H_x E_x^*$, $H_y E_x^*$, and $E_x E_x^*$. The quantities μ and ν are weighting functions for the cross-powers $E_y E_x^*$, $H_x E_x^*$, and $H_y E_x^*$.

This method of weighted averages was tested using computer-simulated data with the three different sets of weighting functions

Table II. Examples of three sets of weighting functions for weighted average method.

Trial	λ	λ'	ξ	ξ'
(a)	E_y^*	$E_y^* E_y^* H_x$	E_x^*	$E_x^* E_x^* H_x$
(b)	E_y^*	$E_y^* E_y^* H_y$	E_x^*	$E_x^* E_x^* H_y$
(c)	$E_y^* E_y^* H_x$	$E_y^* E_y^* H_y$	$E_x^* E_x^* H_x$	$E_x^* E_x^* H_y$

shown in table II for the same impedance tensor, noise-to-signal power ratios and N as in the test of method I. The results obtained for the functions (a) are shown in table III, and should be compared with those obtained using method I in table I. The weighted average technique yields unbiased impedance elements, but the sample variances are three or four times greater than those obtained with method I. Similar results were obtained using weighting functions (b) and (c) of table II.

The apparent resistivities calculated via this method from the Grass Valley data were hopelessly scattered and also appeared to have some upward bias. Occasionally values greater than 10^6 Ω-m were obtained.

In the spirit of warning future investigators away from certain failure I should mention that various weighted averages containing autopowers that would bias the estimate of $\underline{\underline{Z}}$ were tried. It was hoped that the higher moment calculations would reduce the autopower bias by weighting periods of high signal levels more heavily. They did not.

Method III - One Reference Channel

In order to obtain an estimate that is stable for any tensor and does not have the large random error of method II it is necessary to include more information in the calculation. This section considers the possible uses of one simultaneously recorded reference channel. During the 1976 survey a third diagonal telluric dipole as shown in figure 7 was used to measure such a signal, E_r. This gave us a second independent measurement of each of the electric field components:

Table III. Calculation of impedance tensor elements from computer simulated data using weighted averages, and the weighting functions (a) from table II. The noise-to-signal power ratios were 1.5 and 1.0 for the electric and magnetic fields respectively. 100 independent calculations were used to obtain the average values and standard deviations.

Element	True value	Calculated value, $\bar{Z}_{ij}$	σ_{ij}	$\Delta\bar{Z}_{ij}$
Z_{xx}	2(1 - i)	2.10 - 2.43 i	± 4.2	± 0.42
Z_{xy}	3(1 - i)	3.18 - 2.37 i	± 6.4	± 0.64
Z_{yx}	-3(1 - i)	-3.47 - 1.92 i	± 8.3	± 0.83
Z_{yy}	-2(1 - i)	-1.74 - 2.65 i	± 6.0	± 0.60

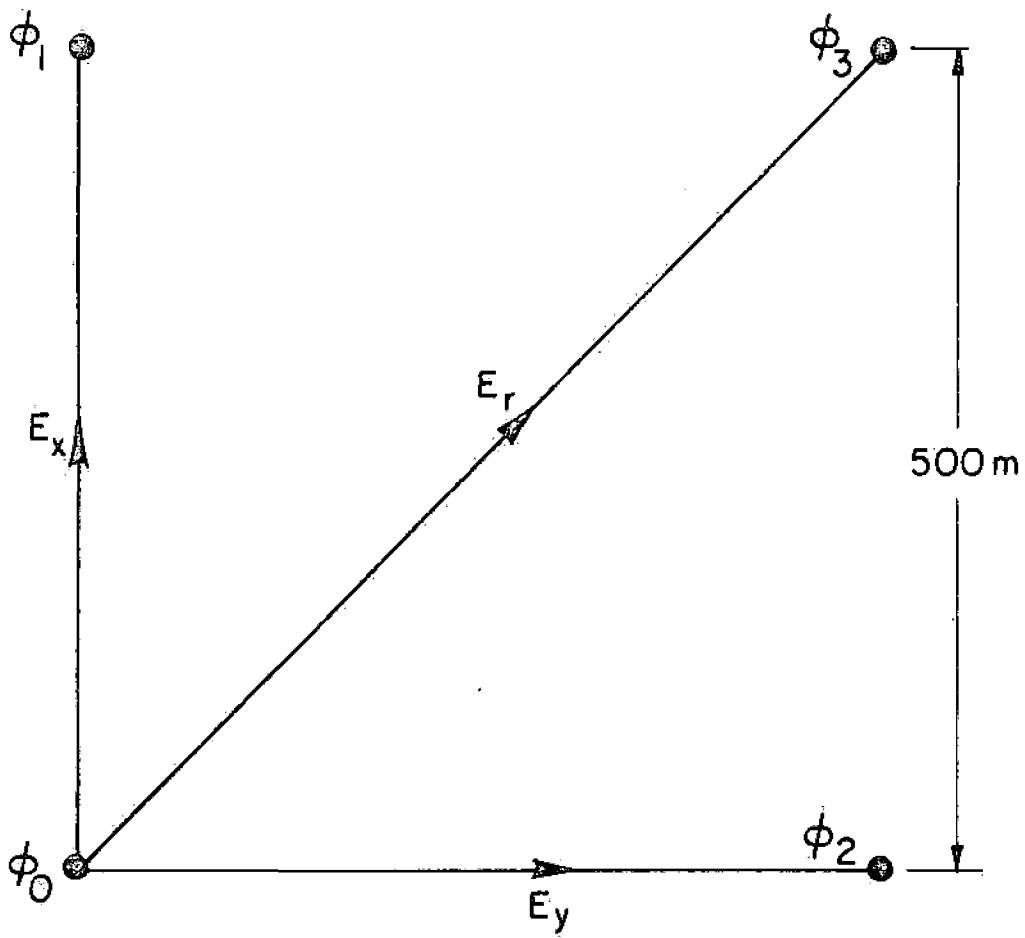

Fig. 7. Electrode configuration used in the 1976 survey to obtain an extra measurement of the telluric voltages, E_r, for use as a reference.

$$E'_x = \sqrt{2}\ E_r - E_y \tag{4.36}$$

and

$$E'_y = \sqrt{2}\ E_r - E_x \tag{4.37}$$

Sims and Bostick[29] have suggested that with such independent measurements one could replace the autopowers $\overline{|E_x|^2}$ and $\overline{|E_y|^2}$ in $\underline{\underline{Z}}^E$ with the crosspowers $\overline{E'_x E^*_x}$ and $\overline{E'_y E^*_y}$ to obtain an unbiased estimator. There is one disadvantage with this technique. Errors in the placement of the diagonal electrode and inhomogenieties in the ground will cause fractions of E_x and E_y to appear as noise in E'_y and E'_x respectively. Since the magnitudes of E_x and E_y often differ by more than an order of magnitude the noise in the channel with the smaller signal can be substantial. There are a number of alternatives that circumvent this difficulty.

Any two of the four field components of $\vec{E}$ and $\vec{H}$, A and B, can be related to the other two, P and Q, by a transconductance matrix G defined by

$$A = G_{11}P + G_{12}Q \tag{4.38}$$

and

$$B = G_{21}P + G_{22}Q\ . \tag{4.39}$$

If R is the field from a fifth channel one can obtain an unbiased estimate of $\underline{\underline{G}}$ by multiplying equation (4.38) by B^* and R^* in turn, and equation (4.39) by A^* and R^*, and averaging each of the equations over all data to find

$$\overline{AB^*} = G_{11}\,\overline{PB^*} + G_{12}\,\overline{QB^*} \quad ,$$

$$\overline{AR^*} = G_{11}\,\overline{PR^*} + G_{12}\,\overline{QR^*} \quad , \qquad (4.40$$

$$\overline{BA^*} = G_{21}\,\overline{PA^*} + G_{22}\,\overline{QA^*} \quad ,$$

and

$$\overline{BR^*} = G_{21}\,\overline{PR^*} + G_{22}\,\overline{QR^*} \quad .$$

Once $\underline{\underline{G}}$ is known, $\underline{\underline{Z}}$ can be computed. For five data channels one can show that there are six independent pairs of equations (4.38) and (4.39) leading to six independent estimates for $\underline{\underline{Z}}$ that contain no autopowers. If $A = E_x$, $B = E_y$, $P = H_x$, $Q = H_y$, and $R = E_r$, one has $\underline{\underline{G}} = \underline{\underline{Z}}$, whereas if $A = H_x$, $B = H_y$, $P = E_x$, $Q = E_y$, and $R = E_r$, one has $\underline{\underline{G}} = \underline{\underline{Y}}$.

The rotated apparent resistivities calculated via these straightforward crosspower methods from the Grass Valley data of location 2 are plotted in figure 8. Part a used the suggestion of Sims and Bostick, part b used the transconductance $\underline{\underline{G}} = \underline{\underline{Z}}$ and part c used $\underline{\underline{G}} = \underline{\underline{Y}}$ and $\underline{\underline{Z}} = \underline{\underline{G}}^{-1}$. All should be compared with the least squares estimate $\underline{\underline{Z}}^E$ from the same data in figure 6(a). They all show the physically unreasonable large values and sharp peak in apparent resistivity and are essentially identical, even though they were derived from expressions containing different crosspowers. For example part b depends on $\overline{E_x E_y^*}$ but not $\overline{H_x H_y^*}$ and vice versa for part c. Since none of these estimates contains autopowers some of the noises must be correlated. The results from $\underline{\underline{Z}}^H$, figure 3(b) do not show any such extremes of bias. Consequently, it is unlikely that there is any significant noise correlation in the crosspowers in $\underline{\underline{Z}}^H$, that is, $\overline{H_x H_y^*}$, $\overline{E_x H_x^*}$, $\overline{E_x H_y^*}$, $\overline{E_y H_x^*}$, and $\overline{E_y H_y^*}$. Therefor the bias introduced into the 5-channel cross power analysis must

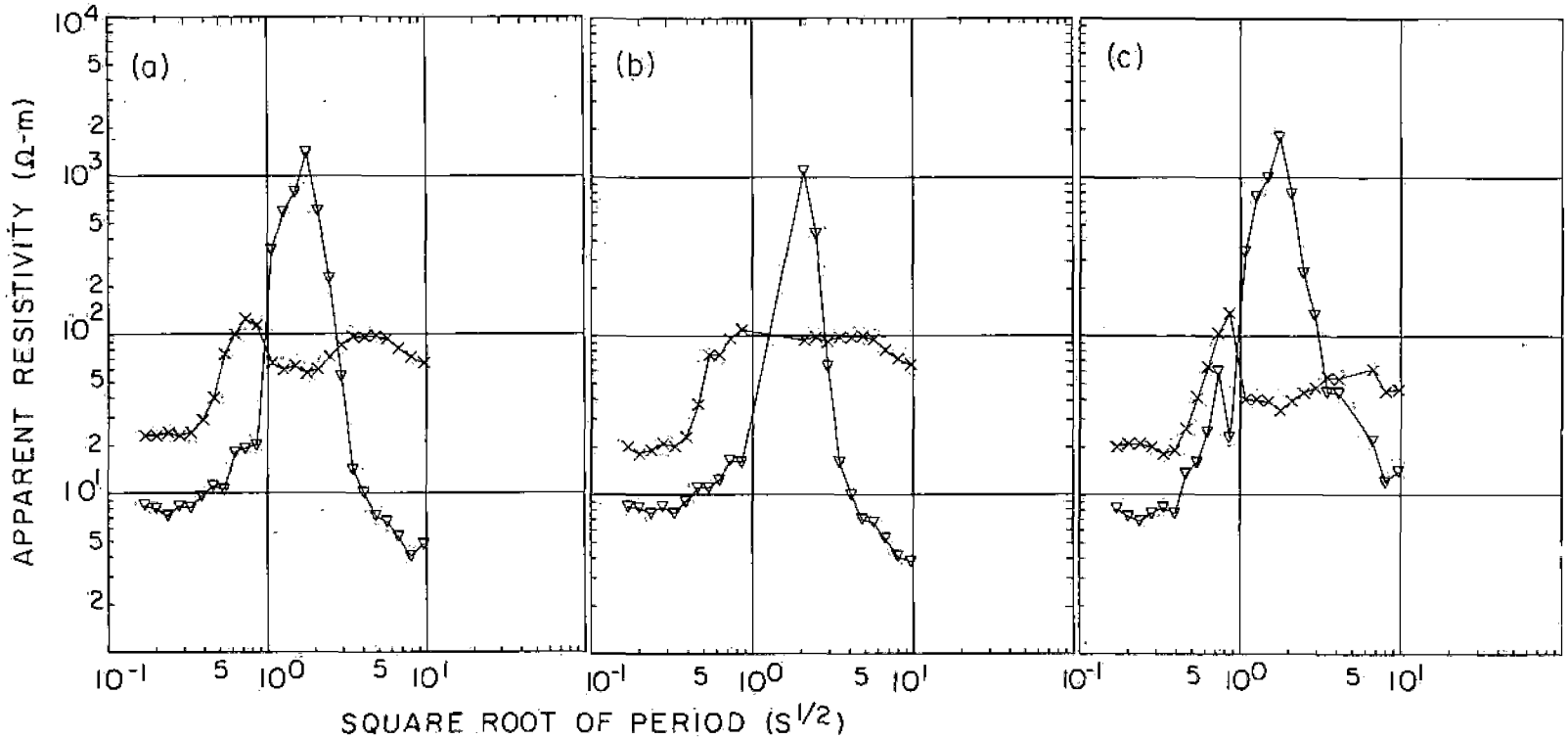

Fig. 8. Rotated apparent resistivities versus square root of period from the one reference channel analysis, method III, of the 1976 data from location 2. a) substitution of $\overline{E_i' E_i^*}$ for the electric field autopowers in $\underset{\approx}{Z}^E$, b) equations (4.40) with $\underset{\approx}{G} = \underset{\approx}{Z}$, c) equations (4.40) with $\underset{\approx}{G} = \underset{\approx}{Y}$ and $\underset{\approx}{Z} = \underset{\approx}{G}^{-1}$. XBL 775-5420

-57-

arise from crosspowers of the electric fields, that is, the noises in the electric channels are correlated.

The agreement between the apparent resistivities from $\underline{\underline{Z}}^E$ and those obtained by replacing the autopowers in $\underline{\underline{Z}}^E$ by $\overline{E_i' E_i^*}$ indicates that $E_i' \simeq E_i$, that is, the potential differences $\phi_1 - \phi_o$ and $\phi_3 - \phi_2$ are approximately the same. This result implies that there were no major noise sources in our measurement equipment, such as electrode noise (in particular, common electrode noise), amplifier noise, or tape recorder noise, as their contributions would be different for $\phi_1 - \phi_0$, which was recorded on one channel (E_x), than $\phi_3 - \phi_2$, which was recorded as the difference of two other channels (E_y and E_r). Thus, it appears that the dominant noise in the electric field measurement is due to real potential differences correlated over distances of a least the maximum electrode separation, 700 m.

There are several possible sources of electric field fluctuations that would be correlated over such distances. Corwin[9] has found self-potentials as large as 50 mV at Grass Valley. He indicates that these are most likely streaming potentials, generated by the flow of spring water through the ground. The large changes in water pressure that are often associated with hot springs could cause the streaming potential to fluctuate. Corwin has also suggested that thermoelectric voltages generated by the temperature gradients of a geothermal area may be a source of significant self-potential. If these gradients fluctuate the voltage would also fluctuate. However, we would expect these fluctuations to be primarily at frequencies well below 0.3 Hz, the frequency at which the large peaks occur in figures 6 and 8. Even if the source of self-potential remains constant, fluctuations in the surface self-potential can be

generated by the variations in the resistivity of the ground caused by seismic waves, surface temperature changes, water table changes, or underground pressure changes. Finally any local electromagnetic source, natural or artificial, would of course give rise to correlated electric field variations.

Method IV - Double Averaging

None of the other methods of analysis in this thesis makes any assumptions about the statistical nature of the signals. The ionospheric signals are often quasisinusoidal fluctuations of only very slowly varying polarization and frequency. It was hoped this property of the signals could be used to distinguish the signals from the noise. In fact this approach was the most successful one tried for the data collected in Grass Valley. However, because the success of the method depends on the statistics of the signals its accuracy can not be predicted. Further, no method that depends only on local measurements can be totally immune to noise correlations.

This method begins with the calculation of the average crosspowers of the components of $\vec{E}$ and $\vec{H}$ with a reference channel R_x. For example

$$\overline{E_x R_x^*}^n = Z_{xx} \overline{H_x R_x^*}^n + Z_{xy} \overline{H_y R_x^*}^n \quad . \tag{4.41}$$

This average is not carried out over all N crossproducts but only over a small subset n at adjacent Fourier harmonics of the same data segment. The superscript n denotes the average over such a subset. Thus we have a large number, m, of values for each average crosspower where m could be as large as the number of ways of choosing a subset n from N objects,

$N!/(N-\hat{n})!n!$. If $\hat{n}$ is large enough that the noise crosspowers in equation (4.44) average to zero then the equation is accurately satisfied by the true value of $\underline{Z}$ for each of the m subsets. If in addition the polarizations of the signals are different for some of these subsets then we have linearly independent solutions of equation (4.44) and we can solve for Z_{xx} and Z_{xy}. One can include all m subsets by picking Z_{xx} and Z_{xy} to minimize the squared error in the prediction of $\overline{E_x R_x^{*n}}$ from $\overline{H_x R_x^{*n}}$ and $\overline{H_y R_x^{*n}}$. That is

$$Z_{xx} = \frac{\overline{\overline{E_x R_x^{*n}}\ \overline{H^* R_x^{n}}}^{m}\ \overline{\overline{H_y R_x^{*n}}\ \overline{H^* R_x^{n}}}^{m} - \overline{\overline{E_x R_x^{*n}}\ \overline{H^* R_x^{n}}}^{m}\ \overline{\overline{H_y R_x^{*n}}\ \overline{H^* R_x^{n}}}^{m}}{\overline{\left|\overline{H_y R_x^{*n}}\right|^2}^{m}\ \overline{\left|\overline{H_x R_x^{*n}}\right|^2}^{m} - \overline{\left|\overline{H_x R_x^{*n}}\ \overline{H^* R_x^{n}}\right|^2}^{m}}$$

and (4.42)

$$Z_{xy} = \frac{\overline{\overline{E_x R_x^{*n}}\ \overline{H^* R_x^{n}}}^{m}\ \overline{\overline{H_x R_x^{*n}}\ \overline{H^* R_x^{n}}}^{m} - \overline{\overline{E_x R_x^{*n}}\ \overline{H^* R_x^{n}}}^{m}\ \overline{\overline{H_x R_x^{*n}}\ \overline{H^* R_x^{n}}}^{m}}{\overline{\left|\overline{H_y R_x^{*n}}\right|^2}^{m}\ \overline{\left|\overline{H_x R_x^{*n}}\right|^2}^{m} - \overline{\left|\overline{H_x R_x^{*n}}\ \overline{H^* R_x^{n}}\right|^2}^{m}}$$

where the superscript m denotes the average over the m subsets. The equations for Z_{yx} and Z_{yy} can be derived in an identical manner.

$$Z_{yx} = \frac{\overline{\overline{E_y R_y^{*n}}^m \overline{H_x^* R_y^n}^m \overline{H_y R_y^{*n}}^m \overline{H_y^* R_y^n}^m} - \overline{\overline{E_y R_y^{*n}}^m \overline{H_y^* R_y^n}^m \overline{H_y R_y^{*n}}^m \overline{H_x^* R_y^n}^m}}{\overline{|\overline{H_y R_y^{*n}}|^2}^m \overline{|\overline{H_x R_y^{*n}}|^2}^m - \overline{|\overline{H_x R_y^{*n}} \overline{H_y^* R_y^n}|^2}^m}$$

and (4.43)

$$Z_{yy} = \frac{\overline{\overline{E_y R_y^{*n}}^m \overline{H_y^* R_y^n}^m \overline{H_x R_y^{*n}}^m \overline{H_x^* R_y^n}^m} - \overline{\overline{E_y R_y^{*n}}^m \overline{H_x^* R_y^n}^m \overline{H_x R_y^{*n}}^m \overline{H_y^* R_y^n}^m}}{\overline{|\overline{H_y R_y^{*n}}|^2}^m \overline{|\overline{H_x R_y^{*n}}|^2}^m - \overline{|\overline{H_x R_y^{*n}} \overline{H_y^* R_y^n}|^2}^m} .$$

One is free to pick the value of n and the way in which the n crossproducts are selected. If no extra reference channel has been recorded then one must use E_y for R_x and E_x for R_y. If an extra telluric measurement is available then one has the additional freedom to chose any combination of E_x and E_r for R_y and E_y and E_r for R_x.

Note that if n=1 this estimate is identical to $\underline{\underline{Z}}^H$ except that the average has been weighted by the reference power. In that case one would expect essentially the same bias as in $\underline{\underline{Z}}^H$.

In the computer test with the simulated data of stationary signals and noises the double average technique did not, and was not expected to, yield significant improvements in the results. With an electric reference aligned with E_x or E_y, only the estimates of Z_{xx} and Z_{xy} or Z_{yx} and Z_{yy} respectively could be improved. With the reference in a diagonal direction as in figure 7 the polarization of the signals averaged to zero at the same rate as the noise in the first average with the result that the estimates were biased the same as $\underline{\underline{Z}}^H$ for all n.

The method behaved as expected when tested on the real data. As n was increased the bias decreased and the random errors increased. At frequencies below 1 Hz where the signals are often quasisinusoidal all of the evident bias in the apparent resistivities could be removed while increasing the random scatter between adjacent frequency windows to an rms value of about a factor of 5. At higher frequencies where the signals are very impulsive the method yielded only very slight improvement.

Several different choices for R were tried including $R_x=E_y$, $R_x=E_r$, $R_x=\sqrt{2}\,E_r - E_y$ and $R_x = E_r - E_y$. There was a relatively small amount of bias, either up or down, that depended on the choice of R.

The first average was performed only over crossproducts from adjacent frequencies. Since it was desireable to keep the results from adjacent frequency windows as independent as possible this limited the number in the first average, n, to the number of Fourier harmonics in the constant Q window. Then various values of n were tried to see what value would minimize the bias without unduely increasing the random errors. The final choice below 1 Hz was n equal to the smallest of the three numbers: the number of Fourier harmonics in the window, $\sqrt{N}$ and 36. For frequencies above 1 Hz any n greater than 2 greatly increased the random error so n equal to 2 was used.

The rotated apparent resistivities calculated via this method with $R_x = E_r - E_y$ and $R_y = E_r - E_x$. are shown in part c of figures 2 - 5 for comparison with the resistivities from $\underline{\underline{Z}}^H$. Because of the large random error in this method the logarithmic mean and standard deviation

of disjoint sets of apparent resistivities from adjacent frequency windows were plotted for the poorer data rather than the individual resistivities. For data that had been rated poor the average was over 5 windows and for fair, 3.

Although the double average method gave the only physically reasonable results from our Grass Valley data the method must still be considered at best an ambiguous success. Some bias still remains, depending on the choice of reference. Since the success of the method depends on the statistical nature of the signals, predictions about its success are nearly impossible. The random errors are comparatively large.

SECTION V. REMOTE REFERENCE

The Estimate

In the analysis of the 5 channel data two of the five channels were used as references for the other three channels. If the noise in either of the two references is correlated with the noises in the other three channels the impedance estimates will be biased. For our 5 channel data from Grass Valley such bias was obvious.

If two reference channels are available one can obtain an unbiased estimate of $\underline{\underline{Z}}$ even if the noise in $\vec{E}$ is correlated with the noise in $\vec{H}$ as long as these noises are not correlated with the reference, $\vec{R}$. In addition the equations are simple, stable for any $\underline{\underline{Z}}$ and have small random error. As opposed to the least squares approach, which gives six possible estimates for $\underline{\underline{Z}}$, or the 37 solutions that can be selected from equations (4.3) through (4.10), the remote reference estimate is unique.

Quite analogously to Madden's generation of equation (1.23) for $\underline{\underline{Z}}^H$, the equation for the remote reference estimate $\underline{\underline{Z}}^R$ can be derived by multiplying the defining equation for $\underline{\underline{Z}}$, (1.11), by $\vec{R}^*$ to form the diadic products, averaging and then solving for $\underline{\underline{Z}}$ to obtain

$$\underline{\underline{Z}}^R = [ER][HR]^{-1} \tag{5.1}$$

One might suppose, then, that other referenced estimates for $\underline{\underline{Z}}$ would exist corresponding to the other least squares estimates but in fact they are all identical. For instance, corresponding to the least squares estimate for the admittance, equation (1.25), the referenced

admittance tensor estimate

$$\underline{\underline{Y}}^{R} = [HR][ER]^{-1} \quad . \tag{5.2}$$

If we then attempt to use this to generate an independent estimate of $\underline{\underline{Z}}$ via $\underline{\underline{Z}} = \underline{\underline{Y}}^{-1}$ we obtain

$$(\underline{\underline{Y}}^{R})^{-1} = [ER][HR]^{-1} = \underline{\underline{Z}}^{R} \quad , \tag{5.3}$$

the identical estimate.

The reference can be either electric or magnetic. The distance it must be removed in order to avoid noise correlations depends, of course, on the range of the noise source. If the source is fluctuations in the streaming potential surface voltages then moving the reference beyond the local water flow field would be sufficient. If the noises are artificial they could be either very short range such as agricultural equipment or they could range over 50 miles like the fields from the Bay Area Rapid Transit system.

Since one has to have an incident wave homogeneous over a large number of skin depths for the impedance to have a stable value, no additional physical conditions are required to use a remote reference. In fact one can guarantee that the signals are homogeneous over a long range by placing the reference at a great distance. The random error of the estimate will increase, however, as the coherence between the signals at the sounding site and the reference decreases with distance.

$\underline{\underline{Z}}^{R}$ contains $\vec{R}$ in both the numerator and denominator in such a way that it is completely independent of the frequency response of the

instruments used to measure $\vec{R}$. This can greatly relax the demands on telemetry used to transmit the reference.

Error Analysis - Variances of $\underline{\underline{Z}}^R$

Equation (5.1) is such a simple linear equation that one can calculate the expected random errors in $\underline{\underline{Z}}^R$ and in any function of $\underline{\underline{Z}}^R$. One way to proceed is to relate the error in $\underline{\underline{Z}}^R$, $\underline{\underline{Z}}^R - \underline{\underline{Z}}$, to $\vec{\eta}$ where $\vec{\eta}$ is the combined noise in the measurements as defined in equation (1.18). An ensemble of experiments must then be specified to calculate the variance of the elements of $\underline{\underline{Z}}^R$. The usual propagation of errors formula can then be used to calculate the error in any function of Z^R. In this section I will derive expressions for the variances of the apparent resistivity, phase angles of the impedance tensor elements and the skewness in a fixed coordinate system. Quantities calculated in the coordinate system aligned with the apparent strike direction are more uncertain because of the uncertainty in the apparent strike direction. Equations for the variances in that coordinate system will also be derived.

To compute $\underline{\underline{Z}}^R - \underline{\underline{Z}}$ it is convenient to introduce the error $\vec{\eta}^P$ predicted when $\underline{\underline{Z}}^R$ is substituted for $\underline{\underline{Z}}$ in equation (1.18):

$$\vec{\eta}^P = \vec{E} - \underline{\underline{Z}}^R \vec{H} \ . \tag{5.4}$$

On eliminating $\vec{E}$ between equations (1.18) and (5.4) one finds

$$\vec{\eta} = \vec{\eta}^P + \underline{\underline{\Delta}} \vec{H} \ , \tag{5.5}$$

where $\underline{\underline{\Delta}} = \underline{\underline{Z}}^R - \underline{\underline{Z}}$. Forming the diadic product of equation (5.5) with $\vec{R}^*$ and averaging gives

$$[\eta R] = [\eta^P R] + \Delta[H\Gamma] \quad . \tag{5.6}$$

Since $[\eta^P R] = 0$ from the definition of $\underline{\underline{Z}}^R$, equation (1.5),

$$\underline{\underline{\Delta}} = [\eta R][HR]^{-1} \quad . \tag{5.7}$$

Thus

$$\Delta_{ij} = \overline{\eta_i A_j}^* \; / \; D, (i = x,y,\; j = x,y) \quad , \tag{5.8}$$

where

$$A_x = R_x \; \overline{H_y^* R_y} \; - \; R_y \; \overline{H_y^* R_x} \quad , \tag{5.9}$$

$$A_y = R_y \; \overline{H_x^* R_x} \; - \; R_x \; \overline{H_x^* R_y} \quad , \tag{5.10}$$

and

$$D = \overline{H_x R_x}^* \; \overline{H_y R_y}^* - \overline{H_x R_y}^* \; \overline{H_y R_x}^* \quad . \tag{5.11}$$

These equations are exact by definition. The following equations are accurate only for large N. This condition is not a significant limitation on the accuracy of any practical estimate of errors. Equations valid for small N can not be accurate unless the distributions of the noises in the measurements are specified. An experimenter can rarely guarantee the distributions of his noises without a large number of measurements.

To compute the expected variances assume that we have an ensemble of estimates for $\underline{\underline{Z}}^R$ and that each value of $\underline{\underline{Z}}^R$ was computed from

identical sets of signals and stationary random noises. Define the variance, $\mathrm{Var}(Z_{ij}^R)$, by

$$\mathrm{Var}(Z_{ij}^R) = \langle |\Delta_{ij}|^2 \rangle - |\langle \Delta_{ij} \rangle|^2 , \tag{5.12}$$

where $\langle\ \rangle$ is the ensemble average. This variance is the sum of the variances of the real and imaginary parts of Z_{ij}^R. We assume that $\vec{R}$ is uncorrelated with $\vec{\eta}$ so that $\langle \Delta_{ij} \rangle = 0$. Then, from equation (5.8),

$$\mathrm{Var}(Z_{ij}^R) = \left\langle \frac{|\eta_i A_j|^2}{|D|^2} \right\rangle . \tag{5.13}$$

If we substitute the measured value of $|D|^2$ in equation (5.13), $\mathrm{Var}(Z_{ij}^R)$ can be written in expended form as

$$\mathrm{Var}(Z_{ij}^R) = \frac{1}{N^2|D|^2} \left\langle \sum_{n=1}^{N} \sum_{m=1}^{N} \eta_{i,m}\eta_{i,n}^* A_{j,m}A_{j,n}^* \right\rangle , \tag{5.14}$$

where N is the number of independent determinations of each field. This approximation introduces an error into the variance of order 1/N. For $m \neq n$, $\eta_{i,m}$ and $A_{j,m}$ are statistically independant of $\eta_{i,n}$ and $A_{j,n}$ (assuming that the analog filtering and Fourier transforming are performed appropriately). Thus, equation (5.14) reduces to

$$\mathrm{Var}(Z_{ij}^R) = \frac{1}{N^2|D|^2} \sum_{m=1}^{N} \left\langle |\eta_{i,m}|^2 |A_{j,m}|^2 \right\rangle . \tag{5.15}$$

If $\eta_{i,m}$ and $A_{j,m}$ are statistically independent, $\langle |\eta_{i,m}|^2 |A_{j,m}|^2 \rangle = \langle |\eta_{i,m}|^2 \rangle \langle |A_{j,m}|^2 \rangle$. Since the crosspowers in the $A_{j,m}$ are in fact

not independent of the $\eta_{i,m}$, the equality is not exact. However, provided $\vec{R}$ is independent of $\vec{\eta}$, the error introduced is of order 1/N, and can be neglected for large N. If the noises are stationary, $\langle |\eta_{i,m}|^2 \rangle$ is independent of m, and equal to $\overline{|\eta_i|^2}$. Under these conditions, equation (5.15) simplifies to

$$\mathrm{Var}(Z_{ij}^R) = |\eta_i|^2 \, |A_j|^2 \, / \, N|D|^2 \, . \tag{5.16}$$

It is easy to show, using equations (5.5), (5.8), and (5.16), that $\overline{|\eta_i|^2} = \overline{|\eta_i^P|^2} \, [1 + 0(1/N)]$. Thus, for large N, one can replace $\overline{|\eta_i|^2}$ in equation (5.16) with

$$\overline{|\eta_i^P|^2} = \overline{|E_i|^2} - 2\mathrm{Re}\left[Z_{ix}^R \, \overline{H_x E_i^*} + Z_{iy}^R \, \overline{H_y E_i^*} - Z_{ix}^R Z_{iy}^{R*} \, H_x H_y^* \right]$$

$$+ |Z_{ix}^R|^2 \, \overline{|H_x|^2} + |Z_{iy}^R|^2 \, \overline{|H_y|^2} \, . \tag{5.17}$$

The variance of Z_{ij}^R is correctly given by equation (5.16) for arbitrary levels of noise but only if: (1) the noises in $\vec{R}$ are uncorrelated with the noises in $\vec{E}$ and $\vec{H}$, (2) the noises in $\vec{E}$ and $\vec{H}$ are independent of the signals, and (3) the noises are stationary. The purpose of the remote reference technique is to ensure that the first condition is satisfied. The second assumption is likely to be well satisfied if the noises are generated locally. On the other hand, if the noises arise from inhomogeneous atmospheric sources, both assumptions 1 and 2 may be violated. Assumption 2 could also be violated if the measuring equipment produces errors that are proportional

to the signals. The requirement (3) of stationarity is not particularly restrictive. We require only that the ensemble average and measured time average of the noise powers be equal. Stationarity does not require that the noise in short segments of our data be the same for all segments. For example, magnetic fields from passing vehicles might introduce much more noise into some data segments than others, yet the ensemble and time averages of the noise power will still be equal, provided the times at which vehicles pass by in each experiment in the ensemble are random. I would like to emphasize that we do not need to assume that the signals are stationary. $\underline{\underline{Z}}^R$ and the errors in $\underline{\underline{Z}}^R$ involve only the ratios of average crosspowers, and, since $\vec{E}$, $\vec{H}$, and $\vec{R}$ are causally related, these ratios do not depend on the statistics of the fields.

It is important to note from equation (5.16) that $\mathrm{Var}(Z^R_{ij}) = 0$ when there is no noise in $\vec{E}$ and $\vec{H}$, regardless of the noise power in $\vec{R}$. Also, when the noise power in $\vec{R}$ is negligible and the crosspowers in A_j and D can be approximated by their noise-free values, it can be shown that $\mathrm{Var}(Z^R_{ij})$ is independent of the tensor relating $\vec{R}$ and $\vec{H}$. Under these conditions, for given $\overline{|\eta|^2}$, $\mathrm{Var}(Z^R_{ij})$ diverges as $\overline{|H_{sx}|^2}\ \overline{|H_{sy}|^2} - \overline{|H_{sx}\, H^*_{sy}|}^2 \to 0$, that is, as the polarization of the signal, $\vec{H}_s$, increases. When there is noise in the reference, one can easily verify that the contribution of the noise power to $\mathrm{Var}(Z^R_{ij})$ increases as the polarization of $\vec{R}$ increases. Thus, the electric field from a telluric array in a location with a highly anisotropic apparent resistivity may not be a suitable reference.

If $\vec{H}$ is noise-free, and if one replaces $\vec{R}$ by $\vec{H}$ in equation (5.7), equation (5.16) gives the expected variance* in the least-squares estimate of $\underline{\underline{Z}}^H$. Since $\underline{\underline{\Delta}}$ is independent of the orientation of $\vec{R}$ relative to $\vec{H}$, the variance in $\underline{\underline{Z}}^R$ is identical with the variance in $\underline{\underline{Z}}^H$ for any noise-free $\vec{R}$ if $\vec{H}$ is also noise-free. Thus, because $\underline{\underline{Z}}^H$ is obtained by minimizing the mean square error in equation (1.24), $\underline{\underline{Z}}^R$ also minimizes the mean square error. On the other hand, if there is noise in $\vec{H}$, for large N the bias errors in $\underline{\underline{Z}}^H$ are large compared to the random errors in either $\underline{\underline{Z}}^H$ or $\underline{\underline{Z}}^R$. Therefore, when there is noise in $\vec{H}$, $\underline{\underline{Z}}^H$ is not a good estimate of $\underline{\underline{Z}}$, and the question of the relative random errors in $\underline{\underline{Z}}^R$ and $\underline{\underline{Z}}^H$ becomes academic.

There are two attempts in the literature to calculate the expected errors in estimates of the individual elements of the impedance tensor. Bentley[3] attempted such a calculation for $\underline{\underline{Z}}^H$. His calculation assumes that there is no noise in the measured fields, that the signals have stationary power spectra, and that the only source of error is the sampling distribution of the random signals. In fact, only the ratios of power spectra enter into the estimate of $\underline{\underline{Z}}$, and these ratios are not affected by sampling errors. Thus, Bentley should have obtained a null estimate for the errors, but did not because he neglected the correlations between the errors in the estimates of the power spectra.

---

*In arriving at equation (5.16), terms of order 1/N were neglected in estimating $\overline{|\eta_i|^2}$. If the only noise is in the electric field, it is easy to show that the unbiased estimator of $\overline{|\eta_i|^2}$ is $[N/(N-2)]\ \overline{|\eta_i^P|^2}$ for all N and for any noise-free $\vec{R}$.

Reddy et al[25] have estimated the random errors in the individual elements of $\underline{\underline{Z}}^H$ using an expression derived from the error in a combination of the elements[12,15,2] via a very rough approximation. The approximation is necessarily very rough because the error distribution of the combination does not contain enough information to specify the individual errors, and, in addition, the expression for the joint errors is valid only for a noise-free magnetic field. Thus, neither approach appears to be appropriate for magnetotellurics.

Variances of Functions of $\underline{\underline{Z}}^R$

However large the noise, the expected magnitude of the error matrix $\underline{\underline{\Delta}}$ can be made arbitrarily small by making N sufficiently large. For small errors, any function ξ of $\underline{\underline{Z}}^R$ can be expanded to first order in Δ_{ij} and Δ_{ij}^*. In these expansions, it is convenient to shorten the notation as follows:

$$\Delta_{ij} \ (i=x,y,\ j=x,y) \leftrightarrow \Delta_k \ (k=1,2,3,4),$$

where 1 = xx, 2 = xy, 3 = yx, 4 = yy. I will also drop the superscript R from $\underline{\underline{Z}}^R$. In terms of Δ_k and Δ_k^*, the error, $\delta\xi$, in ξ is given by

$$\delta\xi = \sum_{k=1}^{4} \left(\frac{d\xi}{dZ_k} \Delta_k + \frac{d\xi}{dZ_k^*} \Delta_k^* \right) . \qquad (5.18)$$

Since $\langle \Delta_k \rangle = 0$, the variance in ξ is $\mathrm{Var}(\xi) = \langle |\delta\xi|^2 \rangle$. If $\vec{\eta}$ and $\vec{R}$ are uncorrelated, $\langle \Delta_k \Delta_\ell \rangle = 0$ for all k and ℓ, since the signals and noises are complex numbers of random phase. Thus $\mathrm{Var}(\xi)$ has the form

$$\mathrm{Var}(\xi) = \sum_{k=1}^{4} \sum_{\ell=1}^{4} \frac{d\xi}{dz_k} \frac{d\xi^*}{dz_\ell^*} \langle \Delta_k \Delta_\ell^* \rangle + \frac{d\xi}{dz_k^*} \frac{d\xi^*}{dz_\ell} \langle \Delta_k^* \Delta_\ell \rangle \quad . \tag{5.19}$$

which simplifies to

$$\mathrm{Var}(\xi) = \sum_{k=1}^{4} \sum_{\ell=1}^{4} G_{k\ell} \langle \Delta_k \Delta_\ell^* \rangle \quad . \tag{5.20}$$

Here,

$$G_{k\ell} = G_{\ell k}^* = \frac{d\xi}{dz_k^*} \frac{d\xi^*}{dz_\ell^*} + \frac{d\xi}{dz_k} \frac{d\xi^*}{dz_\ell} \quad , \tag{5.21}$$

If ξ is real, $G_{k\ell} = 2\mathrm{Re}\left(\frac{d\xi}{dz_k} \frac{d\xi^*}{dz_\ell^*} \right)$. The ensemble average $\langle \Delta_k \Delta_\ell^* \rangle$ can be evaluated with the same assumptions that were used in obtaining equation (5.16). Returning to our original notation and using equations (5.9) and (5.10) we find that

$$\langle \Delta_k \Delta_\ell^* \rangle = \langle \Delta_{ij} \Delta_{nm}^* \rangle = \frac{\overline{\eta_i^P \eta_n^{P*}} \; \overline{A_j A_m^*}}{N|D|^2} \tag{5.22}$$

where we have approximated $\langle \eta_i \eta_n^* \rangle$ by $\overline{\eta_i^P \eta_n^{P*}}$. In equation (5.22) $\overline{\eta_i^P \eta_n^{P*}}$ and $\overline{A_j A_m^*}$ can be expressed in terms of measured crosspowers and autopowers as follows:

$$\overline{\eta_i^P \eta_n^{P*}} = \overline{E_i E_n^*} - Z_{ix} \overline{H_x E_n^*} - Z_{iy} \overline{H_y E_n^*} - Z_{nx}^* \overline{H_x^* E_i} - Z_{ny}^* \overline{H_y^* E_i} + Z_{ix} Z_{nx}^* \overline{|H_x|^2}$$

$$+ Z_{iy} Z_{nx}^* \overline{H_y H_x^*} + Z_{ix} Z_{ny}^* \overline{H_x H_y^*} + Z_{iy} Z_{ny}^* \overline{|H_y|^2} \quad , \tag{5.23}$$

and

$$\overline{A_j A_m^*} = \overline{R_j R_m^*}\ \overline{H_k^* R_k}\ \overline{H_\ell R_\ell^*} + \overline{R_k R_\ell^*}\ \overline{H_k^* R_j}\ \overline{H_\ell R_m^*} - \overline{R_j R_\ell^*}\ \overline{H_k^* R_k}\ \overline{H_\ell R_m^*} - \overline{R_k R_m^*}\ \overline{H_k^* R_j}\ \overline{H_\ell R_\ell^*} , \tag{5.24}$$

where $k = x,y$, $\ell = x,y$, and $k \neq j$ and $\ell \neq m$. It is apparent that $\mathrm{Var}(\xi)$ will, in general, depend on all 15 crosspowers and 6 autopowers of the components of the fields.

To illustrate the use of equation (5.20), let us compute the variance in $\mathrm{Re}(Z_\mu)$, where $\mu = 1,2,3$, or 4. Substituting $\xi = \xi^* = (Z_\mu + Z_\mu^*)/2$ and $d\xi/dZ_k = d\xi^*/dZ_k^* = 1/2\ \delta_{\mu k}$ (δ is the Kronecker delta), one finds $\mathrm{Var}[\mathrm{Re}(Z_\mu)] = 1/2\ (|\Delta_\mu|^2) = 1/2\ \mathrm{Var}(Z_\mu)$. Since $\mathrm{Var}(Z_\mu) = \mathrm{Var}[\mathrm{Re}(Z_\mu)] + \mathrm{Var}[\mathrm{Im}(Z_\mu)]$ this example proves that $\mathrm{Var}[\mathrm{Re}(Z_\mu)] = \mathrm{Var}[\mathrm{Im}(Z_\mu)]$.

The elements of the apparent resistivity matrix $\underline{\underline{\rho}}$ associated with $\underline{\underline{Z}}$ are defined by $\underline{\underline{\rho}}_k = 0.2T\ |\underline{\underline{Z}}_k|^2$, where T is the period in seconds and $\underline{\underline{Z}}$ has dimensions of $mV/(km\gamma)$. If we choose $\xi = \xi^* = Z_\mu Z_\mu^*$ in equation (5.20) then $d\xi/dZ_k = Z_\mu^* \delta_{\mu k}$, $G_{k\ell} = 2|Z_\mu|^2\ \delta_{\mu k}\delta_{\mu \ell}$, and $\mathrm{Var}(\xi) = 2|Z_\mu|^2\ (|\Delta_\mu|^2)$. Thus the variance of the element ρ_μ is given by

$$\mathrm{Var}(\rho_\mu) = (0.2T)^2\ \mathrm{Var}(\xi) = 0.4T\rho_\mu\ (|\Delta_\mu|^2) . \tag{5.25}$$

The phase, ϕ_μ of Z_μ^* is defined by

$$\tan \phi_\mu = (Z_\mu - Z_\mu^*)/i(Z_\mu + Z_\mu^*) , \tag{5.26}$$

where $i = \sqrt{-1}$. If $\xi = \tan\phi_\mu$, $\mathrm{Var}(\phi_\mu) = \cos^4\phi_\mu \, \mathrm{Var}(\xi)$. In equation (5.21)

$$d\xi/dz_k = \delta_{\mu k} \, 2z_\mu^*/i(z_\mu + z_\mu^*)^2 ,$$

and

$$G_{k\ell} = 8 \, |z_\mu|^2 \, \delta_{\mu k} \, \delta_{\mu \ell} / |z_\mu + z_\mu^*|^4 .$$

Thus

$$\mathrm{Var}(\phi_\mu) = 8\cos^4\phi_\mu \, \langle |\Delta_\mu|^2 \rangle \, |z_\mu|^2 / |z_\mu + z_\mu^*|^4 . \qquad (5.27)$$

To find the variance in the skewness, W, we define $\xi = W^2 = |z_{xx} + z_{yy}|^2 / |z_{xy} - z_{yx}|^2$. One obtains

$$\mathrm{Var}(W) = \mathrm{Var}(\xi)/4W , \qquad (5.28)$$

whre $\mathrm{Var}(\xi)$ is given by equation (5.20) with the following values of $G_{k\ell}$:

$$G_{11} = G_{14} = G_{44} = 2W^2/|z_{xy} - z_{yx}|^2 , \qquad (5.29)$$

$$G_{22} = G_{33} = -G_{23} = W^2 G_{11},$$

and

$$G_{12} = G_{24} = -G_{13} = -G_{34} = -G_{11} \frac{\mathrm{Re}[(z_{xx} + z_{yy})(z_{xy}^* - z_{yx}^*)]}{|z_{xy} - z_{yx}|^2} . \qquad (5.30)$$

The rotation angle, θ, to align one of the axes with the apparent strike direction satisfies the equation

$$\tan 4\theta = \frac{2\mathrm{Re}[(z_{yy} - z_{xx})(z_{xy}^* + z_{yx}^*)]}{|z_{xy} + z_{yx}|^2 - |z_{yy} - z_{xx}|^2} . \qquad (5.31)$$

For any integer, m, $\Theta \pm m\pi/4$ also satisfies equation (5.31), but the solutions with odd m maximize $|Z_{xx} - Z_{yy}|^2$. If we choose $\xi = \xi^* = \tan 4\Theta$, then $\mathrm{Var}(\Theta) = \cos^4 4\Theta \, \mathrm{Var}(\xi)/16$. $\mathrm{Var}(\xi)$ is given by equation (5.20) with

$$G_{11} = G_{44} = -G_{14} = 2|\alpha|^2 \, |Z_{xy} + Z_{yx}|^2 ,$$

$$G_{22} = G_{33} = G_{23} = 2|\alpha|^2 \, |Z_{xx} - Z_{yy}|^2 , \qquad (5.32)$$

and

$$G_{12} = G_{13} = -G_{24} = -G_{34} = 2|\alpha|^2 \, \mathrm{Re}[(Z_{xy}^* + Z_{yx}^*)(Z_{yy} - Z_{xx})],$$

where

$$\alpha = \frac{(Z_{xy} + Z_{yx})^2 + (Z_{yy} - Z_{xx})^2}{[|Z_{xy} + Z_{yx}|^2 - |Z_{yy} - Z_{xx}|^2]^2} . \qquad (5.33)$$

The above equations can be used to calculate variances in any coordinate system provided one first rotates the measured spectral density matrixes to the desired orientation. However, if the rotation angle of the coordinate system is itself determined from the data, additional errors will be introduced in the calculated quantities because of the uncertainty in the rotation angle. The following expressions are for the variances of the apparent resistivities and of the phases of the elements of the impedance tensor in the coordinate system rotated by the angle θ obtained from equation (5.31).

Define the rotated apparent resistivity matrix (which is not a tensor) by $\rho_\mu' = 0.2T|Z_\mu'|^2$, where $\underset{\approx}{Z}'$ is the impedance tensor in the rotated coordinate system. Then, if $\xi_\mu = |Z_\mu'|^2$, $\mathrm{Var}(\rho_\mu') = (0.2T)^2 \mathrm{Var}(\xi_\mu)$. $\mathrm{Var}(\xi_\mu)$ is given by equation (5.20) with

$$G_{k\ell} = 2\mathrm{Re}\left(\frac{d\xi_\mu}{dz_k}\ \frac{d\xi_\mu}{dz_\ell}\right)^* \quad , \tag{5.34}$$

and

$$\frac{d\xi_\mu}{dz_k} = \frac{\partial\xi_\mu}{\partial z_k} + \frac{\partial\xi_\mu}{\partial\theta}\ \frac{\partial\theta}{\partial z_k} \quad . \tag{5.35}$$

Using equations (1.15) and (5.35) we find

$$\frac{d\xi_\mu}{dz_k} = z'^*_\mu\ U_\mu(k) + 2\mathrm{Re}[z'^*_\mu V_\mu]\ \frac{\partial\theta}{\partial z_k} \quad , \tag{5.36}$$

where

$$\underset{\approx}{U}(k) = \underset{\approx}{R}\ \frac{\partial \underset{\approx}{Z}}{\partial z_k}\ \underset{\approx}{R}^{-1} \quad , \tag{5.37}$$

and

$$V = \frac{\partial \underset{\approx}{R}}{\partial\theta}\ \underset{\approx}{Z}\ \underset{\approx}{R}^{-1} + \underset{\approx}{R}\ \underset{\approx}{Z}\ \frac{\partial \underset{\approx}{R}^{-1}}{\partial\theta} \tag{5.38}$$

where $\underset{\approx}{R}$ is defined in equation 1.16.

The elements of equation (5.37) are

$$\underset{\approx}{U}(xx) = \begin{pmatrix} \cos^2\theta & -\sin\theta\cos\theta \\ -\sin\theta\cos\theta & \sin^2\theta \end{pmatrix} \quad ,$$

$$\underset{\approx}{U}(xy) = \begin{pmatrix} \sin\theta\cos\theta & \cos^2\theta \\ -\sin^2\theta & -\sin\theta\cos\theta \end{pmatrix} \quad , \tag{5.39}$$

$$\underset{\approx}{U}(yx) = \begin{pmatrix} \sin\theta\cos\theta & -\sin^2\theta \\ \cos^2\theta & -\sin\theta\cos\theta \end{pmatrix} \quad ,$$

and

$$\underset{\approx}{U}(yy) = \begin{pmatrix} \sin^2\theta & \sin\theta\cos\theta \\ \sin\theta\cos\theta & \cos^2\theta \end{pmatrix} \quad .$$

$\underset{\approx}{V}$ can be written as

$$\underset{\approx}{V} = \begin{pmatrix} -\sin 2\theta & \cos 2\theta \\ -\cos 2\theta & -\sin 2\theta \end{pmatrix} \begin{pmatrix} Z_{xx} - Z_{yy} & Z_{xy} + Z_{yx} \\ Z_{xy} + Z_{yx} & Z_{yy} - Z_{xx} \end{pmatrix} \tag{5.40}$$

From equation (5.31),

$$\partial\theta/\partial Z_{xx} = -\partial\theta/\partial Z_{yy} = -\alpha^* \cos^2 4\theta (Z_{xy} + Z_{yx})/4 \ , \tag{5.41}$$

and

$$\partial\theta/Z_{yx} = \partial\theta/\partial Z_{xy} = \alpha^* \cos^2 4\theta (Z_{xx} - Z_{yy})/4 \ ,$$

where α is defined in equation (5.33).

Now consider ϕ'_μ, the phase of Z'_μ, and define

$$\xi_\mu = \tan\phi'_\mu = \frac{Z'_\mu - Z'^*_\mu}{i(Z'_\mu + Z'^*_\mu)} \ . \tag{5.42}$$

Then, $\mathrm{Var}(\phi'_\mu) = \cos^4\phi'_\mu \ \mathrm{Var}(\xi_\mu)$, and $\mathrm{Var}(\xi_\mu)$ is given by equation (5.20). From equations (5.42) and (5.35), we find

$$\begin{aligned} \frac{d\xi_\mu}{dZ_k} &= -2i \left[\frac{Z'^*_\mu \ \frac{dZ'_\mu}{dZ_k} - Z'_\mu \ \frac{dZ'^*_\mu}{dZ_k}}{(Z'_\mu + Z'^*_\mu)^2} \right] \\ &= -2i \left[\frac{Z'^*_\mu \ U_\mu(k) + 2i\,\mathrm{Im}[Z'^*_\mu \ V_\mu]\partial\theta/\partial Z_k}{(Z'_\mu + Z'^*_\mu)^2} \right] , \end{aligned} \tag{5.43}$$

where $\underset{=}{U}(k)$, $\underset{=}{V}$, and $\partial\theta/\partial Z_k$ have been defined in equations (5.39) through (5.41).

Confidence Limits

Although least squares linear regression is not the best method of determining $\underline{\underline{Z}}$, the least squares principle is appropriate for the comparison of different estimates of $\underline{\underline{Z}}$. For example, the best model of the ground in a statistical sense minimizes the mean square of the magnitudes of the differences between the modeled and measured values of $\underline{\underline{Z}}$, weighted in inverse proportion to the variances. However, to determine the statistical significance of this discrepancy, one requires the distribution of the errors of the estimates, not just the variances.

In equation (5.8) for the error Δ_{ij}, D can be approximated by its noise-free value for large N. In this approximation, Δ_{ij} is just the sum of N complex random errors (one for each k, $1 \leqslant k \leqslant N$) and, by the central limit theorem, its real and imaginary parts are normally distributed. Since the error Δ_{ij} is of random phase $\langle \mathrm{Re}(\Delta_{ij})\mathrm{Im}(\Delta_{ij}) \rangle = 0$. Thus $\mathrm{Re}(\Delta_{ij})$ and $\mathrm{Im}(\Delta_{ij})$ are also statistically independent. The sums of the squares of n independent normally distributed random variables with unity variance and zero mean has a χ^2_n distribution. Thus, if $\vec{H}$ and $\vec{R}$ are noise-free,

$$\delta_{ij} \equiv |\Delta_{ij}|^2/\mathrm{Var}[\mathrm{Re}(\Delta_{ij})] = 2|\Delta_{ij}|^2 N|D|^2/\langle|\eta_i|^2\rangle \overline{|A_j|^2} \qquad (5.44)$$

has a χ^2_2 distribution. In this expression, the unknown quantity $\langle |\eta_i|^2 \rangle$ is best approximated by $\overline{|\eta_i^P|^2}$. The errors introduced by this approximation must be included to obtain an unbiased estimate of

the confidence limits. Since $\beta \equiv (2N-4)\ |\eta_i^P|^2/(|\eta_i|^2)$ can be shown to have a χ^2_{2N-4} distribution[15] the quantity δ_{ij}/β is the ratio of two variables with χ^2 distributions. Thus $(2N-4)\delta_{ij}/(2\beta)$ has a Fisher F distribution with 2 and 2N-4 degrees of freedom, $F_{2,2N-4}$. For large N the modification introduced by $\overline{|\eta_i^P|^2}$ is small. For example, for N > 25, the confidence limits for the $F_{2,2N-4}$ distribution are less than 6% larger than those for the χ^2_2 distribution up to the 95% confidence level. If the signal-to-noise ratios of $\vec{R}$ and $\vec{H}$ are much greater than the signal-to-noise ratio of $\vec{E}$, this small correction to the confidence limits may be significant. If the noise is not predominantly in $\vec{E}$, the other corrections of order 1/N that we have neglected will cause modifications of the distribution comparable with the difference between the χ^2 and F distributions. These modifications cannot be described in terms of elementary distribution functions. Thus, for most applications, the χ^2 distribution should be adequate, and as accurate as can be obtained without extraordinary effort.

Errors estimated from the first-order Taylor expansion, equation (5.18), for example errors in the apparent resistivity, are linear functions of the errors in the real and imaginary parts of $\underline{\underline{Z}}^R$. Therefore, within the limits of accuracy of the Taylor expansion, these errors are also normally distributed. The confidence limits of these quantities are again modified by the estimation of $(|\eta_i|^2)$ by $\overline{|\eta_i^P|^2}$ so that the proper distribution is that of the ratio of a normally distributed to a χ^2 distributed variable, or a Student t distribution. However, the corrections to a normal distribution will be significant only when

the confidence intervals are so small that the Taylor expansion introduces a negligible error, and, as before, the noise is predominantly in $\vec{E}$. For most purposes, a normal distribution should be entirely adequate.

As an example, consider two independent sets, a and b, of M estimates of $Z_{ij}(\omega)$, $Z^a_{ij}(\omega_k)$ and $Z^b_{ij}(\omega_k)$, where $1 \leqslant k \leqslant M$. We calculate the probability that the disagreement between the sets arose from random errors alone assuming that the errors in set b are negligible compared to the errors in set a. Such a calculation would be required if one wanted to determine the significance of the difference between a model of the ground (set b) and a sounding (set a), or if one considered rejecting a small subset of the data (set a) because of its disagreement with the rest of the data (set b). If the quantities $\delta^a_{ij}(\omega_k)$ have χ^2_2 distributions then the total discrepancy, $\sum_{k=1}^{M} \delta^a_{ij}(\omega_k)$, has a χ^2_{2M} distribution. Neglecting the errors in $Z^b_{ij}(\omega_k)$, we find

$$\sum_{k=1}^{M} \delta^a_{ij}(\omega_k) \equiv \zeta = \sum_{k=1}^{M} \frac{2\left|Z^a_{ij}(\omega_k) - Z^b_{ij}(\omega_k)\right|^2 N^a |D^a|^2}{\overline{|\eta^{Pa}_i|^2}\ \overline{|A^a_j|^2}} \quad . \tag{5.45}$$

Thus the probability that $\zeta > \alpha$ through random errors alone is $1 - \chi^2_{2M}(\alpha)$.

Determination of Signal and Noise Powers

The random errors in $\underline{\underline{Z}}^R$ depend only on the combined noise, $\vec{\eta}$, rather than on individual noises in $\vec{E}$ and $\vec{H}$. Nevertheless, the determination of the noises in the individual fields is obviously

of practical interest. With a remote reference the signal and noise power spectral densities can be evaluated as follows.

The value of $\underline{\underline{Z}}^R$ obtained from equation (5.1) and the measured magnetic field, $\vec{H}$, predict an electric field $\vec{E}^P$, where

$$\vec{E}^P = \underline{\underline{Z}}^R \vec{H} \quad . \tag{5.46}$$

$\vec{E}^P$ contains contributions from the signal $\vec{H}_s$ and the noise $\vec{H}_n = \vec{H} - \vec{H}_s$. If the noises are uncorrelated with each other and with the signals, the spectral density matrix

$$[E^P E] = \underline{\underline{Z}}^R [HE] = [ER][HR]^{-1}[HE] \tag{5.47}$$

has the expectation value of the spectral density matrix $[E_s E_s]$, where

$$[E_s E_s] = \begin{bmatrix} \overline{|E_{sx}|^2} & \overline{E_{sx} E_{sy}^*} \\ \overline{E_{sy} E_{sx}^*} & \overline{|E_{sy}|^2} \end{bmatrix} .$$

The matrix $[E_s E_s]$ is Hermitian: The diagonal elements are real, and the off-diagonal elements are complex conjugates of each other. On the other hand, $[E^P E]$ is, in general, not Hermitian because of the noises $\vec{E}_n$, $\vec{H}_n$, and $\vec{R}_n$. If the phases of the errors are unknown, it seems reasonable to estimate $[E_s E_s]$ by the Hermitian part of $[E^P E]$, $[E_s E_s]^P$ given by

$$[E_s E_s]^P = \frac{1}{2} \{[E^P E] + [E^P E]^\dagger\} = ([E^P E] + [E E^P])/2 \ . \tag{5.48}$$

This estimate of the signal power can be derived in a second way. Equation (5.46) predicts the electric field from the magnetic field using $\vec{R}$ as a reference. This idea can easily be generalized. If any three quantities are linearly related, each of them can be predicted from either of the others, with the third as a reference. If all the noises are uncorrelated then each of the linear relationships between the three quantities can be estimated in a stable, unbiased manner. For instance, the electric field can be predicted from $\vec{R}$, using $\vec{H}$ as the reference. That is, we can estimate $\underset{\approx}{G}$, defined by

$$\vec{E}_s = \underset{\approx}{G}\, \vec{R}_s \tag{5.49}$$

from

$$\underset{\approx}{G}^R = [EH][RH]^{-1} \ . \tag{5.50}$$

Thus we have a second estimate of the electric field signal power:

$$[E^P E]' = \underset{\approx}{G}^R [RE] = [EH][RH]^{-1} [RE] \ . \tag{5.51}$$

Comparing this with (5.47), we see that $[E^P E]' = [E^P E]^\dagger$! Thus we obtain equation (5.48) by taking the Hermetian part of either estimate. Alternatively, considering (5.47) and (5.51) as two equally valid estimates, one would want to obtain the best estimate by taking their average, again producing equation (5.48). Thus we see that both $\underset{\approx}{Z}^R$ and the signal power estimates are unique and contain remarkable symmetry.

Following these symmetries, we can immediately write down the predicted signal powers for $\vec{H}$ and $\vec{R}$:

$$[H_s H_s]^P = ([H^P H] + [HH^P])/2 \ , \tag{5.52}$$

and

$$[R_s R_s]^P = ([R^P R] + [RR^P])/2 \ , \tag{5.53}$$

where

$$[H^P H] = [HR][ER]^{-1}[EH] \ , \tag{5.54}$$

and

$$[R^P R] = [RE][HE]^{-1}[HR] \ . \tag{5.55}$$

One can calculate the spectral density matrices for the noises by subtracting the estimated signal density matrices from the measured spectral density matrices, for example

$$[E_n E_n] = [EE] - [E_s E_s]^P \ . \tag{5.56}$$

The noise matrixes contain the crosspowers $\overline{E_{nx} E^*_{ny}}$, $\overline{H_{nx} H^*_{ny}}$, and $\overline{R_{nx} R^*_{ny}}$. Thus, one can determine whether there are significant correlations between the noises in the two components of each field. Such correlations may be indicative of measurement errors, and could be generated, for example, by noise from a common electrode, or by a moving magnetic object.

The remote reference method requires the measurement of the three fields $\vec{E}$, $\vec{H}$, and $\vec{R}$, each with two components. Correlations between the noises in the two components of each field do not bias the estimates of $\underline{\underline{Z}}^R$, the errors in $\underline{\underline{Z}}^R$, or the signal and noise power spectral density matrices. However, any correlation between a measured field and the noise in another field will bias the estimates of the signal and noise power spectra. Such correlations would usually cause a significant non-Hermitian part in the matrices $[E^P E]$, $[H^P H]$, and $[R^P R]$.

$\underline{\underline{Z}}^R$ will be biased only by correlations between $\vec{\eta}$ and $\vec{R}$. Thus, under most circumstances, the requirement that $[E^P E]$, $[H^P H]$, and $[R^P R]$ be Hermitian provides a sufficient but not necessary check on the correlations that would bias $\underline{\underline{Z}}^R$. However, if the ionospheric signal is from a fixed inhomogeneous source, these matrices would still be Hermitian, but $\underline{\underline{Z}}^R$ would be biased.

Generalizations - the referenced tipper

All of the referenced tensor equations obviously hold for any rank tensor and can be immediately applied to the measurement of any tensor response function. The unbiased estimation of a tensor of rank n in the presence of correlated noises requires n reference channels with uncorrelated noises. As a simple example of this I will include here the equations for the measurement of a quantity often investigated in conjunction with magnetotelluric surveys, the tipper $\vec{T}$.

The tipper is the linear relationship between the vertical and horizontal magnetic field components, defined by $H_{sz} = \vec{T}\,\vec{H}_s$. The referenced estimate for the tipper is

$$\vec{T}^R = [H_z R][HR]^{-1} \tag{5.57}$$

where

$$[H_z R] = (\overline{H_z R_x^*},\ \overline{H_z R_y^*}) \quad .$$

The vertical magnetic signal power is

$$\mathrm{Re}(H_z^P H_z) = \mathrm{Re}([H_z R][HR]^{-1}\ [HH_z]). \tag{5.58}$$

The error in the estimate of $\vec{T}$ is

$$\vec{\Delta} = [\tau R][HR]^{-1} \tag{5.59}$$

where

$$\tau = H_z - \vec{T}\,\vec{H} .$$

Thus the variances of the elements of $\vec{T}$ are

$$\mathrm{Var}(T_i^R) = \overline{|\tau^P|^2}\ \overline{|A_i|^2}\ /(N|D|^2) \tag{5.60}$$

where the A_i and D are given in equations (5.9) - (5.11) and

$$\overline{|\tau^P|^2} = \overline{|H_z|^2} + |T_x|^2\,\overline{|H_x|^2} + |T_y|^2\,\overline{|H_y|^2} - 2\mathrm{Re}(\overline{H_x H_z^*}\ T_x + \overline{H_y H_z^*}\ T_y - \overline{H_x H_y^*}\ T_x T_y^*) . \tag{5.61}$$

The apparent tipper strike is the direction of the horizontal magnetic field component that has the smallest linear relationship with H_z. The angle of rotation about the $\hat{z}$ axis that will align the $\hat{x}$ axis with the tipper strike, θ_T, satisfies the equation

$$\tan 2\theta_T = \frac{2\mathrm{Re}(T_x T_y^*)}{|T_x|^2 - |T_y|^2} \tag{5.62}$$

Caution must be exercised because $\theta_T \pm \frac{m\pi}{2}$ also satisfies equation (5.62) for any integer m and the solutions for odd m maximize $|T_x(\theta)|^2$. Therefore θ_T obviously also maximizes $|T_y(\theta)|^2$ and $|T_y(\theta)|^2 - |T_x(\theta)|^2$. $|T_x|^2 + |T_y|^2 = |\vec{T}|^2$ is independent of rotation and is a measure of the total horizontal contrast in resistivity. One may also wish to know just how well $T_x(\theta)$ can be minimized. The minimum $|T_x(\theta)|^2$ is

$$f = (|T_x|^2 \cos^2\theta - |T_y|^2 \sin^2\theta)/\cos 2\theta \ . \qquad (5.63)$$

Thus θ_T, $|T|^2$ and f are interesting parameters of $\vec{T}$ for physical interpretation. Their variances can be calculated via the Taylor expansion analogous to equation (5.18) and for small errors the distribution of errors should be normal. Dropping the superscript R and calculating $\partial|T|^2/\partial T_i$ we obtain

$$\mathrm{Var}(|T|^2) = Q(|T_x|^2 \overline{|A_x|^2} + |T_y|^2 \overline{|A_y|^2} + 2\mathrm{Re}(T_x T_y^*)\ \mathrm{Re}(\overline{A_x A_y})) \qquad (5.64)$$

where $\overline{A_x A_y^*}$ is given by equation (5.24) and

$$Q = 2\overline{|\tau^P|^2} / (N|D|^2). \quad \text{Let } \xi = \tan 2\theta_T \ .$$

Then $\mathrm{Var}(\theta_T) = \cos^4 2\theta_T \ \mathrm{Var}(\xi)/4$ and

$$\mathrm{Var}(\xi) = |P|^2 Q(|T_y|^2 \overline{|A_x|^2} + |T_x|^2 \overline{|A_y|^2} - 2\mathrm{Re}(T_y T_x^*)\ \mathrm{Re}(\overline{A_x A_y^*})) \qquad (5.65)$$

where

$$P = (T_x^2 + T_y^2)/(|T_x|^2 - |T_y|^2)^2 \ .$$

$$\mathrm{Var}(f) = Q\left(2\mathrm{Re}\left(\frac{df}{dT_x}\left(\frac{df}{dT_y}\right)^*\right) \mathrm{Re}\ \overline{A_x A_y^*} + \left|\frac{df}{dT_x}\right|^2 \overline{|A_x|^2} + \left|\frac{df}{dT_y}\right|^2 \overline{|A_y|^2}\right). \qquad (5.66)$$

$$\frac{df}{dT_i} = \frac{\partial f}{\partial T_i} + \frac{\partial f}{\partial \theta}\ \frac{\partial \theta}{\partial T_i} \ , \qquad (5.67)$$

where

$$\frac{\partial f}{\partial \theta} = \frac{2\mathrm{Re}(T_x T_y^*)}{\cos 2\theta} \ , \qquad (5.68)$$

$$\frac{\partial f}{\partial T_x} = \frac{T_x^* \cos^2\theta}{\cos 2\theta} \ , \qquad (5.69)$$

$$\frac{\partial f}{\partial T_y} = \frac{-T_y^* \sin^2\theta}{\cos 2\theta} \tag{5.70}$$

$$\frac{\partial \theta}{\partial T_x} = - BT_y \tag{5.71}$$

and

$$\frac{\partial \theta}{\partial T_y} = BT_x \tag{5.72}$$

where

$$B = \cos^2 2\theta_T \, P^*/2 \ . \tag{5.73}$$

SECTION VI. TEST OF THE REMOTE REFERENCE METHOD

This section describes in detail a test of the remote reference technique using data collected simultaneously at two sounding sites called Upper and Lower La Gloria. To assess the quality of the data as compared with those obtained from other surveys they were analyzed using $\underline{\underline{Z}}^H$. I also include the apparent resistivities as calculated via $\underline{\underline{Z}}^E$ and method I, the crosspower solution of the eight equations. The data from Upper La Gloria were among the best we have collected, those from Lower La Gloria were among the worst. $\underline{\underline{Z}}^R$ produced excellent results in every case.

Data

We established two complete magnetotelluric sounding stations separated by 4.8 km on La Gloria road in Bear Valley, California, at the sites shown in figure 9. The Upper La Gloria station is in hilly terrain where the geology consists chiefly of granites, while the Lower La Gloria station is in a level area over a zone of low resistivity,[18] and is slightly east of a fault that separates this zone from the granites. Lower La Gloria is about 2 km west of the San Andreas Rift Zone which runs in a northwesterly direction.

For the electric field measurements we used the Pb electrodes installed by Corwin for dipole-dipole resistivity monitoring.[20] The location of the electrodes is shown in figure 9. Electrodes E_1 and E_2 were the common electrodes at the lower and upper stations, respectively. The nonorthogonality of the telluric arrays was taken into account in the analysis. For the magnetic field measurements we used our dc

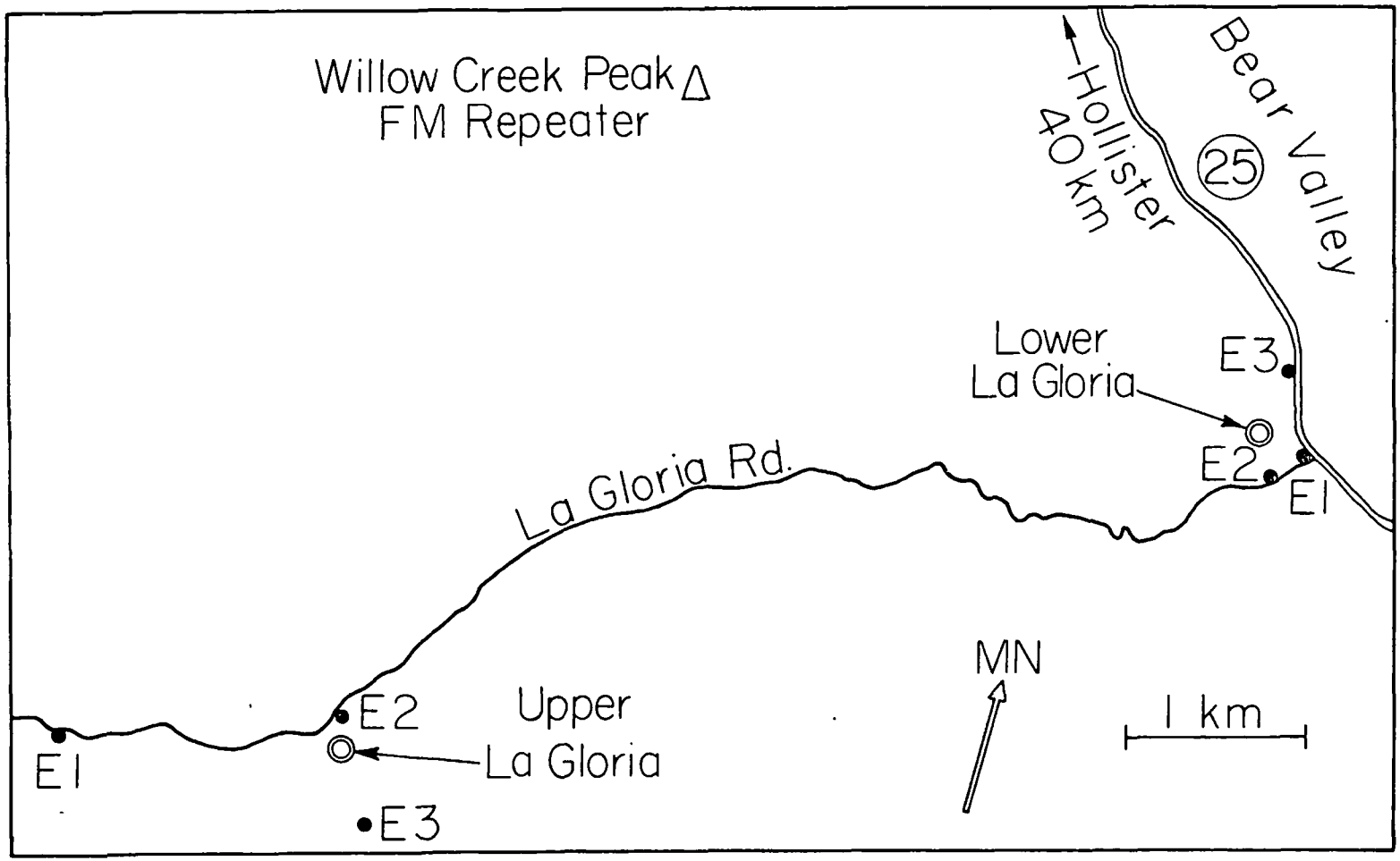

Fig. 9. Sites near Hollister, California, where magnetotelluric data were recorded simultaneously. Dots denote electrodes, double circles denote magnetometers.

XBL7712-6514

SQUID magnetometer at Lower La Gloria, and an rf SQUID magnetometer manufactured by S.H.E. Corporation at Upper La Gloria whose magnetic field sensitivity was approximately 10^{-4} γ $Hz^{-1/2}$. The magnetometer at each site was used as the reference for the signals at the other site.

The data from both sites were recorded simultaneously. A block diagram of the measurement electronics appears in figure 10. The equipment at Lower La Gloria was battery powered, while that at Upper La Gloria was powered by a 60 Hz generator. Each signal was passed through a preamplifier that contained a high-pass filter to attenuate the large-amplitude low-frequency signals that could have exceeded the dynamic range of the electronics. Each preamplifier was followed by a 60-Hz notch filter. The signals from Lower La Gloria were transmitted to Upper La Gloria by FM telemetry via a repeater on Willow Creek Peak. At Upper La Gloria we passed each of the signals through a four-pole band-pass filter, digitized the signals with 12-bit resolution, and recorded the data on a nine-track digital recorder. The data were acquired in the four overlapping bands listed in table IV. Band 4 was intended to include periods from 30 s to 1000 s, but an error in setting the highpass filter of the telemetry preamplifier at the remote site resulted in the longest period being 100 s. The times required for data collection and the sampling periods are also listed in table IV. We recorded all the data within a 40 hour period, making only brief interruptions to change gains and filter bands and to replace batteries. All the recorded data were processed using the

Table IV. Summary of filter bands, recording time per band, digitizer sampling period, and the number of points per fast Fourier transform (FFT).

Filter band no.	Filter band (s)	Total recording time (h)	Digitizer sampling periods (s)	No. of points in data segments
1	0.02 - 1	0.54	0.005	1024
2	0.33 - 5	4.22	0.1	512
3	3 - 100	10.52	1	512
4	30 - 100	14.9	10	256

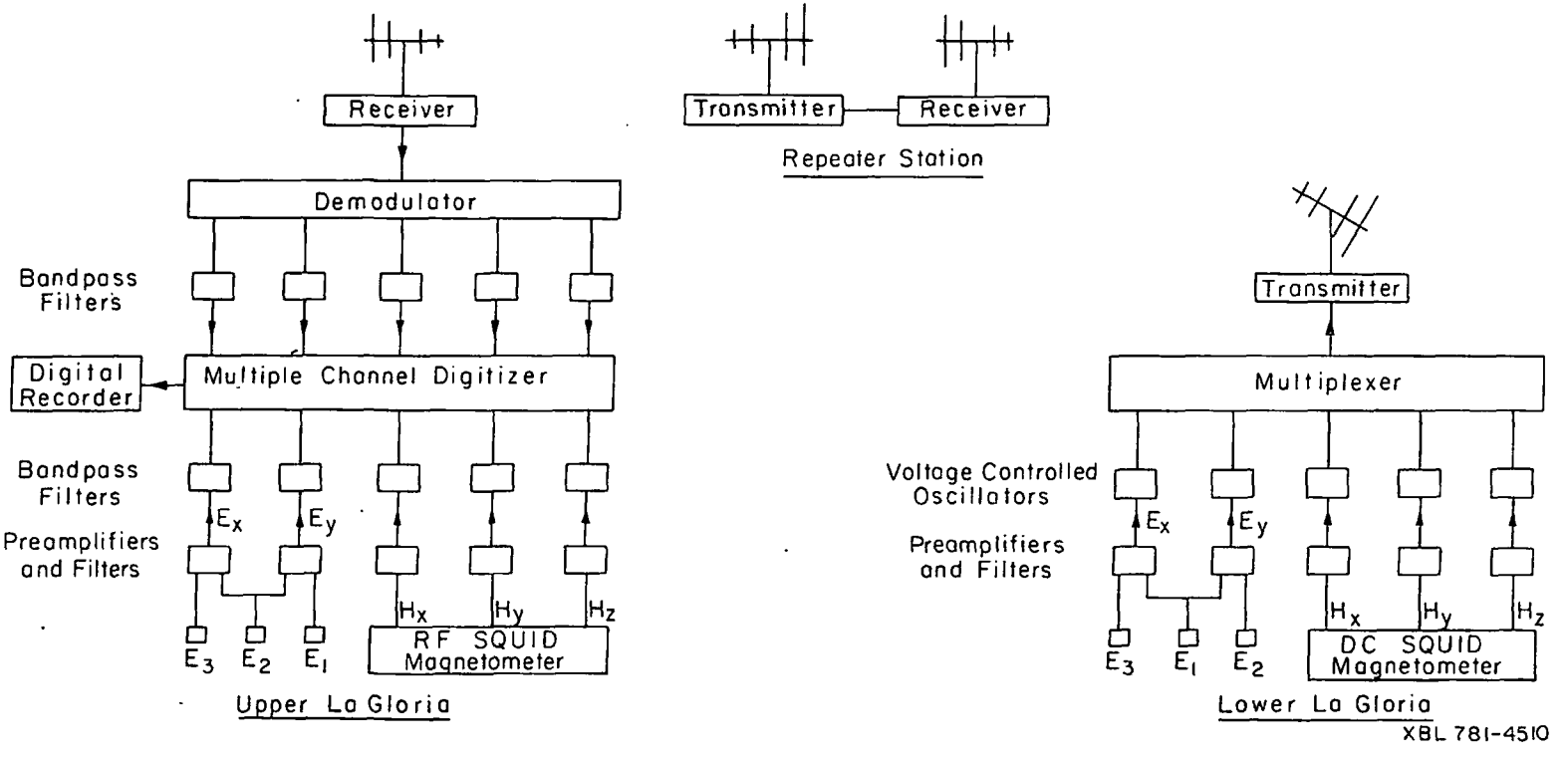

Fig. 10. Block diagram of data acquisition.

procedures in section III except those rendered meaningless by equipment failure, amplifier saturation or obvious magnetic interference from passing vehicles. The lengths of the data segments are shown in table IV. The center period of each frequency window, the number of harmonics in each window and the number of data segments are given in table V.

Results

The results are graphed versus period for Upper La Gloria in figures 11 through 21 and for Lower La Gloria in figure 22 through 32. Figure 11 contains the correlation coefficients C_x and C_y in the rotated coordinate system. Figures 12 through 14 contain the rotated apparent resistivies from $\underline{\underline{Z}}^E$, method I, and $\underline{\underline{Z}}^H$, respectively. The apparent resistivities from the remote reference method are indicated on these figures by a dashed line to facilitate comparison of the methods and are plotted with their probable errors in figure 16.

Consider the apparent resistivities from $\underline{\underline{Z}}^E$, $\underline{\underline{Z}}^H$ and $\underline{\underline{Z}}^R$, figures 12, 14 and 16. In 60 of 64 cases the apparent resitivity from $\underline{\underline{Z}}^E$ is larger than, and that from $\underline{\underline{Z}}^H$ is smaller than, that from $\underline{\underline{Z}}^R$. This regular ordering of the apparent resistivities demonstrates that the bias error in at least two of the estimates is large compared to the random error in any of them and it strongly suggests that the bias is due to the measured autopowers in the least squares estimates. Comparing the differences between $\underline{\underline{Z}}^E$ and $\underline{\underline{Z}}^H$, figures 12 and 14, with C, figure 11, we see that the relative bias usually but not always increases as C decreases. For instance, ρ_{yx} from $\underline{\underline{Z}}^H$ at 0.032 second period has the

Table V. Number of harmonics per window, and numbers of sets of data segments for each station.

Band no. 1		Band no. 2		Band no. 3		Band no. 4	
Period (s)	Harmonics per window	Period (s)	Harmonics per window	Period (s)	Harmonics per window	Period (s)	Harmonics per window
0.023	75	0.325	52	3.3	52	32.0	13
0.032	53	0.45	37	4.5	37	41.1	9
0.044	38	0.63	27	6.3	27	60.9	7
0.062	27	0.88	19	8.8	19	85.3	5
0.085	19	1.2	14	12	14		
0.12	14	1.7	10	17	10		
0.16	10	2.4	7	24	7		
0.22	7	3.4	5	34	5		
0.30	5			49	4		
0.41	4						
0.57	3						
0.79	2						

	Number of sets of data segments			
Upper La Gloria	476	297	73	21
Lower La Gloria	381	297	73	21

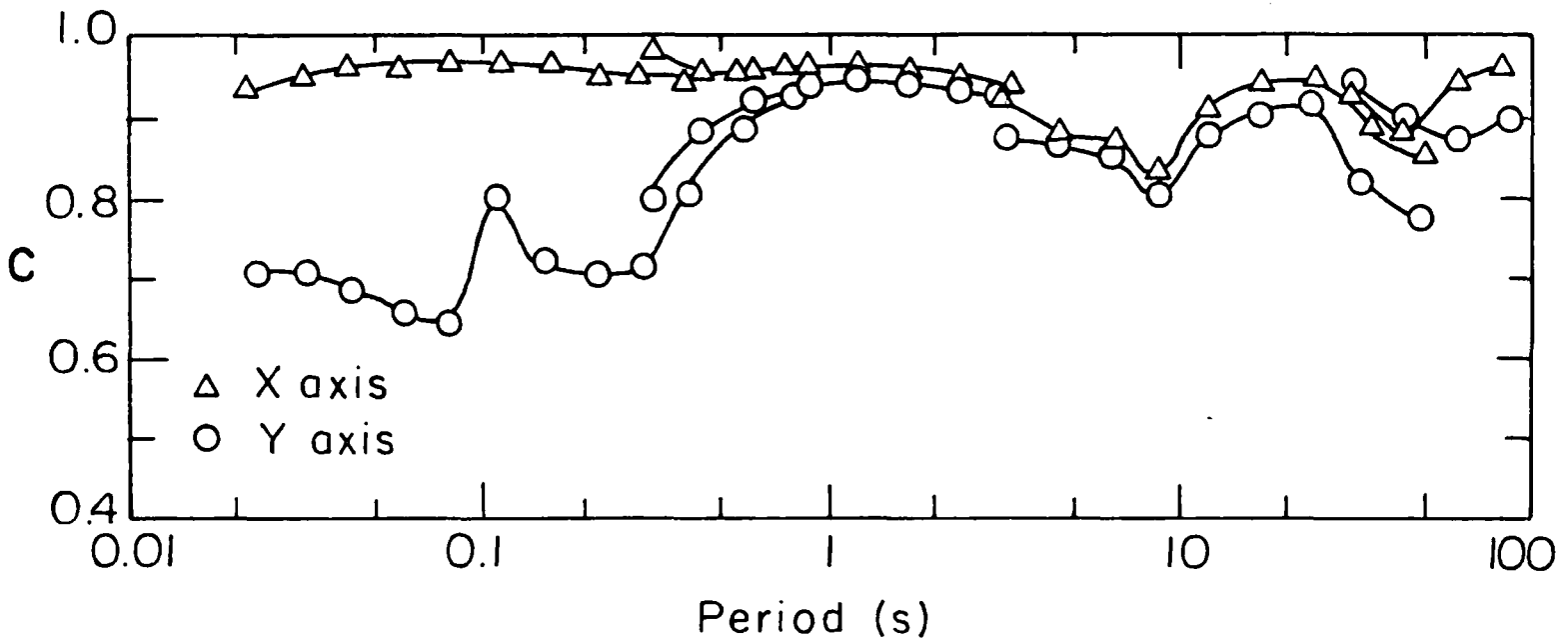

XBL 7712-6516

Fig. 11. Correlation coefficients, C_x and C_y from equation (1.29), versus period for the data from Upper La Gloria.

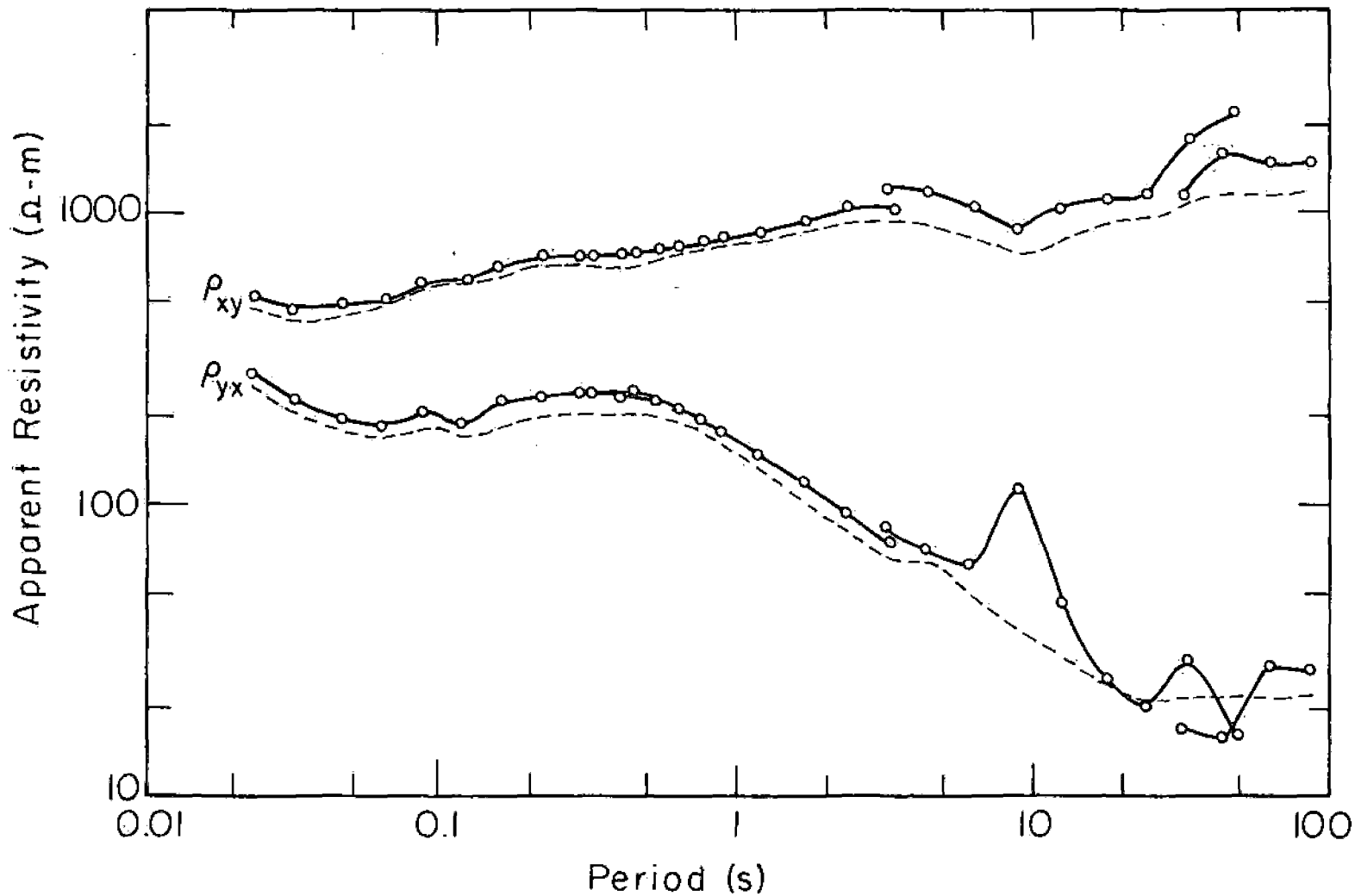

XBL 7712-6517

Fig. 12. Rotated apparent resistivities from $\underline{\underline{Z}}^{E}$ versus period, Upper La Gloria. ------ remote reference results.

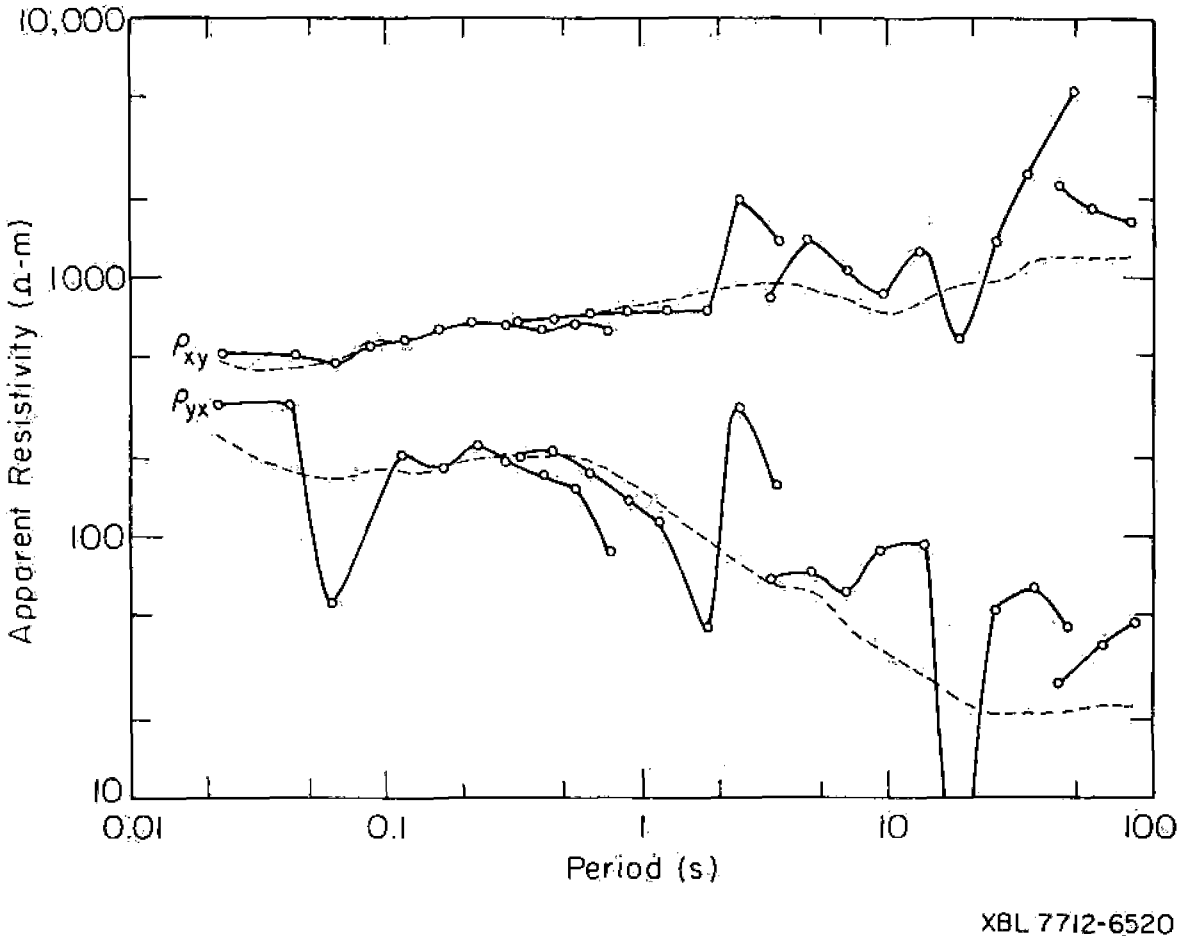

Fig. 13. Rotated apparent resistivities from method I, crosspower solution of eight equations, versus period, Upper La Gloria. ------remote reference results.

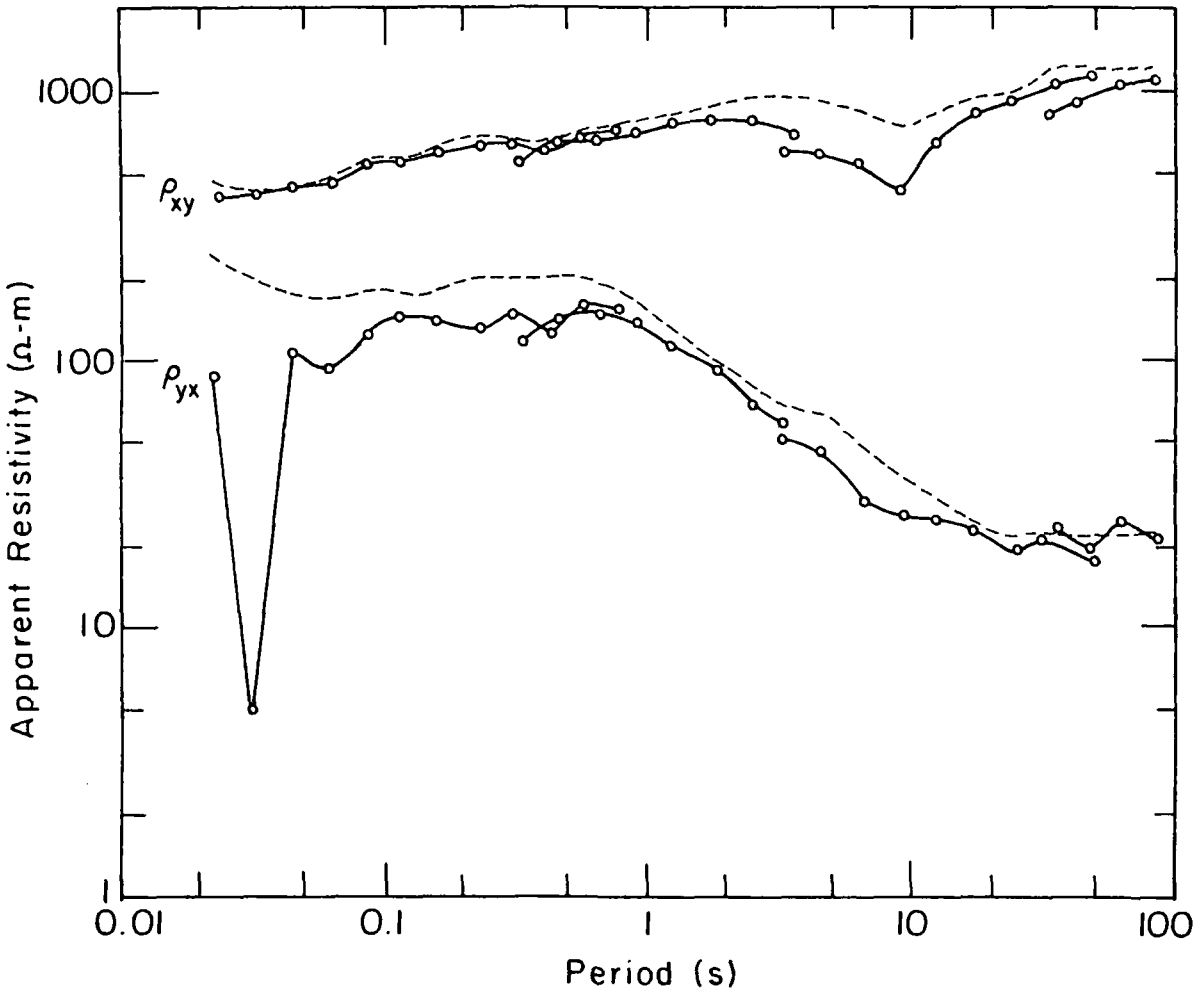

Fig. 14. Rotated apparent resistivities from $\underline{\underline{Z}}^H$ versus period, Upper La Gloria. ------ remote reference results.

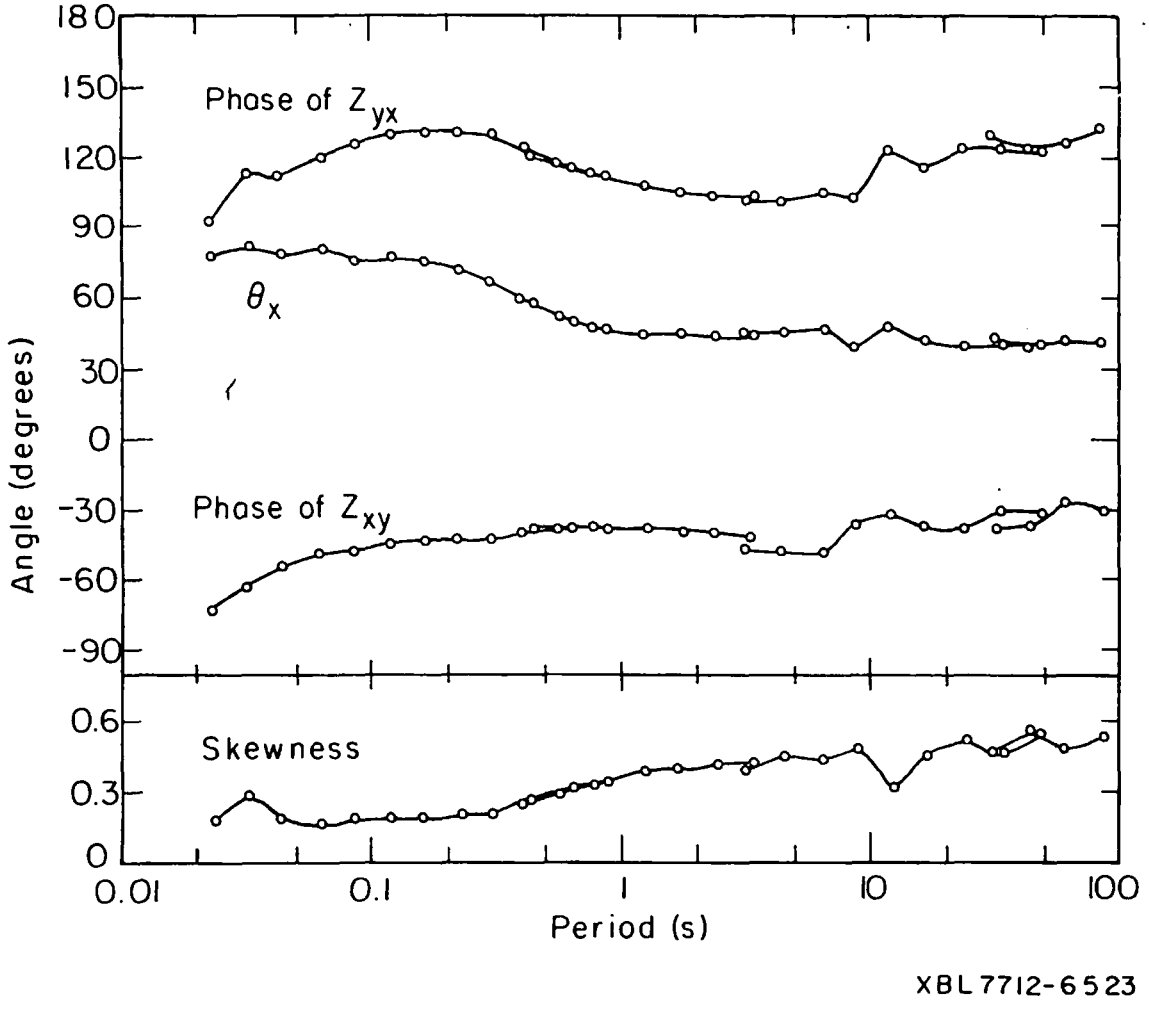

Fig. 15. The angle, θ_x, between magnetic north and the $\hat{x}$ axis of the coordinate system aligned with the apparent strike direction, skewness, and phases of Z_{xy} and Z_{yx} versus period from $\underset{\approx}{Z}^H$, Upper La Gloria.

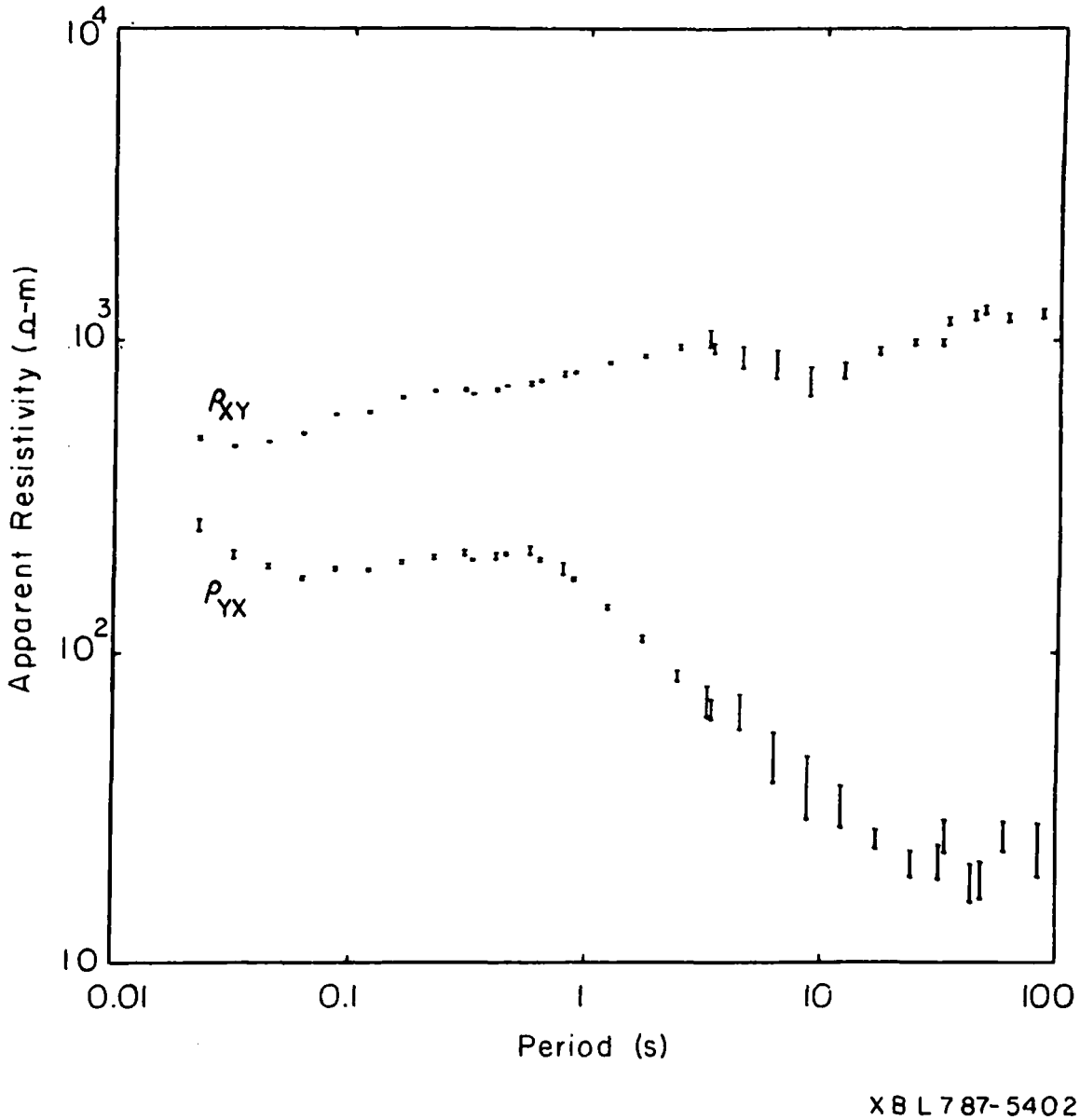

Fig. 16. Rotated apparent resistivities from $\overset{\approx}{Z}^R$ and their probable errors versus period, Upper La Gloria.

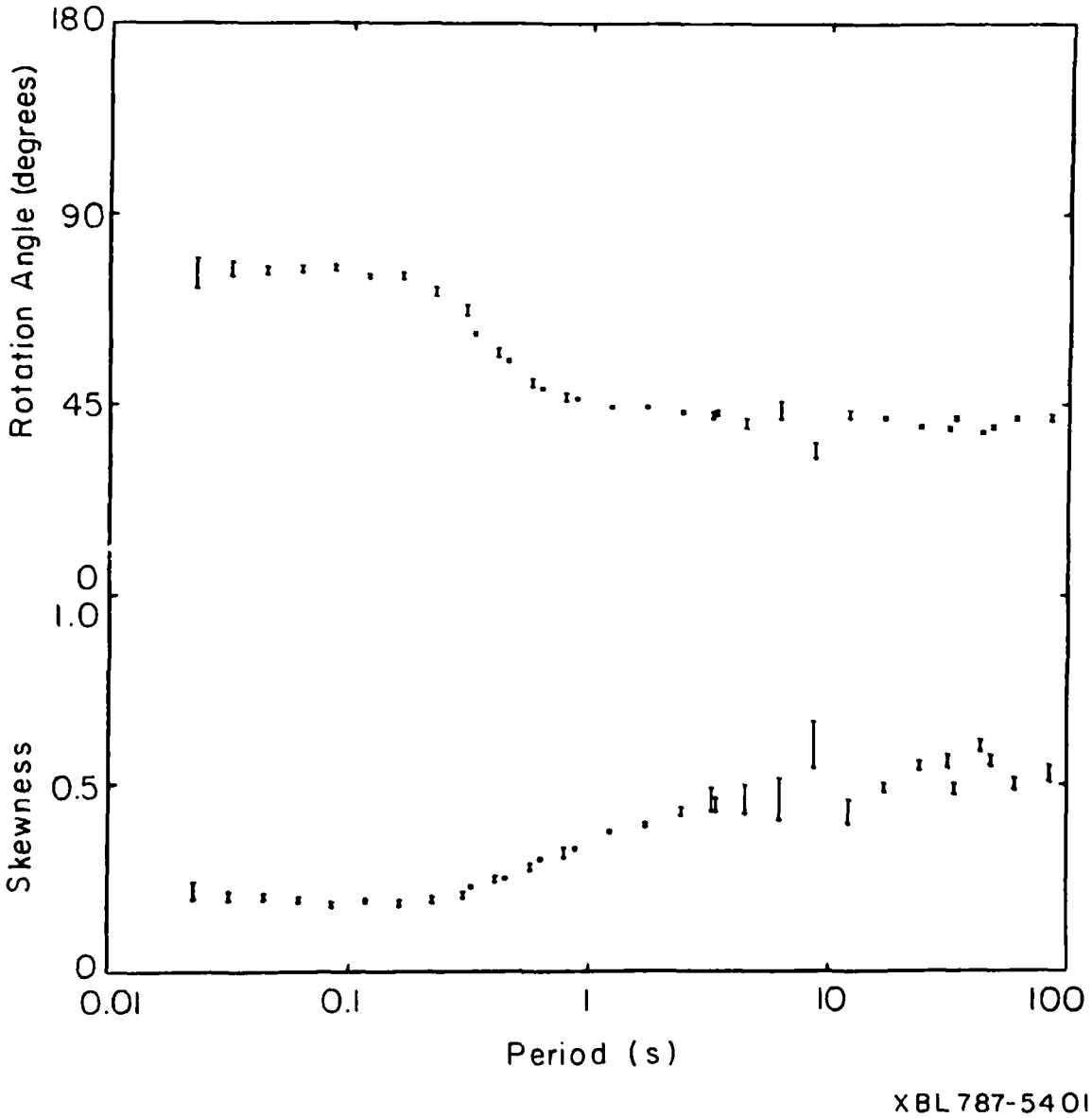

Fig. 17. The angle between magnetic north and the $\hat{x}$ axis of the coordinate system aligned with the apparent strike direction and the skewness from Z^R with their probable errors versus period, Upper La Gloria.

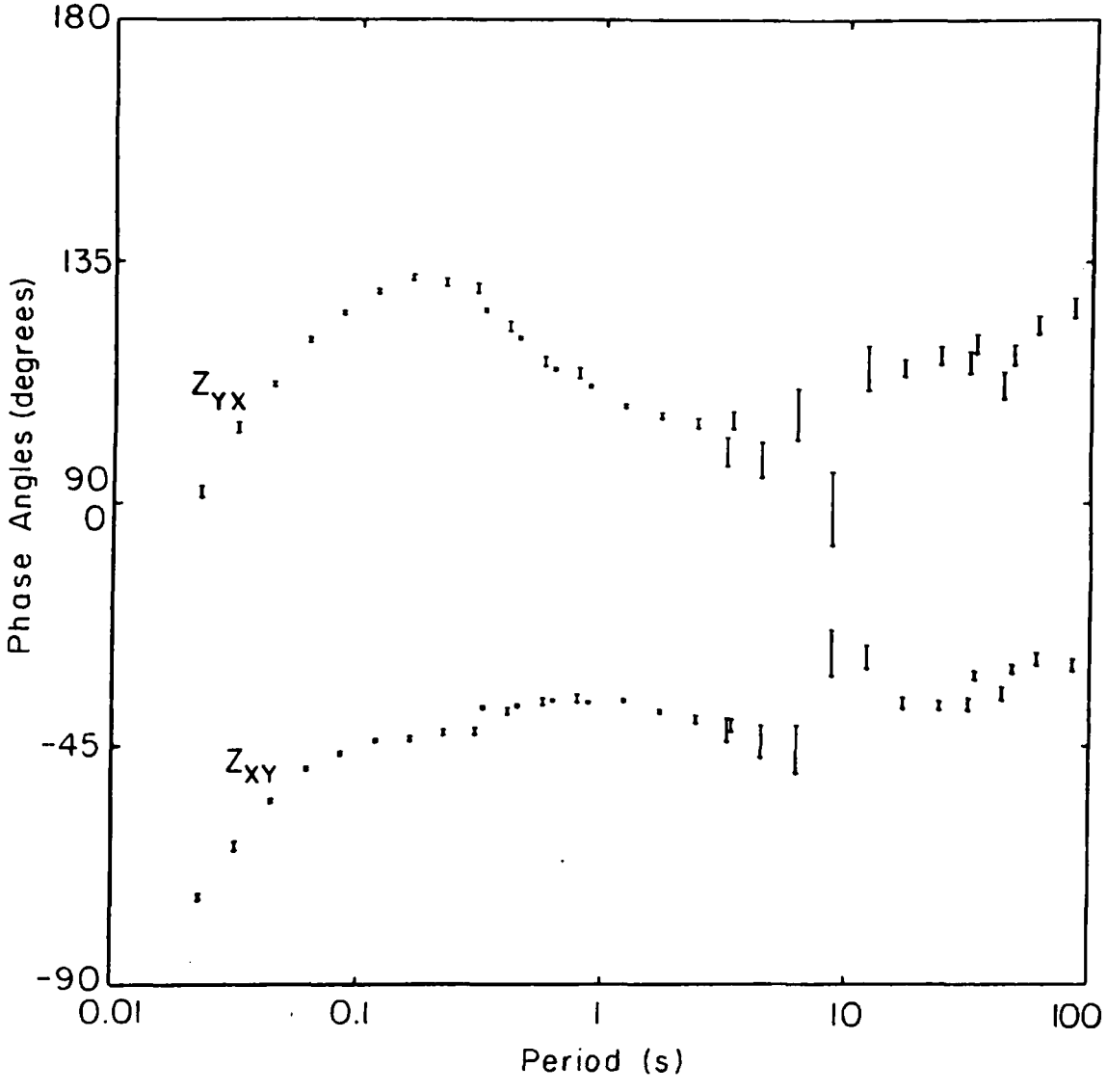

Fig. 18. Phases from $\underset{\approx}{Z}^{R}$ and their probable errors versus period, Upper La Gloria.

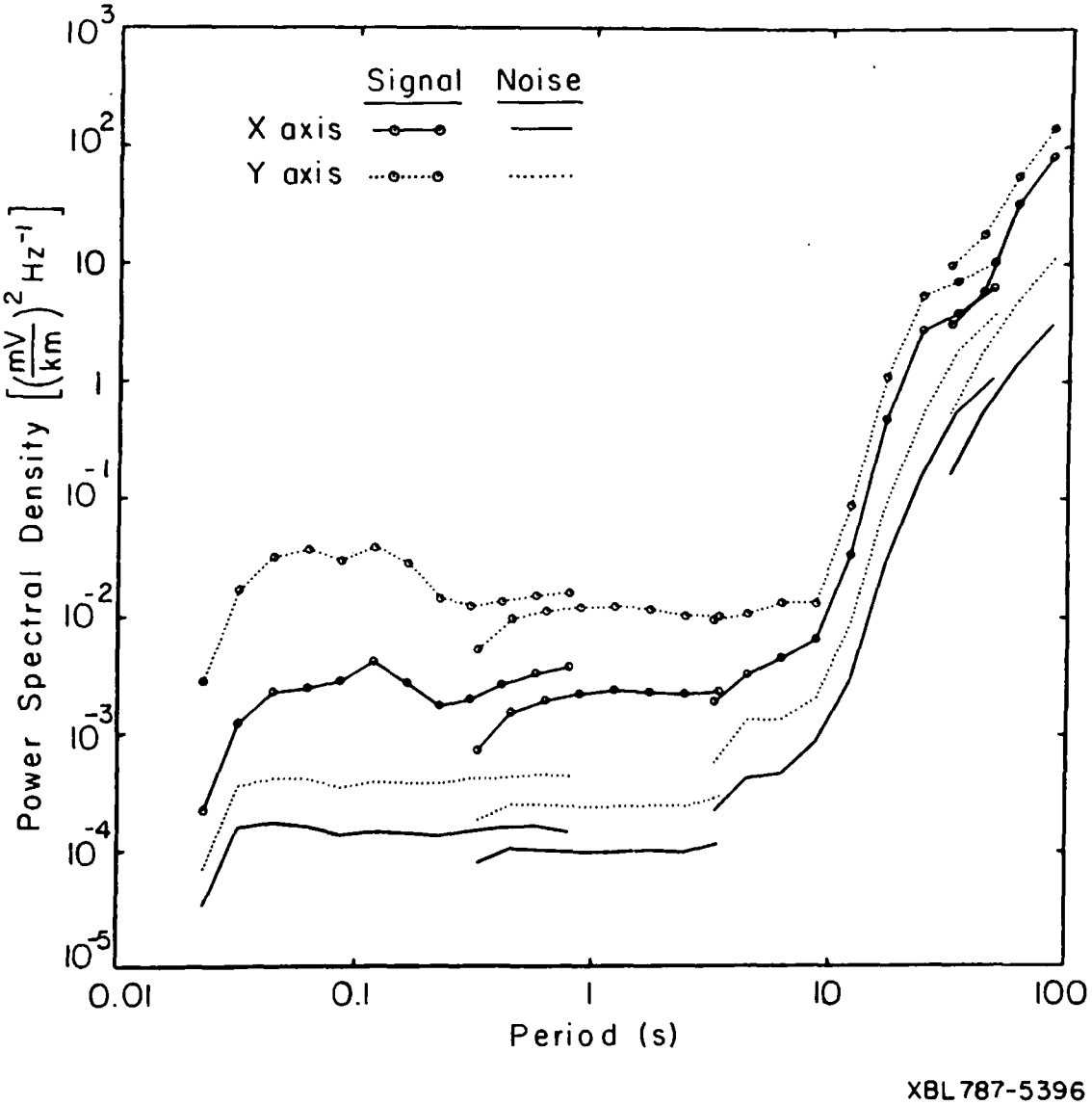

Fig. 19. Electric field signal and noise power spectra versus period, Upper La Gloria.

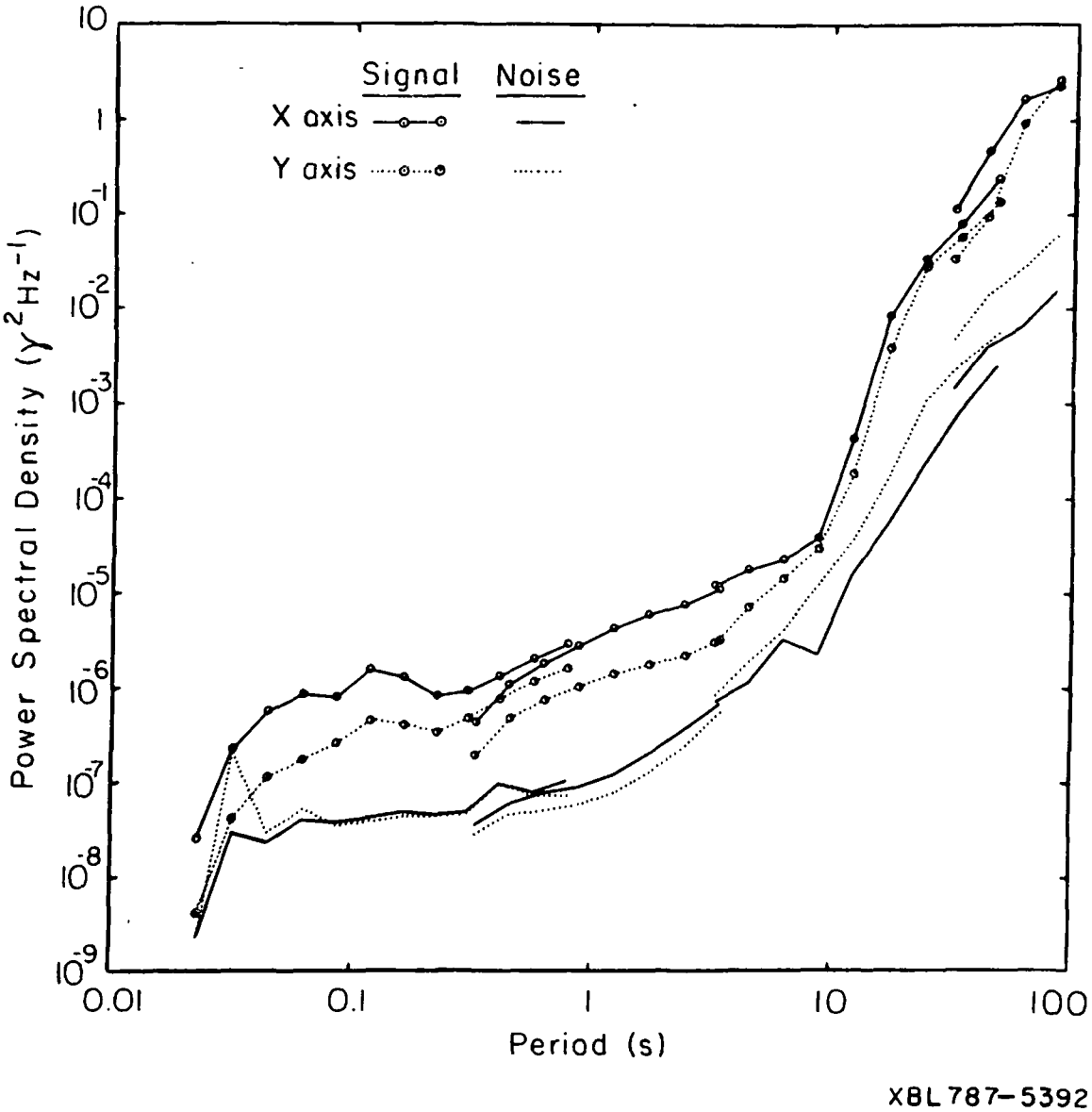

Fig. 20. Magnetic field signal and noise power spectra versus period, Upper La Gloria.

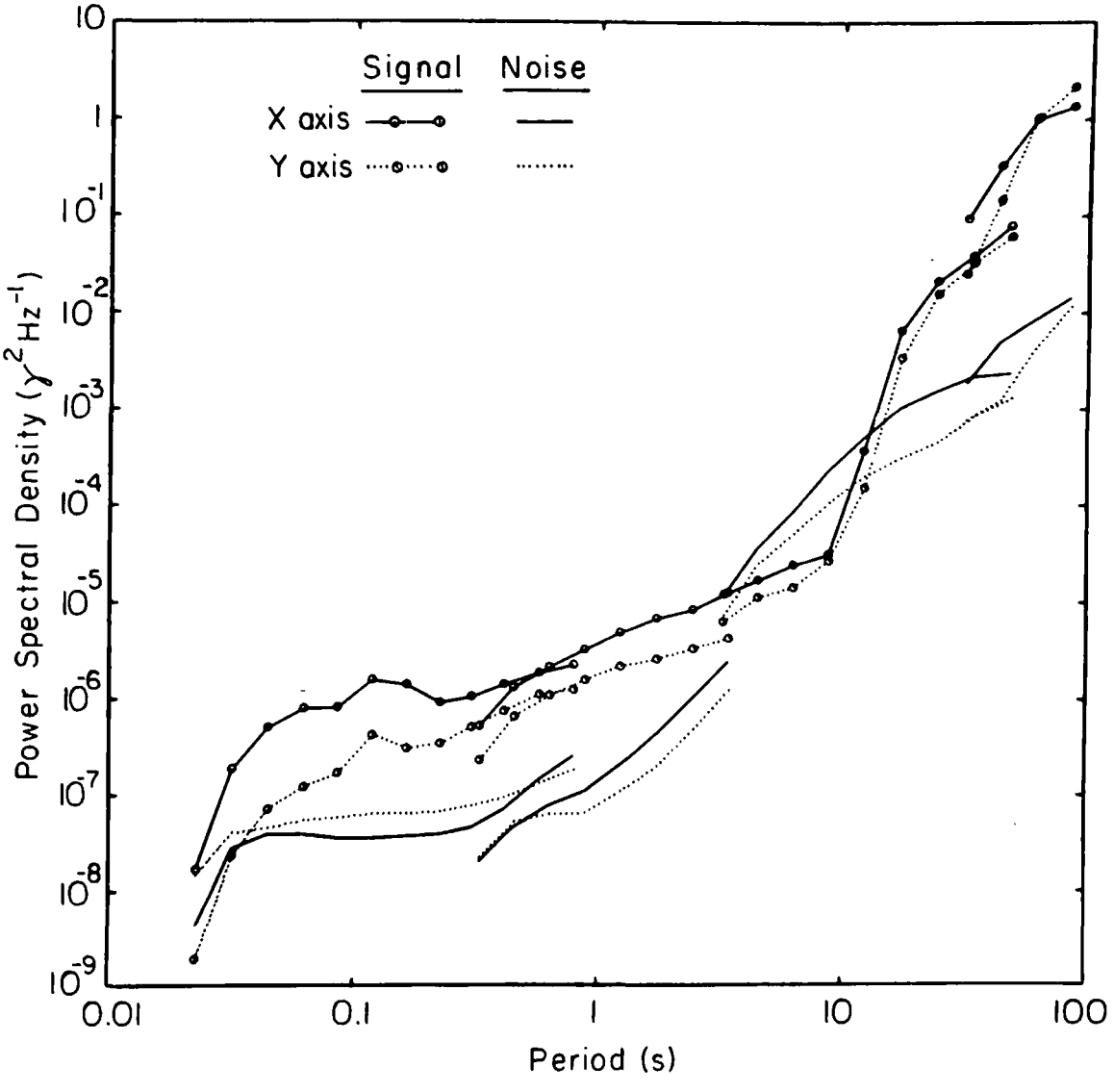

Fig. 21. Remote magnetic reference signal and noise power spectra versus period, Upper La Gloria.

largest bias of any of the results from this station, possibly due to magnetic noise from the 60 Hz generator, and yet C_y for that window is actually higher than for the adjacent frequency windows. Thus C is only a very rough indication of the accuracy of the least squares results.

The apparent resistivities from method I, figure 13, are far more scattered than those from the other estimates. The best results from this method are for ρ_{xy} at periods shorter than 1 s, where C_x is greater than 0.9. Here, they are still scattered over the 10% range of the disagreement between the $\underset{\approx}{Z}^H$ and $\underset{\approx}{Z}^E$ resistivities. Note that no value of apparent resistivity has been plotted at 0.032 s period for method I. This is because the predicted autopowers were not real. Thus we know that there is some significant noise in this window even through C_y is higher than in the adjacent windows.

Because of the large random errors in method I and the bias errors in the two least-squares estimates they are not reliable estimates of the apparent resistivity when the C_i are less than 0.9. If we were to reject all resistivities for which C_y is below 0.9, we could retain only 11 values for ρ_{yx}, all at periods longer than 0.5 seconds.

The remote reference signal and noise spectra, figures 19-21 contain six times as much information as the least squares C_i. They are calculated in a coordinate system with the $\hat{x}$ axis pointing towards magnetic north and have not been corrected for the 60 Hz notch. The peak in the noise power in H_y at 0.032 second period shows up clearly and the bias of the least squares estimates is well predicted by the noise to signal ratio from these spectra.

Because of random errors in the calculated signal spectral density matrices, it is possible for the calculated noise power to be negative. This behavior was never observed at this station, even though the signal-to-noise ratios varied from 100:1 for E_y at 0.1 second period and 200:1 for H_y at 85 second period to 1:7 for R_x at 9 second period. The signal power spectra for these data are particularly steep; for example, around 15 second period they increase roughly as the 8th power of the period. Nonetheless, the calculated noise spectra are comparatively smooth, indicating that the random errors are small.

The non-Hermitian parts of the predicted autopower spectral density matrices were very small. For example, the imaginary parts of the predicted autopowers (such as $\overline{E_x^P E_x^*}$) were always less than 10% of the real parts, and averaged about 1%. For periods shorter than 3 seconds, where we had the most data, they were always less than 2%. Thus, even if the noise coherencies were statistically significant, they were too small to have any practical importance in the remote reference calculations.

$\underline{\underline{Z}}^H$ and $\underline{\underline{Z}}^R$ gave similar estimates of the other parameters: apparent strike direction (equation 5.31), phase angles and skewness (equation 1.17), at Upper La Gloria, figures 15, 17 and 18. The only difference, which may be too small to see in the graphical representation, is that there was a scatter in the value of the apparent strike direction of about $\pm$ 3° when estimated by $\underline{\underline{Z}}^H$ that was absent when $\underline{\underline{Z}}^R$ was used.

While the data from Lower La Gloria were much noisier, the same observations about the bias hold true. Apparent resistivities from

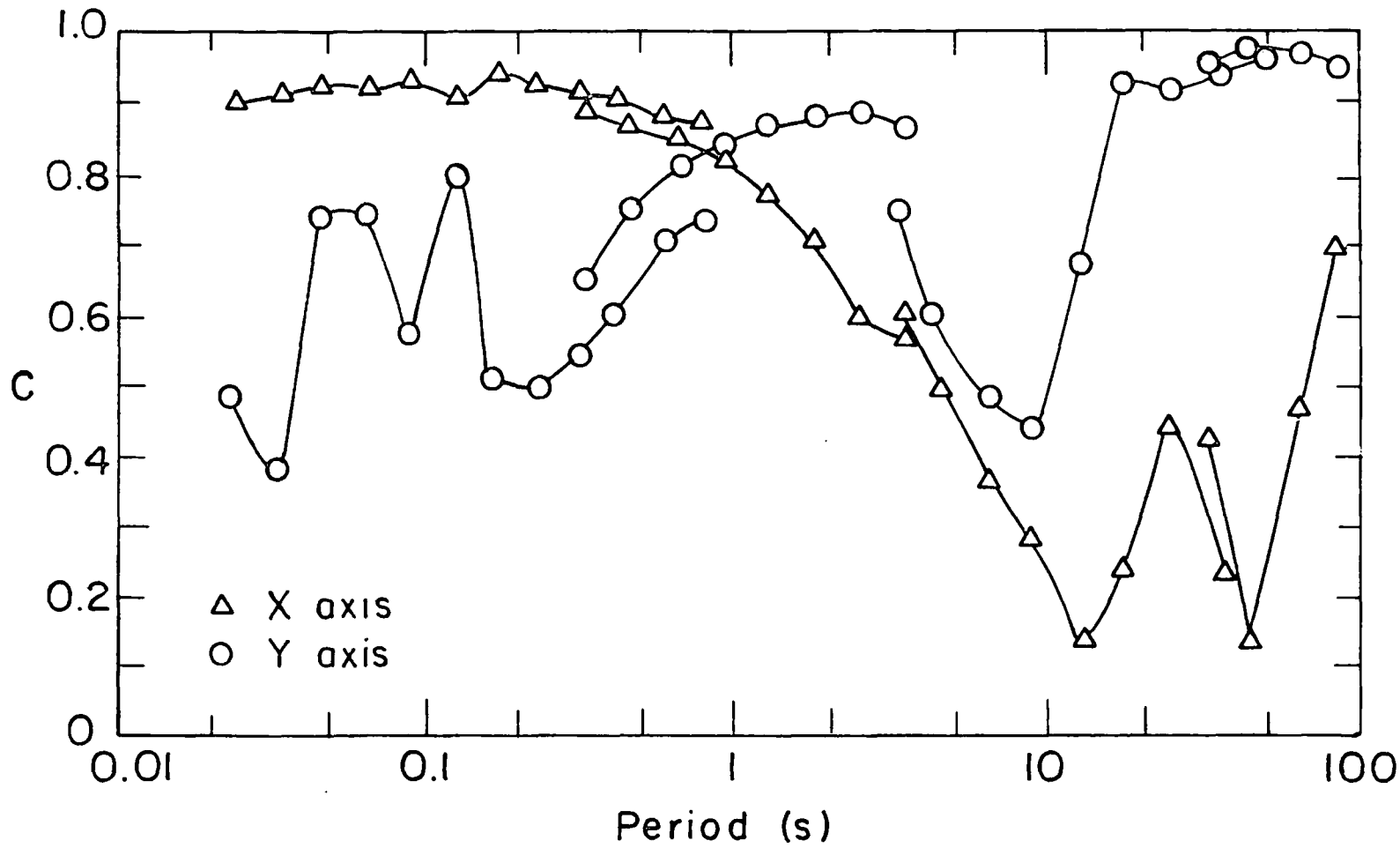

Fig. 22. Correlation coefficients, C_x and C_y from equation (1.29), versus period for the data from Lower La Gloria.

XBL 7712-6515

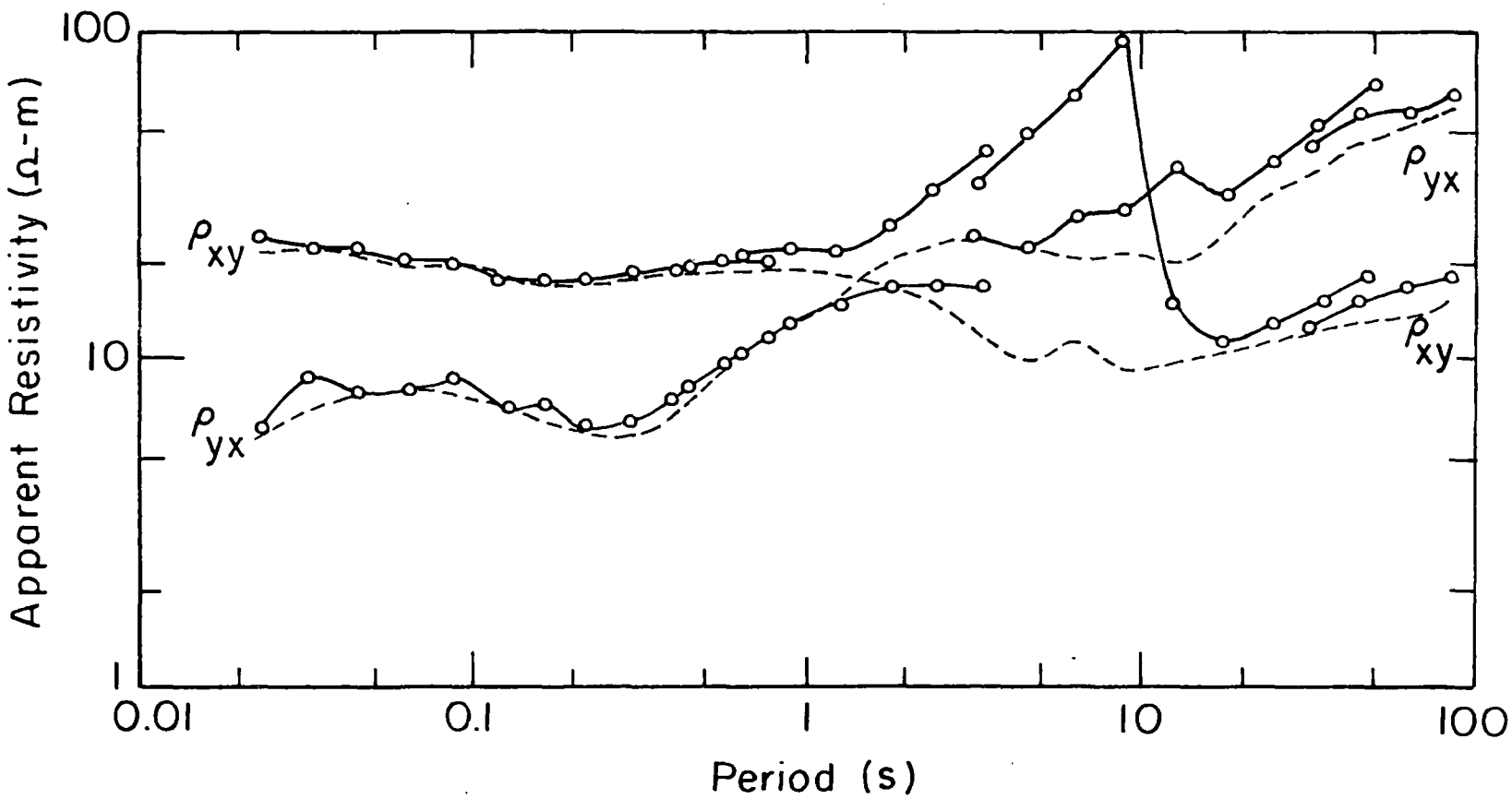

Fig. 23. Rotated apparent resistivities from $\underline{\underline{Z}}^E$ versus period, Lower La Gloria. ----- remote reference results.

XBL7712-6518

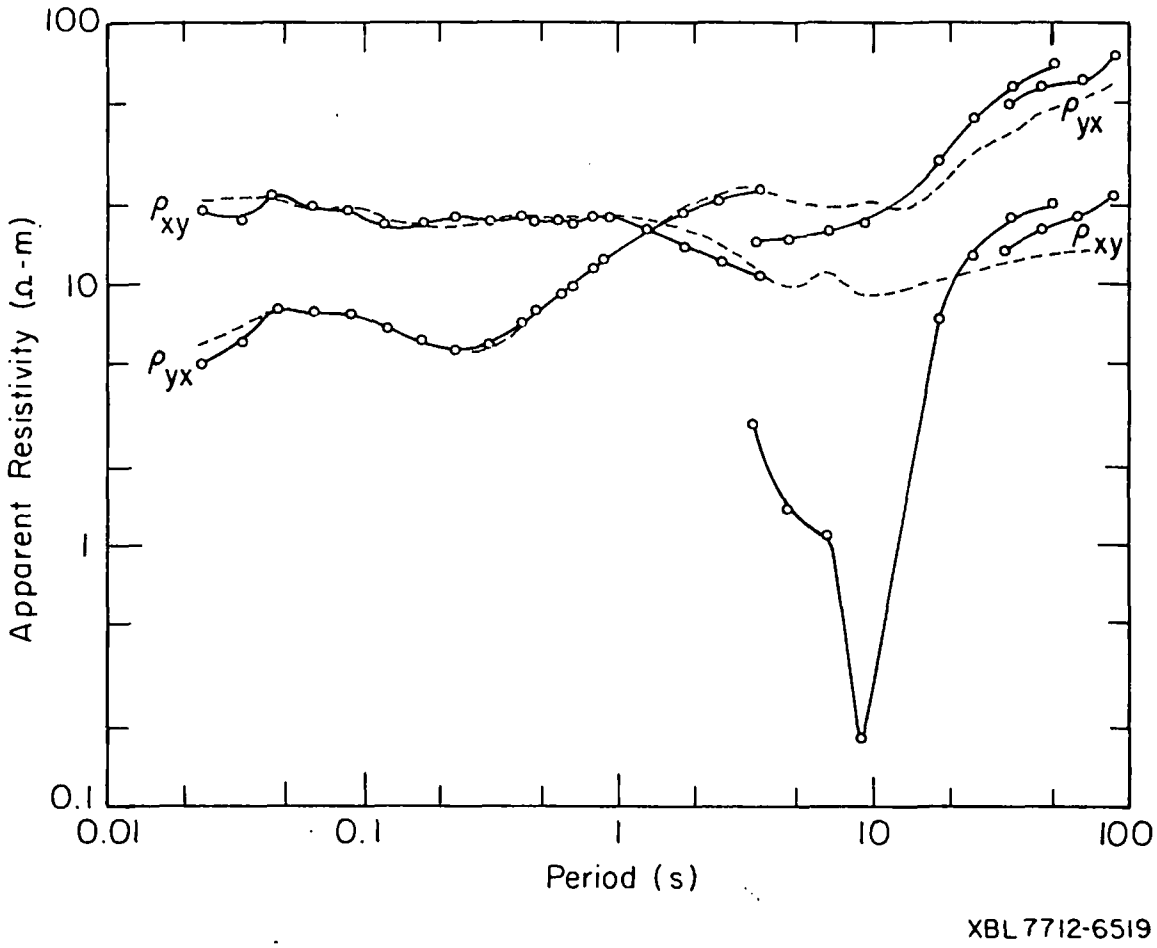

Fig. 24. Rotated apparent resistivities from method I, crosspower solution of eight equations, versus period, Lower La Gloria. ----- remote reference results.

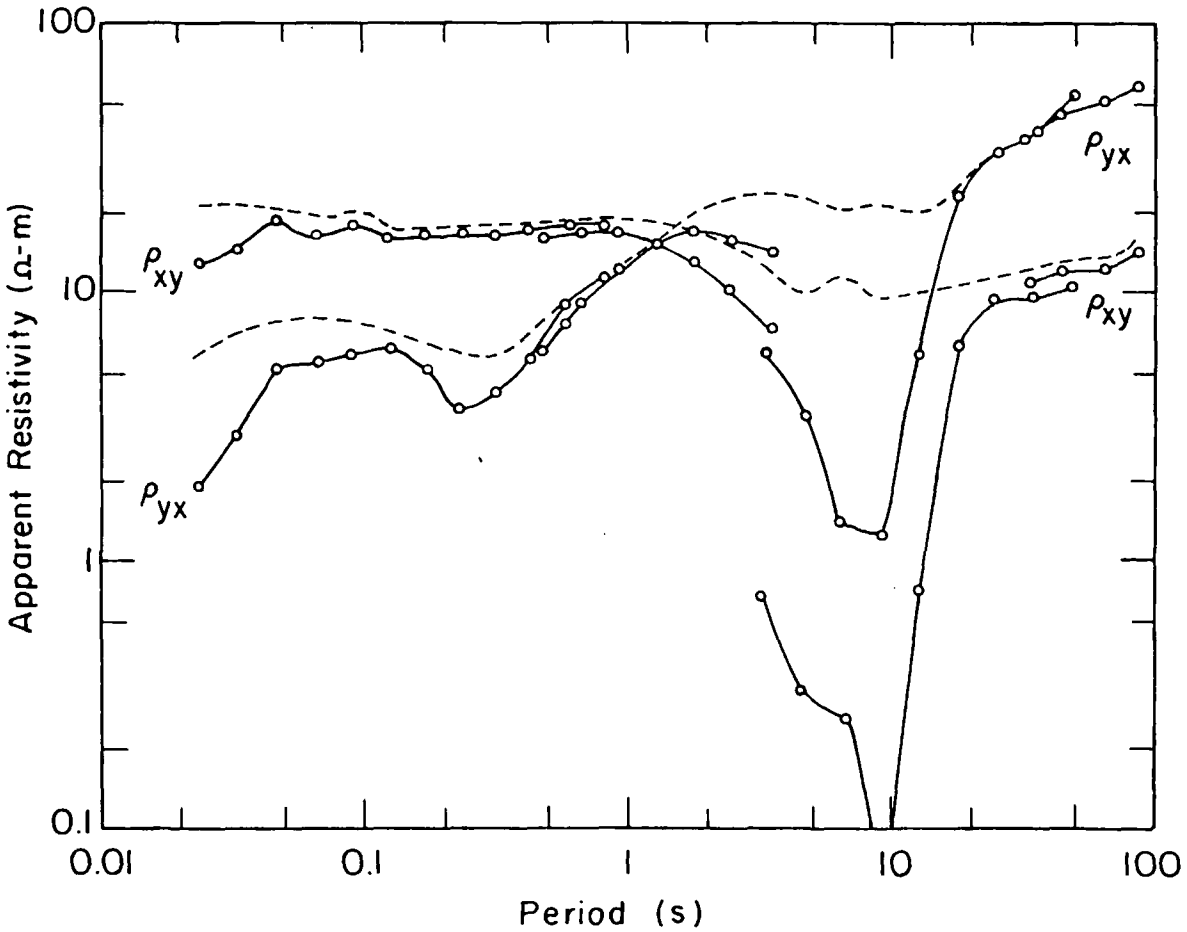

Fig. 25. Rotated apparent resistivities from $\underline{\underline{Z}}^H$ versus period. Lower La Gloria. ----- remote reference results.

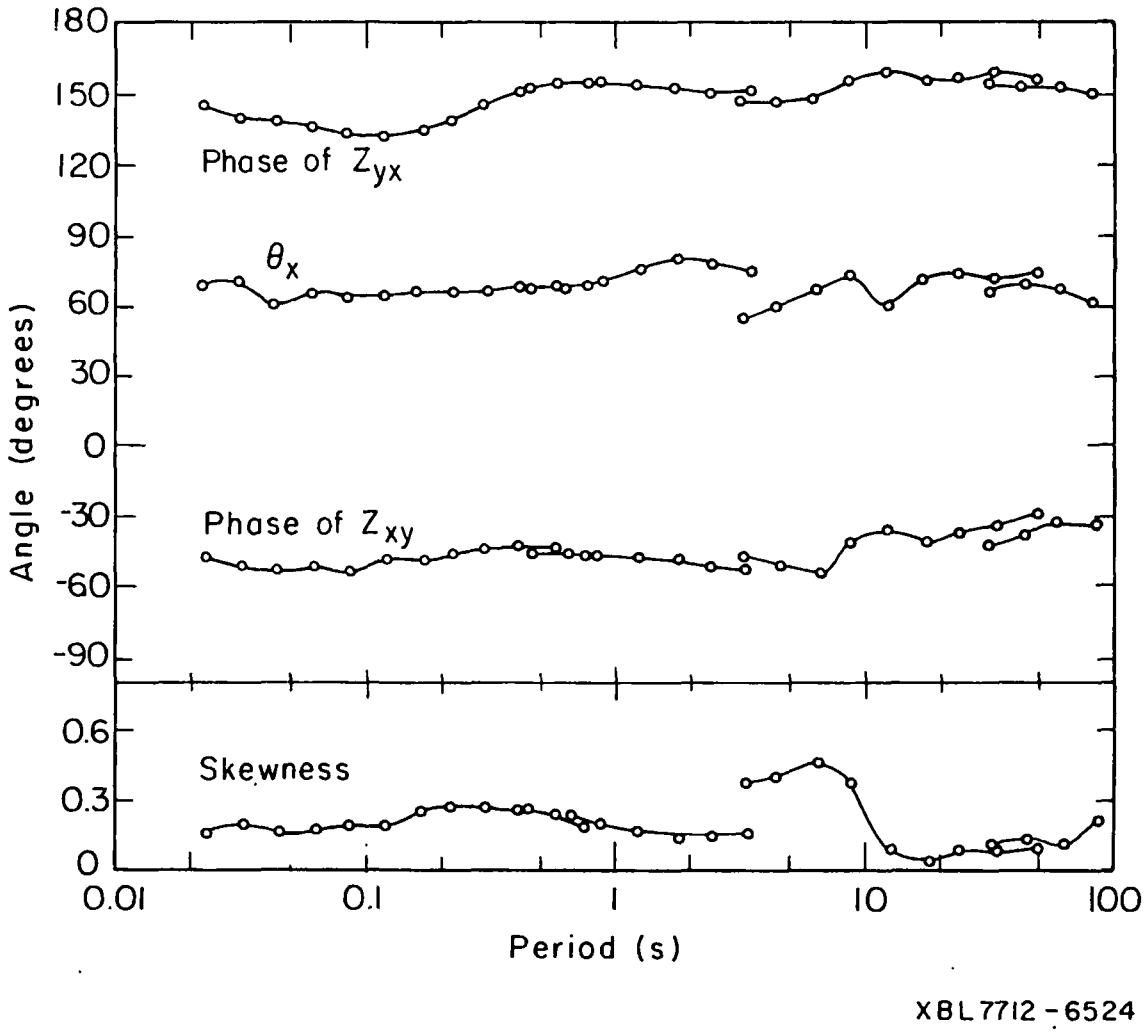

Fig. 26. The angle, θ_x, between magnetic north and the $\hat{x}$ axis of the coordinate system aligned with the apparent strike direction, skewness, and phases of Z_{xy} and Z_{yx} versus period from $\underset{\approx}{Z}^H$, Lower La Gloria.

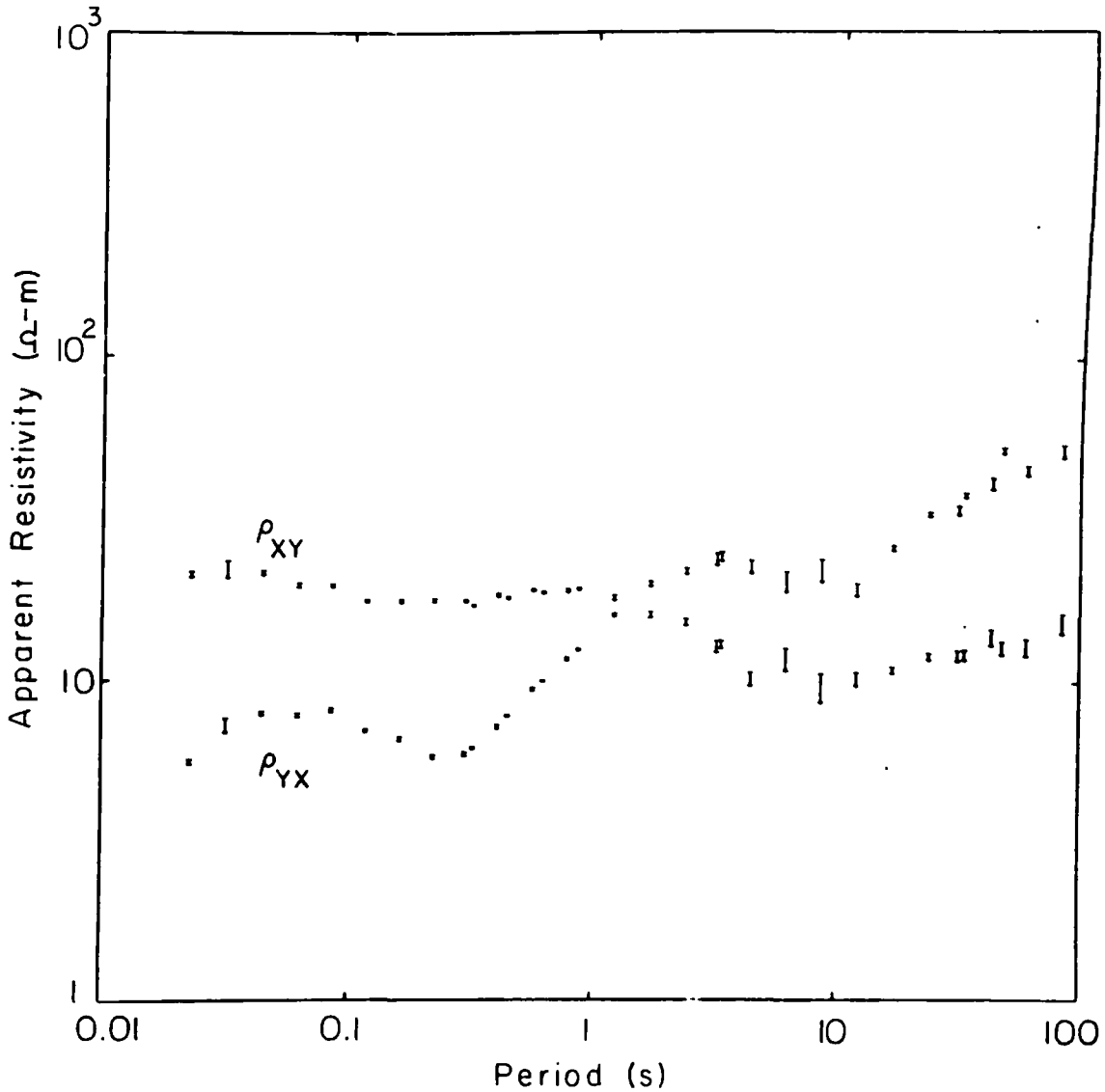

Fig. 27. Rotated apparent resistivities from $\underline{\underline{Z}}^R$ and their probable errors versus period, Lower La Gloria.

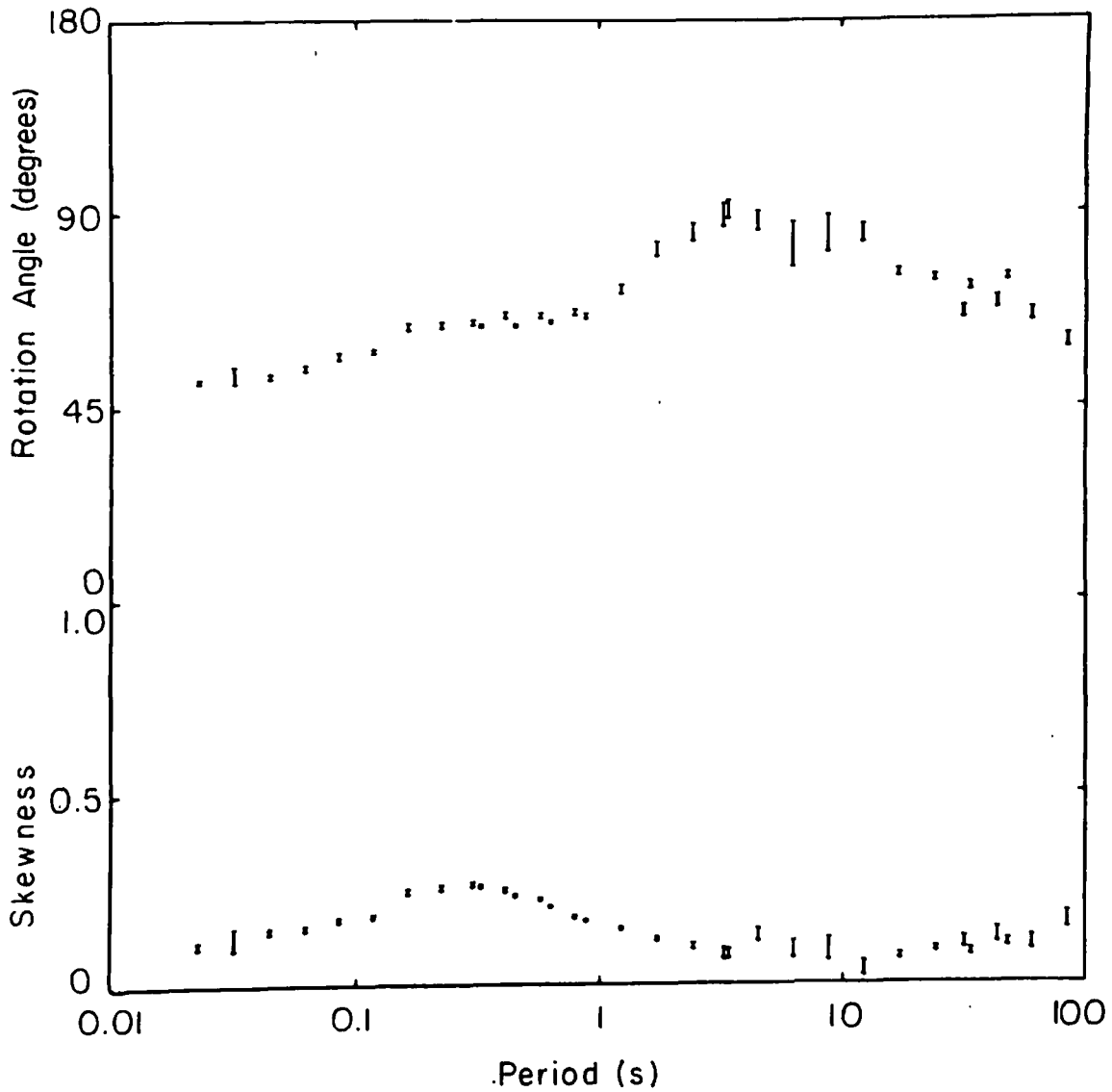

Fig. 28. The angle between magnetic north and the $\hat{x}$ axis of the coordinate system aligned with the apparent strike direction and the skewness from $\underset{\approx}{Z}^R$ with their probable errors versus period, Lower La Gloria.

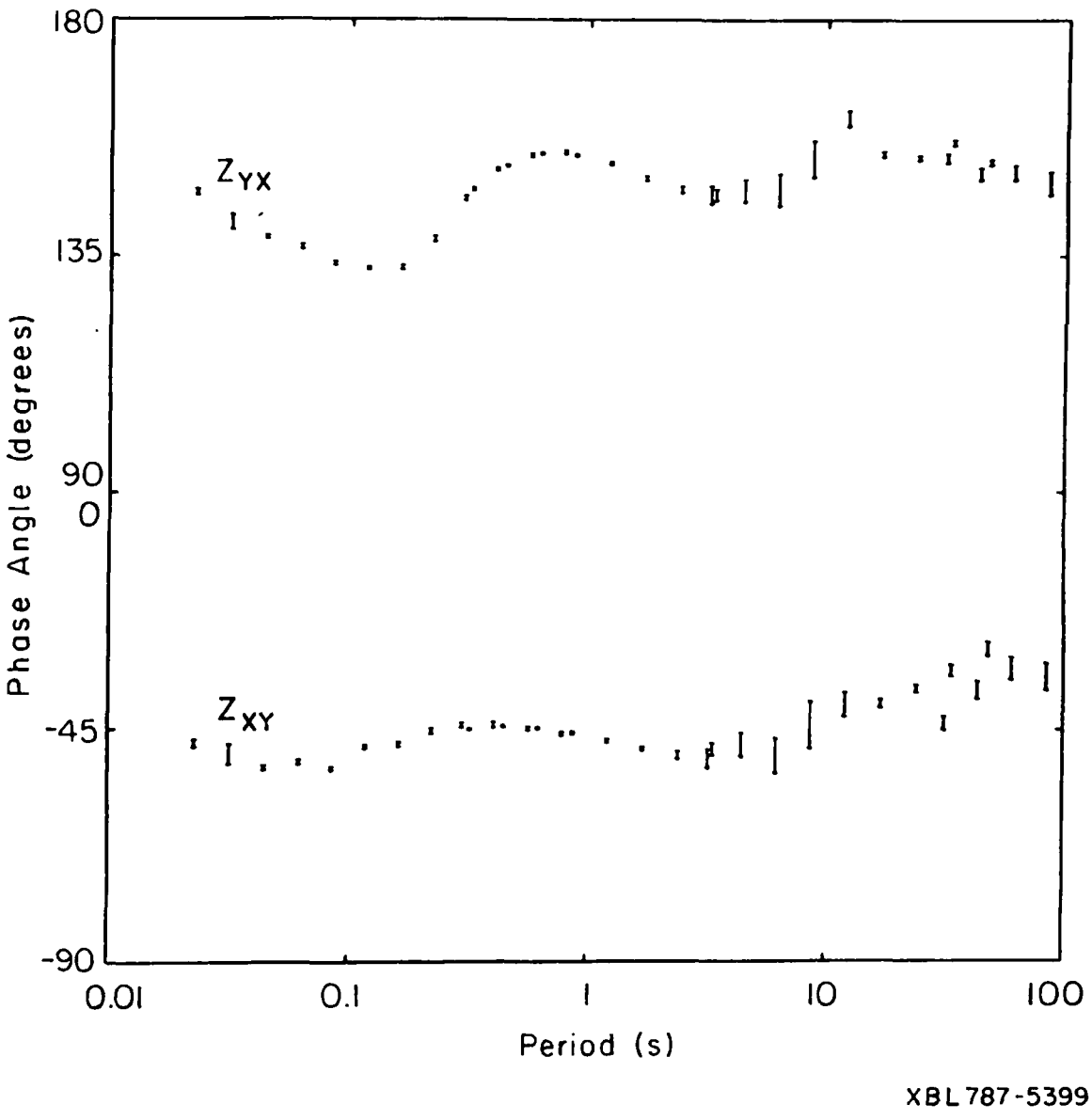

Fig. 29. Phases from $\underline{\underline{Z}}^R$ and their probable errors versus period, Lower La Gloria.

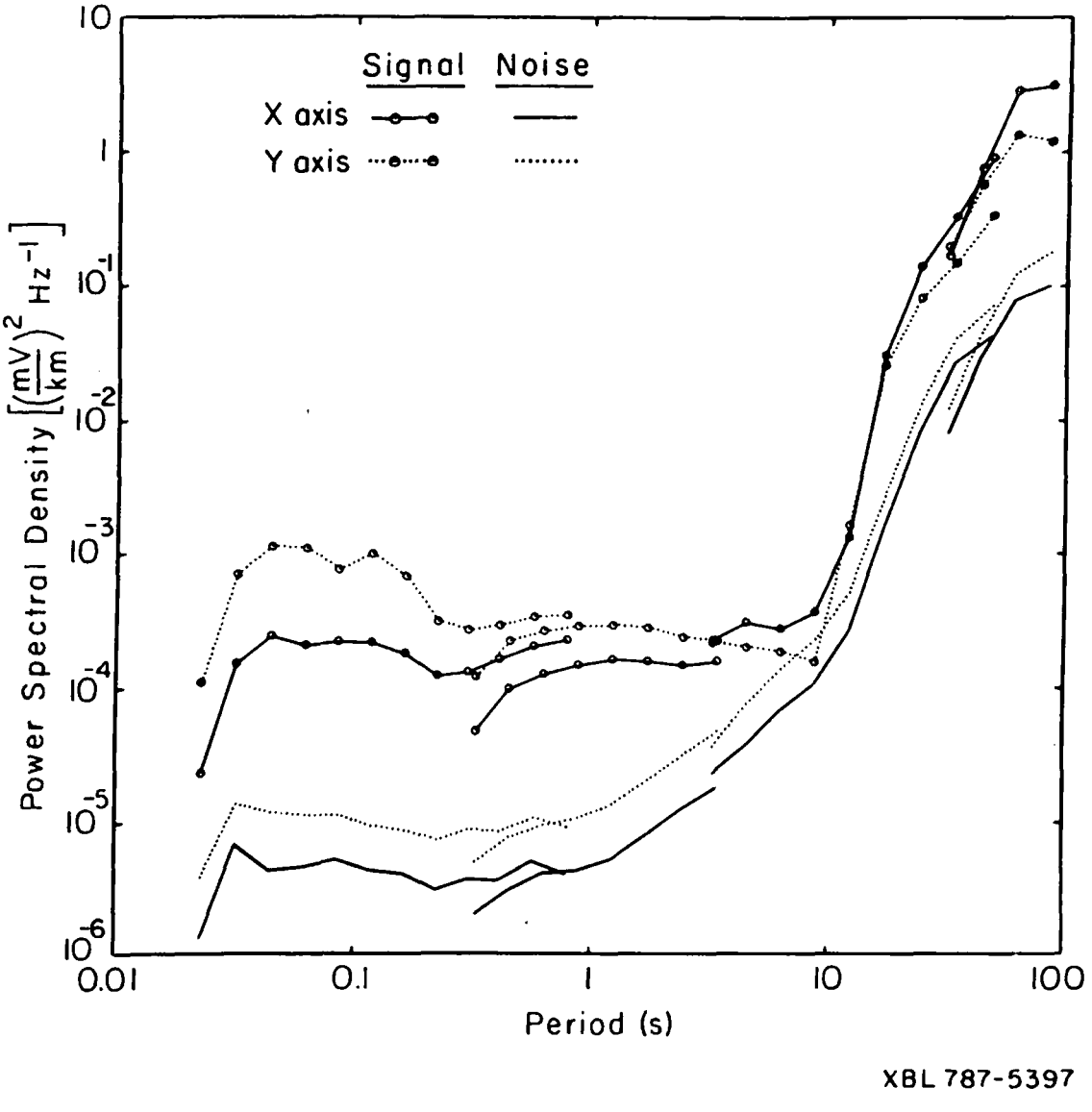

Fig. 30. Electric field signal and noise power spectra versus period, Lower La Gloria.

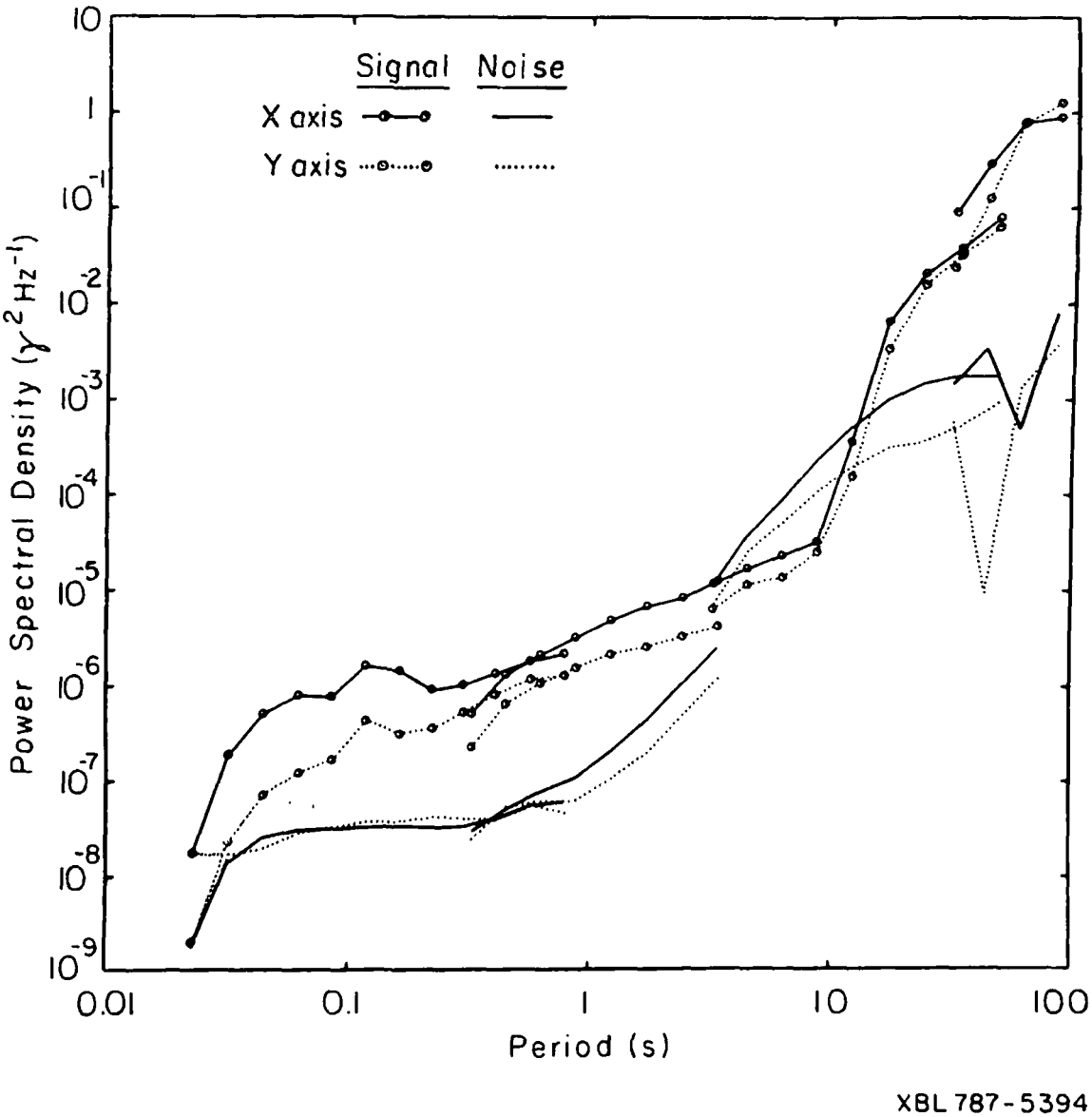

Fig. 31. Magnetic field signal and noise power spectra versus period, Lower La Gloria.

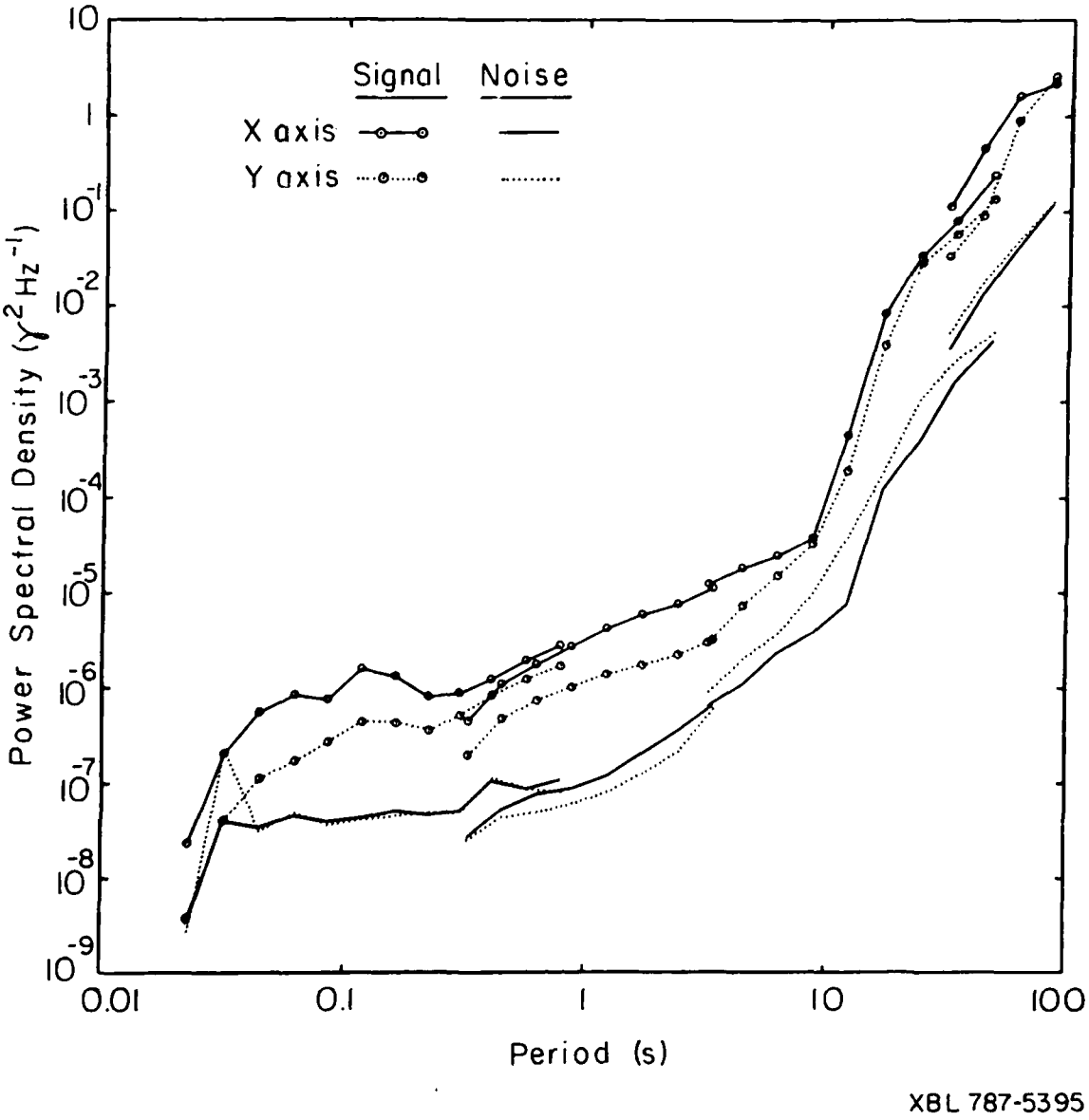

Fig. 32. Remote magnetic reference signal and noise power spectra versus period, Lower La Gloria.

$\underline{\underline{Z}}^E$ were invariably larger than those from $\underline{\underline{Z}}^H$. The difference reached a factor of 100 for ρ_{xy} at 9 second period, figures 23 and 25. This station would have been a wasted effort with conventional analysis since C_x and C_y are never both above 0.9. The source of the bias is evident in the signal and noise power spectra, figures 30 through 31.

Lower La Gloria was the one station where method I was more successful than the least squares methods. For periods shorter than 20 seconds it yielded apparent resistivities, figure 24, that lie between the two least squares resistivities, figure 23 and 25, in 50 of 54 cases. This result indicates that the random errors for the crosspower method are small in this case compared to the bias errors of the least squares methods, and is further evidence that the autopower bias is the major source of error. At periods between 3 and 20 seconds method I produced dips in the apparent resistivity similar to those of the standard analysis, but about a factor of five smaller.

In contrast with the other methods, the remote reference method yields apparent resistivities, figure 27, that vary smoothly over the entire range of periods, even where the coherency is low. The results from overlapping bands agree within the expected random error. At periods shorter than 1 s, the remote reference apparent resistivities agree with the results from the crosspower method to within the random scatter of the crosspower results (± 10%).

It is interesting to compare the signal and noise power spectra for $\vec{H}$ at Lower La Gloria, figure 31, with the spectra for the reference

field for Upper La Gloria, figure 21, since they are, of course, physically the same thing. The difference between the two calculations is that in the former case the electric field at Lower La Gloria was used in equation (5.52) while in the latter the electric field at Upper La Gloria was used in equation (5.53). The converse relation holds for the calculation of the $\vec{H}$ spectra at Upper La Gloria and the reference spectra for Lower La Gloria. The eight pairs of spectra are satifyingly similar except for some noticable random scatter at the longest periods where the number of data is least. In fact at Lower La Gloria there were two values of noise autopower in the magnetic field that came out negative. This would cause problems on a logarithmic plot so the absolute value was plotted.

At Lower La Gloria the standard and remote reference methods yield very similar values for the phase angles, with scatter increasing with period up to about $\pm$ 5° for periods longer than 10 s, figures 26 and 29. The standard analysis yields values of apparent strike and skewness that differ by 20° and 0.2 respectively between bands 2 and 3, while no disagreements are apparent for the remote reference method, figure 28. There are also consistent differences between the two methods. For example, the apparent strike at short periods determined by the remote reference method is about 52°, while by the standard method it is about 65°.

Reproducibility of Apparent Resistivities

The final question to be answered is whether the expected random error is a good estimate of the reproducibility of the results. They

are certainly in qualitative agreement. Where the bands overlap the values usually agree within the calculated probable error. One can draw a very smooth curve through at least 50% of the probable error ranges. One can get a slightly better estimate of the reproducibility by comparing the results obtained from disjoint subsets of the data.

In bands 1 and 2 we had collected about 5 times as many data as were necessary to obtain estimates with reasonably small random errors. I divided these data into M subsets and thus was able to recompute M completely independent estimates for each of the apparent resistivities. If the average of the M values is $\bar{\rho}$ then the expected standard deviation of the average, σ, is given by

$$\sigma^2 = \sum_{i=1}^{M} (\rho_i - \rho)^2 / (M^2 - M) \quad . \tag{6.1}$$

For band 1 at Upper La Gloria I formed 5 subsets and for band 1 at Lower La Gloria and for band 2 at both stations I selected 4. In an attempt to include signals of various polarizations in each of the M subsets I selected for each subset roughly equal numbers of records from two different recording times that were widely separated. Table VI summarizes the recording times and the number of the subset to which the data segments were assigned. There are no entries for the first two recording times in band 1 at Lower La Gloria because we had accidentally removed a set of preamplifiers from some of the channels at that station.

Table VII lists the percentage expected standard deviation of the mean resistivity, 100 $\sigma/\bar{\rho}$, as a function of period for both stations.

Table VI. Arrangement of data from bands 1 and 2 into subsets to estimate the standard deviation of the apparent resistivity at each period. Date refers to September 1977.

Band 1				Band 2			
		Subset number				Subset number	
Recording time	Date	Upper La Gloria	Lower La Gloria	Recording time	Date	Upper La Gloria	Lower La Gloria
11:55 AM - 12:00 PM	14	2	Omitted	9:25 AM - 9:50 AM	14	1	1
12:01 PM - 12:06 PM	14	3	Omitted	9:55 AM - 10:42 AM	14	2	2
7:30 PM - 7:35 PM	14	4	3	10:43 AM - 11:27 AM	14	3	3
7:36 PM - 7:41 PM	14	5	4	6:20 PM - 6:57 PM	14	4	4
1:20 PM - 1:25 PM	15	1	1	7:00 PM - 7:32 PM	14	2	2
1:25 PM - 1:30 PM	15	2	2	10:50 AM - 11:37 AM	15	1	1
1:30 PM - 1.35 PM	15	3	3	11:38 AM - 12:25 PM	15	3	3
1:35 PM - 1:40 PM	15	4	4	12:36 PM - 1:13 PM	15	4	4
1:40 PM - 1:45 PM	15	5	1				
1:45 PM - 1:50 PM	15	1	2				

Table VII. Expected standard deviations, 100 $\sigma_j/\bar{\rho}_j$, of mean apparent resistivities from the remote reference method.

Period (s)	Upper La Gloria		Lower La Gloria	
	100 $\sigma_{xy}/\bar{\rho}_{xy}$	100 $\sigma_{yx}/\bar{\rho}_{yx}$	100 $\sigma_{xy}/\bar{\rho}_{xy}$	100 $\sigma_{yx}/\bar{\rho}_{yx}$
0.03	0.4	3.5	2.0	2.3
0.04	0.5	0.8	0.7	0.8
0.06	0.2	0.8	1.3	0.5
0.08	0.3	2.1	1.1	0.9
0.12	0.5	0.7	0.8	0.7
0.16	0.4	1.4	1.6	1.3
0.22	0.7	0.6	1.9	1.1
0.30	0.6	0.9	0.9	1.8
0.41	0.04	4.4	0.7	1.2
0.57	1.2	2.2	1.3	1.3
0.79	1.2	1.6	1.8	1.5
0.33	2.2	1.6	0.4	0.8
0.45	0.8	1.0	1.2	0.5
0.63	1.2	3.0	1.0	0.5
0.88	1.2	0.9	0.9	0.7
1.2	1.0	1.3	1.4	1.1
1.7	1.1	1.4	0.9	1.5
2.4	0.8	3.4	2.7	1.2
3.4	1.3	2.6	1.7	2.0

We see that the expected fractional standard deviation of both $\bar{\rho}_{xy}$ and $\bar{\rho}_{yx}$ is always less than 5%, and, for 87% of the data, is 2% or less. The average of $\sigma/\bar{\rho}$ over all entries in table VII is 1.3%. For comparison, when I performed the same analysis on the apparent resistivities calculated from Z^H, the average of the fractional standard deviation was 3.3%. At periods less than 3 seconds, the expected deviations are much smaller than the discrepancies caused by bias (typically 20%) that one observes when one compares these results with those obtained from $\underline{\underline{Z}}^R$.

With the number of subsets M being so small these estimates of the standard deviations are very crude, with uncertainties of roughly a factor of 2. Nevertheless they are in qualitative agreement with the expected random error from figures 16 and 27. One can obtain one more certain estimate of the reproducibility by calculating the rms value of σ for a number of the resistivities with comparable σ's. Averaging together 25 of the σ's in this way should produce an estimate of the reproducibility that is accurate to within about 10%. Indeed, for the 25 apparent resistivities with the smallest expected percentage random error, the rms value of σ was equal to 88% of the rms expected standard deviation as calculated from equation 5.20.

CONCLUSION

The remote reference method is a superior method of measuring $\underline{\underline{Z}}$. It makes possible the measurement of $\underline{\underline{Z}}$ with accuracy limited only by the inhomogeneity of the incident fields. This ultimate accuracy should be even better than that of the test in section VI since all the apparent errors in that test were easily accounted for by the expected random error, but will depend on the geology of the sounding site and the nature of the signals.

Of course one should minimize the errors of the measurements and of signal processing. However, the intrinsic noise level of our SQUID magnetometer was usually an insignificant (less than 10%) contribution to the magnetic field noise observed in our measurements. The great superiority of the results of the remote reference method over the other methods of analysis for the same data processed in the identical fashion proves that the errors in that signal processing are not significant. Any digital technique for computing the average powers should be satisfactory if applied with reasonable care.

While the attempts to estimate $\underline{\underline{Z}}$ from local measurements alone, as described in section IV, were not satisfactory, they did demonstrate correlated noises. Since the remote reference method can be used to separate out the ionospherically generated electromagnetic signals, the source of these other "noises" may itself be an interesting area of investigation.

The most exciting thing about the remote reference method is its extreme generality. The best previously used estimator for $\underline{\underline{Z}}$, $\underline{\underline{Z}}^H$, is

an example of least squares linear regression. This regression technique has almost invariably been employed to estimate the linear relationship between any two processes, from the relationship between a person's height and his annual income to the response of an airplane wing to the vibration of an engine. The difficulties of least squares linear regression have long been recognized by statisticians. Mosteller and Tukey,[21] in a chapter titled "The woes of regression analysis" concluded," at this point we can recommend only deep and careful thought." The remote reference method should be valuable in any area where many noisy data are available. The "autopower" bias can be removed from the estimation of any of these linear relationships by the measurement of a third related process, a "remote reference," and the use of the cross-correlation regression technique of section V.

REFERENCES

1. W. H. Barlow, On the Spontaneous Electric Currents Observed in the Wires of the Electric Telegraph: Phil. Trans. R. Soc., p. 61-72 (1849).

2. J. S. Bendat and A. G. Piersol, Random Data: Analysis and Measurement Procedures, New York, John Wiley & Sons, Inc., (1971).

3. C. R. Bentley, Error Estimation in Two Dimensional Magnetotelluric Analysis: Physics of the Earth and Planetary Interiors 7, 423-430, (1973).

4. H. Beyer, A. Dey, A. Liaw, E. Majer, T. V. McEvilly, H. F. Morrison, and H. Wollenberg, Geological and Geophysical Studies in Grass Valley, Nevada: Preliminary Open File Report, Energy and Environmental Division, Lawrence Berkeley Laboratory, University of California, Berkeley. LBL Publication 5262, (1976).

5. L. Cagniard, Basic Theory of the Magnetotelluric Method of Geophysical Prospecting: Geophysics 18, 605-635, (1953).

6. T. Cantwell, Detection and Analysis of Low Frequency Electromagnetic Signals: Ph.D. thesis, Dept. of Geology and Geophysics, M.I.T. (1960).

7. S. Chapman and J. Bartels, Geomagnetism, Oxford, Clarendon Press, (1940).

8. J. Clarke, W. M. Goubau and M. B. Ketchen, Tunnel junction dc SQUID: Fabrication, Operation, and Performance: J. Low Temp. Phys. 25, 99-144, (1976).

9. R. Corwin, Use of the Self-Potential Method for Geothermal Exploration: Lawrence Berkeley Laboratory Report 3235.

10. H. G. Fournier, Essai d'un historique des connaissances magnetotelluriques: note #17, Inst. de Phys. du Globe, Faculte des Sciences, U. de Paris, (1966).

11. T. D. Gamble, W. M. Goubau, M. B. Ketchen, and J. Clarke, Regulator for Controlling Liquid Helium Bath Near 4.2 K: Rev. Sci. Instrum. 49, 119-120, (1978).

12. N. R. Goodman, Measurement of Matrix Frequency Response Functions and Multiple Coherence Functions: AFFDL TR 65-56, Wright Patterson Air Force Base, Air Force Flight Dynamics Laboratory, (1965).

13. H. Hatakeyama, On the Bay Disturbance and the Pulsation of the Earth Current: Geophys. Mag. 12, 189-210 (1938).

14. M. Hirayama, On the Relations Between the Variations of the Earth Potential Gradient and Terrestrial Magnetism: J. Met. Soc. Jap. 12, (1), 16-22, (1934).

15. G. M. Jenkins and D. G. Watts, Spectral Analysis and Its Applications: San Francisco, Holden-Day, (1968).

16. D. W. Kao and D. Rankin, Enhancement of Signal to Noise Ratio in Magnetotelluric Data: Geophysics, 42, 103-110, (1977).

17. T. Madden and P. Nelson, A Defense of Cagniard's Magnetotelluric Method: Off. of Naval Res. Project NR-371-401, Geophys. Lab., M.I.T. (1964).

18. A. T. Mazzella, Deep Resistivity Study Across the San Andreas Fault Zone: Ph.D. thesis, University of California, Berkeley, (1976).

19. H. F. Morrison, A Magnetotelluric Profile Across the State of California: Ph.D. thesis, University of California, Berkeley, (1967).

20. H. F. Morrison, R. F. Corwin and M. Chang, High Accuracy Determination of Temporal Variations of Crustal Resistivity: The Nature and Physical Properties of the Earth's Crust, J. G. Heacock, Ed., p. 593-614, AGU Monograph 20, (1977).

21. F. Mosteller and J. W. Tukey, Data Analysis and Regression, A Second Course in Statistics, Reading, Mass., Addison Wesley.

22. A. T. Price, Theory of Magnetotelluric Methods When the Source Field is Considered; J. Geophys. R., 67, 1907-1918 (1962).

23. C. Quon, Electromagnetic Fields of Elevated Dipoles on a Two-Layer Earth: M.S. thesis, University of Alberta, Edmonton, (1963).

24. C. Quon, K. Vozoff, M. Hoversten, H. F. Morrison, and K-H. Lee, Localized Source Effects on Magnetotelluric Apparent Resistivities: Paper at the 40th EAEG Meeting, Dublin, Ireland, (1978).

25. I. K. Reddy, R. J. Phillips, J. H. Whitcomb, D. M. Cole and R. A. Taylor, Monitoring of Time Dependent Electrical Resistivity by Magnetotellurics: J. Geomagn. Geoelectr. 28, 165-178 (1976).

26. T. Rikitake, Electromagnetism and the Earth's Interior, Amsterdam, London, N.Y., Elsevier Publ. (1966).

27. R. Resnick and D. Halliday, Physics, New York, Wiley, (1966).

28. W. J. Rooney, Earth Currents: Terrestrial Magnetism and Electricity, J. A. Fleming, Ed., New York, McGraw-Hill, p. 270-306 (1939).

29. W. E. Sims and F. X. Bostick, Jr., Methods of Magnetotelluric Analysis: Tech. Rep. 58, Elect. Geophys. Res. Lab., University of Texas, Austin, (1969).

30. W. E. Sims, F. X. Bostick, Jr. and H. W. Smith, The Estimation of Magnetotelluric Impedance Tensor Elements from Measured Data: Geophysics, 36, 938-942, (1971).

31. C. M. Swift, Jr., A. Magnetotelluric Investigation of an Electrical Conductivity Anomaly in the Southwestern United States: Ph.D. Thesis, MIT., (1967).

32. T. Terada, On Rapid Periodic Variations of Terrestrial Magnetism: J. Col. Sci., Tokyo Imp. U. 37, (9), 56-84, (1917).

33. K. Vozoff, The Magnetotelluric Method in the Exploration of Sedimentary Basins: Geophysics, 37, 98-114, (1972).

34. D. F. Wight, F. X. Bostick, Jr. and H. W. Smith, Real Time Fourier Transformation of Magnetotelluric Data, Electrical Geophysics Res. Lab., University of Texas, Austin, (1977).

35. R. Zelwer and H. F. Morrison, Spatial Characteristics of Midlatitude Geomagnetic Micropulsations: J. Geophys. Res. 77, (4), 674-694, (1972).

This report was done with support from the Department of Energy. Any conclusions or opinions expressed in this report represent solely those of the author(s) and not necessarily those of The Regents of the University of California, the Lawrence Berkeley Laboratory or the Department of Energy.

TECHNICAL INFORMATION DEPARTMENT
LAWRENCE BERKELEY LABORATORY
UNIVERSITY OF CALIFORNIA
BERKELEY, CALIFORNIA 94720